5-2007

KINETICS OF SURFACE-INITIATED PHOTOINIFERTER-MEDIATED PHOTOPOLYMERIZATION AND SYNTHESIS OF STIMULI-RESPONSIVE POLYMER BRUSHES

Santosh Rahane
Clemson University, srahane@clemson.edu

KINETICS OF SURFACE-INITIATED PHOTOINIFERTER-MEDIATED PHOTOPOLYMERIZATION AND SYNTHESIS OF STIMULI-RESPONSIVE POLYMER BRUSHES

A Thesis
Presented to
the Graduate School of
Clemson University

In Partial Fulfillment
of the Requirements for the Degree
Doctor of Philosophy
Chemical Engineering

---

by
Santosh Bhagwat Rahane
May 2007

Accepted by:
Dr. S. Michael Kilbey II, Committee Chair
Dr. Andrew T. Metters, Committee Chair
Dr. Scott M. Husson
Dr. Igor Luzinov

ABSTRACT

The focus of this research is to understand the kinetic and mechanistic aspects of surface-initiated photoiniferter-mediated photopolymerization (SI-PMP) and exploit the robustness of SI-PMP to synthesize stimuli-responsive polymer brushes. The “living” characteristics of dithiocarbamate-based photoiniferter-mediated photopolymerization are well documented. However, in this dissertation I show that the growth of poly(methyl methacrylate) (PMMA) brushes by SI-PMP is nonlinear, suggesting loss of radicals during SI-PMP and, in turn, non-living characteristics. Results from kinetic models in conjunction with experimental results suggest that irreversible bimolecular termination reactions are a primary culprit for the loss of radicals during SI-PMP.

To overcome this problem of irreversible termination reactions, tetraethylthiuram disulfide (TED), a source of deactivating dithiocarbamyl radicals, was added to the SI-PMP system. Preaddition of TED successfully reduced irreversible termination reactions. Contention of decrease in irreversible termination reactions is further supported by results from reinitiation studies using styrene: reinitiation efficiency, as indicated by the thickness of the added polystyrene block, increases as TED concentration increases.

The impact of various photopolymerization conditions on SI-PMP is further investigated by simulating the SI-PMP process using a rate-based model. With this approach the effect of photopolymerization conditions such as light intensity, TED concentration, exposure time and initial photoiniferter concentration on the growth kinetics and reinitiation ability of PMMA layers has been studied in detail. The

simulations show that increases in [TED] and decreases in light intensity impact the PMMA layer propagation in similar fashions; these trends are observed in experiments. However, simulations also indicate that the effect of [TED] and light intensity on the reinitiation ability of PMMA layers are significantly different: reinitiation ability increases with increasing [TED], but decreasing light intensity does not improve reinitiation ability. The simulations also show that choice of photopolymerization conditions used during the first polymerization step is critical to the final structure of the polymer brush created upon reinitiation: PMMA layers formed in the presence of TED are more likely to form block copolymers as compared to PMMA layers synthesized without TED and at lower light intensity.

Strategies learned from these simulations and experiments were applied for the synthesis of bi-level, multiresponsive poly(methacrylic acid)-*block*-poly(*N*-isopropyl-acrylamide) (PMAA-*b*-PNIPAM) layers. *In-situ* multi-angle ellipsometry investigations of these layers demonstrate that these layers respond to changes in pH, temperature and ionic strength. While the individual blocks retain their customary responsive characteristics, the overall swelling behavior of the PMAA-*b*-PNIPAM layers can be tuned by any number combinations of pH, temperature and ionic strength.

The efforts described in this dissertation, demonstrate not only the robustness of SI-PMP for making a variety of functional polymer brushes, but also the complex links between synthesis, structure and properties of polymer brushes.

DEDICATION

I dedicate this work to the most wonderful people in the world, my beloved parents:

Aai and Dada.

Aai and Dada, all that I have done to-date and all that I will do in the future is for you!!

ACKNOWLEDGMENTS

There are countless individuals that deserve my sincere gratitude for helping me complete this work. First and foremost, I would like to thank my family: my parents (*Aai and Dada*), my brothers (Suhas and Sandip), Yogitavahini, Seemavahini and last but not the least, little *Pau*. Their support, guidance, words of encouragement and unselfish love inspire me to achieve what I want to achieve. I feel blessed to have such a wonderful family.

I would like to thank my advisors Dr. Kilbey and Dr. Metters for their suggestions, encouragement and constant support that made the job of completing this dissertation lot easier than it would have been. I am also thankful my dissertation committee members: Dr. Husson and Dr. Luzinov for their time, effort and suggestions from time to time.

Thanks to all past and present group members: Amit, Brad, Azi, Srinivas, Jose, Mike Z, Ed, Nihar, Josh, JP, Chien-Chi, Peng and John for the insightful discussions during the numerous group meetings and random discussions in the office. Special thanks to all the hardworking undergraduate students: Alaiiina, Michael, Yulia, Yasin, Abby and Michelle. Special thanks is also due to all the office-mates - Brad, Ed, Srinivas, John, Keisha, Amit, Chun, Rahul, Josh, SiqZhu and Namrata for making the offices “the most-fun places” to work (*work??*).

All the roomies: Amol, Mihir, Shamik, Nripen, Sameer, Rahul and Sourabh deserve special thanks for eating all the special dishes (*which were never special??*) I cooked without any complaints.

Last but not the least, I am also thankful to all the special friends in Clemson: Panya (*you can have half of the car*), Kyo, Rucha (*do I get the chocolates??*), Abhijit, Roma, Shrinivas, Karkha, Vidya, Gaurav, Amitda, Srinivas, Santanu, Giri, Chakra, the "Surabhi" and "AID" teams, and the cricket, softball and football gangs.

I would like to thank everyone else; whose names have skipped mention. Thank you everyone!!

TABLE OF CONTENTS

Table of Contents (Continued)

Table of Contents (Continued)

Page

Table of Contents (Continued)

Page

LIST OF TABLES

LIST OF FIGURES

List of Figures (Continued)

Figure Page

List of Figures (Continued)

List of Figures (Continued)

Figure Page

List of Figures (Continued)

Figure Page

List of Figures (Continued)

Figure Page

List of Figures (Continued)

Figure Page

List of Figures (Continued)

List of Figures (Continued)

Figure Page

CHAPTER 1

INTRODUCTION

Polymer brushes, which are an assembly of polymer chains tethered by one end to a surface or an interface, serve as a general model for studying polymer-modified surfaces, polymer micelles, and microphase separated block copolymers [1-3]. The density of the polymer chains tethered at the interface of a polymer brush is sufficient to force the chains to stretch away from the surface to avoid overlapping. The stretched configuration of chains in a polymer brush differs significantly from the random-coil configuration of polymer chains in solution. This structural difference affects the interfacial behavior of the tethered chains, which in turn, leads to many novel properties of polymer brushes [3].

Therefore, fabricating polymer brushes provides a way to modify the interfacial properties of a material without sacrificing its bulk properties [4]. For example, properties such as biocompatibility, wettability, corrosion resistance, friction, affinity to a specific target molecule, and adsorption capacity can be controlled by modifying a surface with polymer brushes. Owing to these capabilities, polymer brushes have found applications in various areas concerning new adhesive materials [5,6], protein-resistant or protein-adhesive biosurfaces [7], chromatographic devices [8], lubricants [9,10], polymer compatibilizers [1], chemical gates [11,12], microfluidic devices [13] and drug delivery devices [7] to name a few.

In view of such potential, it is crucial to understand the synthesis-structure-property relationship of polymer brushes so that they can cater to the exact needs of a particular application. In this work, to gain insight into synthesis-structure-property relationships of polymer brushes, brush formation from silicon substrates was investigated through experimental studies and modeling. Use of silicon substrates allows common interfacial characterization techniques (for example: ellipsometry, infra-red spectroscopy, contact angle) to be used readily for the characterization and understanding of structure of polymer brush layers. In this chapter, first, various strategies for making polymer brush layers are described. Then, brief overview and contributions from selected previous researchers related to various concepts and techniques, on which the present work is based on, are discussed.

1.1 Strategies for Fabricating Polymer Brushes on Solid Substrates

Methods of fabricating polymer brushes on solid substrates are termed “grafting to” and “grafting from” approaches. While grafting to approach involves tethering premade chains to the surface, either by preferential physisorption or *via* a chemical bond formation between reactive groups on a surface and reactive end groups of polymer chains [14-19], grafting from involves growing chains from surface-anchored initiators [2]. Figure 1.1 schematically depicts the grafting to and grafting from approaches. As suggested in Figure 1.1a, brush formation *via* preferential physisorption involves the self-assembly of amphiphilic block copolymers from dilute solution using a selective

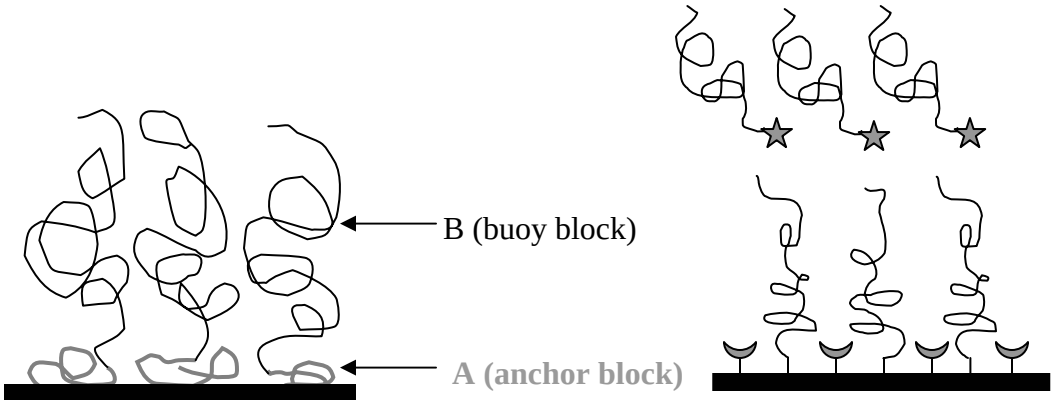

(a) (b)

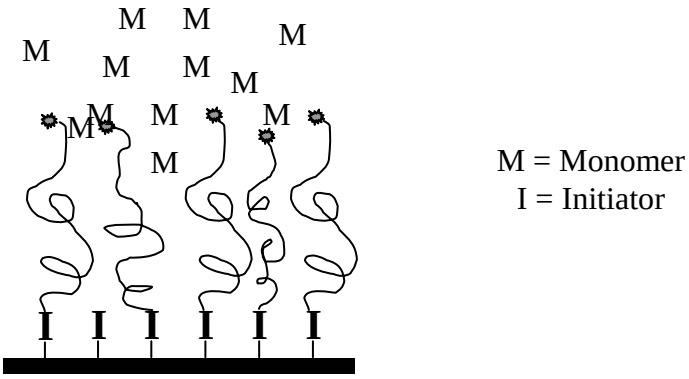

(c)

Figure 1.1 Strategies for forming polymer brushes on solid substrates: a) preferential physisorption of amphiphilc diblock copolymers; b) covalent attachment of pre-made, end-functionalized polymer chains; and c) growing from an initiator-modified substrate.

solvent [20-23]. In a selective solvent, one block is insoluble (referred to as the “anchor” block, A) and the other block is well-solvated (referred to as the “buoy” block, B). This selectivity forces anchor block away from the solvent. In a situation when the anchor block has affinity toward the solid-liquid interface, anchor block tethers the amphiphilic block copolymer to the solid-liquid surface. At sufficiently high grafting density, due to repulsive interactions, the tethered chains stretch away from the surface into the solvent creating polymer brush structure.

However, these physisorbed layers can be dislodged from the surface if the solvent conditions under which these layers were formed are reversed. The approach of covalent attachment overcomes this limitation of physisorption. As mentioned earlier, the covalent attachment method involves reacting end-functionalized polymer chains with an appropriate complementary functionality on the surface (Figure 1.1b) [24-26]. Both of these methods are preferred for fundamental studies because the chain size, composition and architecture can be rigorously controlled and characterized prior to assembly. However, both of the grafting to approaches have an inherent limitation in terms of maximum grafting density achievable. Once the surface is significantly covered, additional polymer molecules are trying to reach the surface face strong steric hindrance from already tethered chains. This steric hindrance impedes the growth of film and grafting density of resultant polymer brushes [16].

The grafting from technique, which involves growing chains from a surface, overcomes limitations of the grafting to approach. In this technique, initiators are immobilized onto the substrate in one or two steps and surface-initiated polymerization is performed to generate surface-tethered polymer chains. A variety of polymerization

methods, including thermally- [27,28] and photo-initiated [29-31] free-radical polymerizations, living anionic and cationic polymerizations [32], and "living" free-radical polymerization (LRP) techniques [33-44] have been used to produce surface-tethered polymer layers *via* the grafting from approach. Of these techniques, LRP techniques, which in general, are based on establishing and maintaining a dynamic equilibrium between active radicals and dormant chains (Figure 1.2), have been most widely used for the following reasons:

i) LRPs are tolerant to impurities and are versatile in terms of monomers that can be polymerized;

ii) LRPs yield polymer chains with low polydispersity;

iii) LRPs allow the molecular weight of chains to be controlled; and

iv) LRPs can be used to synthesize complex polymer architectures, such as multi-block copolymers.

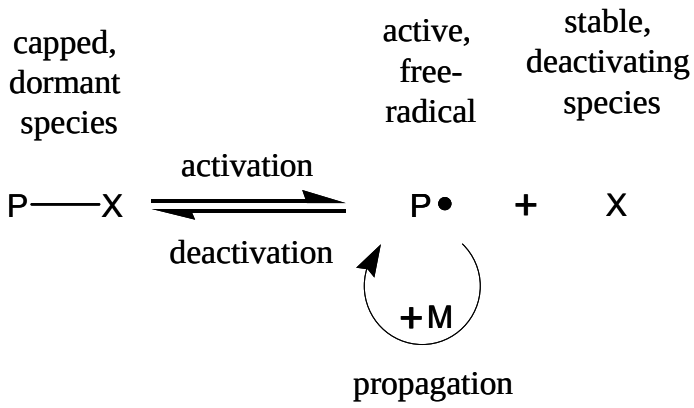

Figure 1.2 Schematic representation of living radical polymerization: equilibrium between capped, dormant chains and propagating free radicals.

Various LRPs, such as atom transfer radical polymerization (ATRP) [33-39], nitroxide-mediated free-radical polymerization (NMP) [40-42], reversible addition fragmentation transfer (RAFT) [43,44], and photoiniferter-mediated photopolymerization (PMP) [45-51] have been used to synthesize surface-tethered polymer brushes using the grafting-from approach. In the current work, PMP was used to produce surface-tethered polymer layers. PMP is based on a dithiocarbamate photoiniferter chemistry first discovered by Otsu et al. [52]. PMP was chosen over other LRPs because PMP has the following advantages [31]:

i) Because PMP involves photochemical initiation, spatial and temporal control over polymerization is enabled by controlling the location, intensity, and duration of light exposure. This allows for micropatterning of the surface.
ii) Because PMP operates at room temperature, it is well-suited for thermally unstable monomers or monomers that include unstable functional groups.
iii) The rate of initiation can be manipulated by simply varying the light intensity at room temperature.

1.2 Brief Overview of Photoiniferter-Mediated Photopolymerization

Photoiniferter molecules, as mentioned earlier, are generally dithiocarbamate derivatives that can *ini*tiate upon exposure to light, act as trans*fer* agents or *ter*minate during polymerization (hence the name photoiniferter). As shown in Figure 1.3, upon exposure to UV light the photoiniferter molecules undergo photolysis, yielding a carbon radical and a dithiocarbamate radical. While the carbon radical is reactive and can initiate

polymerization by reacting with vinyl monomers, the dithiocarbamate radical is stable and reacts weakly, if at all, with vinyl monomers [53,54]. However, the dithiocarbamate radical can reversibly terminate the propagating chains, thereby imparting the “living” characteristics to photoiniferter-mediated photopolymerization.

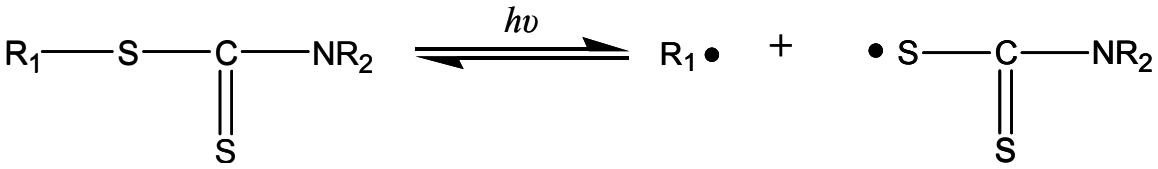

Figure 1.3 Typical reversible activation of dithiocarbamate-based photoiniferter.

Since the discovery of photoiniferter molecules by Otsu et al. [52], various aspects of PMP have been investigated to understand the kinetic mechanism of PMP [52-59]. Otsu et al. [52] showed that PMP of methyl methacrylate (MMA) exhibits living characteristics: the molecular weight of the poly(methyl methacrylate) (PMMA) chains increased linearly with monomer conversion. Otsu and coworkers [55] subsequently demonstrated that the living characteristics allowed for block copolymers of polystyrene and poly(methyl methacrylate) to be made, both in solution and on the surface of microbeads. Turner et al. [56] and Lambrinos et al. [53] also successfully synthesized block copolymers using PMP.

Kannurpatti et al. [58] and Ward et al. [59] investigated the kinetics of PMP of mono- and multifunctional methacrylates in bulk. Both of these research groups concluded that the autoacceleration effect observed in classical free-radical photopolymerization is either reduced or eliminated by using PMP. This phenomenon is a

consequence of the reversible carbon-dithiocarbamyl radical combination reactions, which are not diffusion limited, dominating compared to the diffusion limited, and irreversible carbon-carbon radical termination reactions. This domination of carbon-dithiocarbamyl radical combination reactions also support previously observed living radical mechanism associated with PMP.

Thus, while the mechanisms involved in bulk or solution PMP are well-characterized, mechanism and kinetics of surface-initiated photoiniferter-mediated photopolymerization (SI-PMP) can be significantly different from bulk or solution PMP and have not been investigated adequately. The following section briefly discusses the various works done in the field of SI-PMP.

1.3 Surface-Initiated Photoiniferter-Mediated Photopolymerization (SI-PMP)

Photoiniferter-mediated photopolymerizations from surface-immobilized photoiniferters have been used by several groups [46-52] to modify surface properties of various organic and inorganic substrates. Before learning about the previous studies of SI-PMP in the literature, it is first instructive to understand how a polymer layer should grow by an ideal, living SI-PMP. Eq 1 represents the layer thickness growth rate as a function of monomer concentration and surface-tethered radical concentration,

$$\frac{dT}{dt} = k[STR\bullet][M] \tag{1}$$

where T is the polymer layer thickness, t is exposure time, k is the proportionality constant that relates rate of photopolymerization rate to the thickness growth rate of polymer layer, $[STR\bullet]$ is the surface-tethered radical concentration and $[M]$ is the monomer concentration. The assumptions and simplifications involved in the derivation of Eq 1 are described previously [60] and in Chapter 2 as well. In case of an ideally living SI-PMP, $[STR\bullet]$ should remain constant. Additionally, in typical surface-initiated LRPs, (SI-LRPs) monomer consumption is negligible. Therefore, $[M]$ should also remain constant during the layer growth. Thus, when $[STR\bullet]$ and $[M]$ are constant, analysis of Eq 1 suggests that polymer layer thickness should grow linearly with time.

Luo et al. [47] studied the photopolymerization of poly(ethylene glycol) monomethacrylate from *N*,*N*-diethyldithiocarbamate-functionalized polymer substrates. These *N*,*N*-diethyldithiocarbamate-functionalized polymer substrates were prepared by either thermally- or photo-initiated free radical polymerization of a monomer-iniferter, (methacryloyl ethylene-dioxycarbonyl) benzyl *N*,*N*-diethyldithiocarbamate. SI-PMP of poly(ethylene glycol) monomethacrylate resulted in micron-thick polymer layers in the span of 4 minutes and layer thickness growth was observed to be linear for the time-span investigated. However, a significant amount of gelation was observed in this system, presumably due to significant chain transfer to the poly(ethylene glycol) monomethacrylate macromer. Therefore, polymer layer growth in this system resulted not only from propagation of surface-tethered polymer chains but also from crosslinking between surface-tethered chains and polymer chains or networks in the bulk. Thus, the layers produced were not strictly polymer brushes.

Nakayama et al. [45] investigated the kinetics of SI-PMP by synthesizing polystyrene (PS) layers from dithiocarbamate-modified polystyrene films. SI-PMP was carried out using a lattice-patterned projection mask. As a result, graft-copolymerization of PS was realized only on the unmasked areas. The height difference between non-treated part of the surface and graft-copolymerized regions of the surface was measured using atomic force microscopy (AFM) to determine the thickness of the photopolymerized PS layers. As shown in Figure 1.4, a linear dependence of dry PS layer thickness on exposure time was observed, and they attributed this pattern of behavior as suggesting living radical polymerization. However, these measurements were made only during the early stages of polymerization (20 minutes).

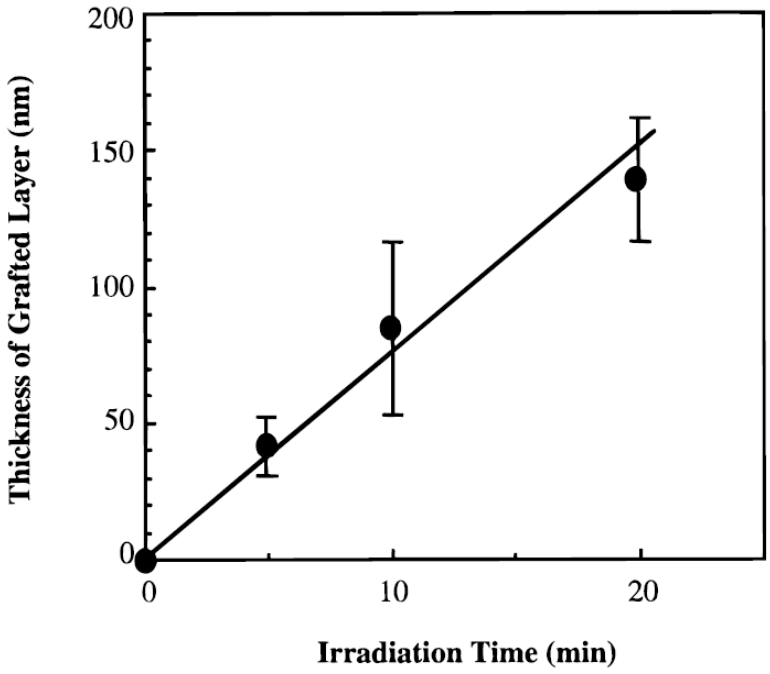

Figure 1.4 Linear dependence of polystyrene layer thickness synthesized using surface-initiated photoiniferter-mediated photopolymerization (SI-PMP) from dithiocarbamate-modified polystyrene films with polymerization time. The linear growth of polystyrene layer was attributed to living radical mechanism of SI-PMP. Reprinted with permission from Ref. [45] (*Macromolecules* **1996**, *29*, 8622; Copyright (1996) American Chemical Society).

de Boer et al. [49] studied the effect of exposure time on the thicknesses of PS layers synthesized from dithiocarbamate-modified glass and silicon substrates over a longer range of exposure times (20 hours). Micropatterned polystyrene layers were synthesized and thicknesses of the polymer layers were estimated by measuring the height differences between polymerized and unpolymerized regions on a substrate using AFM. As shown in Figure 1.5, a linear increase in the measured thickness of the dried polystyrene films with polymerization time was observed. However, the effect of other

photopolymerization conditions such as light intensity and monomer concentration was not investigated.

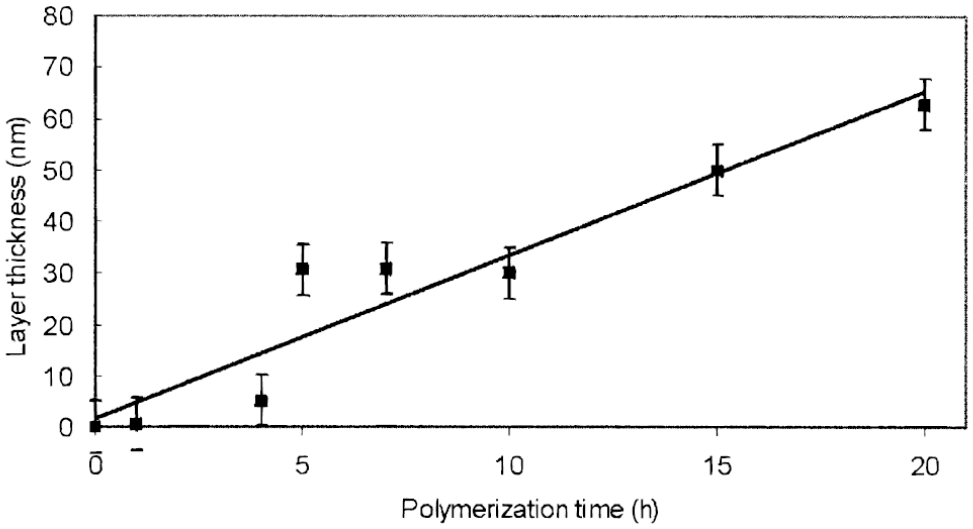

Figure 1.5 Linear dependence of polystyrene layer thickness synthesized using surface-initiated photoiniferter-mediated photopolymerization (SI-PMP) from dithiocarbamate-modified glass substrates with polymerization time. The linear growth of polystyrene layer was attributed to living radical mechanism of SI-PMP. Reprinted with permission from Ref. [49] (*Macromolecules* **2000**, *33*, 349; Copyright (2000) American Chemical Society).

Nakayama et al. [51] extended their efforts to understand SI-PMP by investigating the effect of monomer concentration and light intensity on the kinetics of SI-PMP. Their study of dithiocarbamate-based surface photograft-polymerization of various vinyl monomers, including acrylamides and acrylates, using quartz crystal microbalance (QCM) measurements revealed a linear increase in the rate of polymerization with monomer concentration and intensity (Figure 1.6). However, this study was again limited to short exposure times.

Thus, the question of whether SI-PMP behaves as expected at long exposure times and various intensities still needs to be answered. This information about the effects of various photopolymerization parameters on kinetics of SI-PMP, however, is extremely important if one desires to precisely design surface-tethered polymer brushes that can cater to needs of a particular application. Additionally, it is essential to investigate whether the system retains its living characteristics over a wide array of photopolymerization conditions. To understand the layer growth by SI-PMP, it can be helpful to understand the mechanism of other SI-LRPs: analogy between SI-PMP and other SI-LRPs can be instrumental in delineating the strategies for systematic investigation of SI-PMP through experimental studies and modeling.

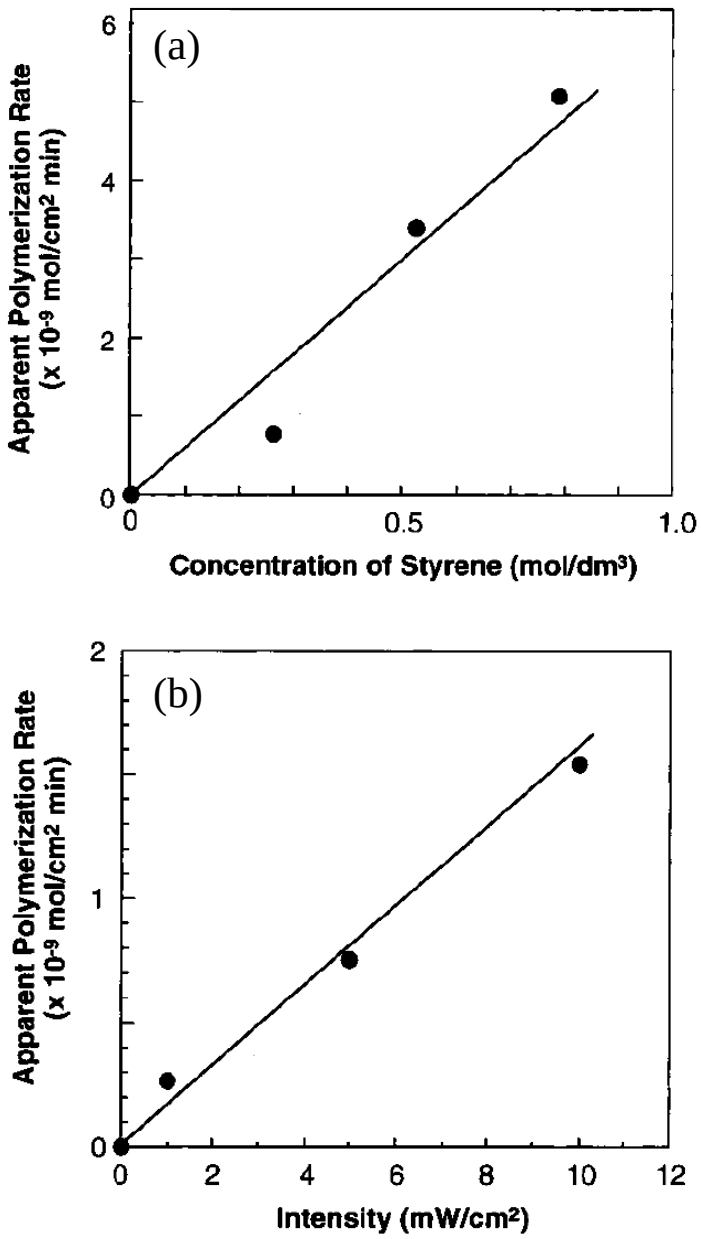

Figure 1.6 Dependence of polymerization rates of SI-PMP of styrene obtained using quartz crystal microbalance on a) monomer concentration and b) light intensity. Over the range of styrene concentration and light intensity investigated, polymerization rate increased linearly with both the parameters. Reprinted with permission from Ref. [51] (*Macromolecules* **1999**, *32*, 5405; Copyright (1999) American Chemical Society).

Previously, it has been shown that living radical polymerizations initiated from flat substrates often show “pseudo-living” characteristics [34,38,60,61]. These pseudo-living characteristics arise due to the loss of radicals by various irreversible termination reactions that occur in the absence of a sufficient concentration of persistent deactivating radicals, and often, the effect of losing radicals does not manifest until longer times. Consequently, polymer layer ceases to grow after certain reaction time. Such a phenomenon has been observed by various groups [34,38,60,61] in their studies of surface-initiated ATRP. Additionally, because the radicals are lost during SI-PMP, the layers formed lack the ability to reinitiate to form multiblock architectures.

To overcome the problem of irreversible termination reactions that lead to cessation of layer growth, in general, the approach of adding a source of deactivating radicals is adapted [35,36,38-41,63-66]. Adding the deactivating species helps establish and maintain an equilibrium between capped, dormant chains and active, free-radical species. This keeps active free-radical concentration low, which consequently helps minimize, irreversible terminations reactions. Such a strategy to minimize irreversible termination reactions has been used by various researchers in their studies of SI-CRP [34,35,39,40,65]. For example, Figure 1.7 shows the effect of added deactivating species, Cu(II) bromide on the kinetics of SI-ATRP of MMA, as reported by Kim et al. [38] As shown in Figure 1.7a, when no Cu(II) bromide is added, the layer initially grows rapidly, followed by a plateau in the thickness suggesting the cessation of layer growth because of irreversible termination reactions. On the other hand, as shown in Figure 1.7b, in the presence of added Cu(II) bromide, initially the layer growth is slow but the layer continues to grow for longer time as compared to that observed in absence of Cu(II)

bromide, suggesting that the irreversible termination reactions are reduced. However, as suggested by the curvature in Figure 1.7b, irreversible termination reactions are not completely eliminated.

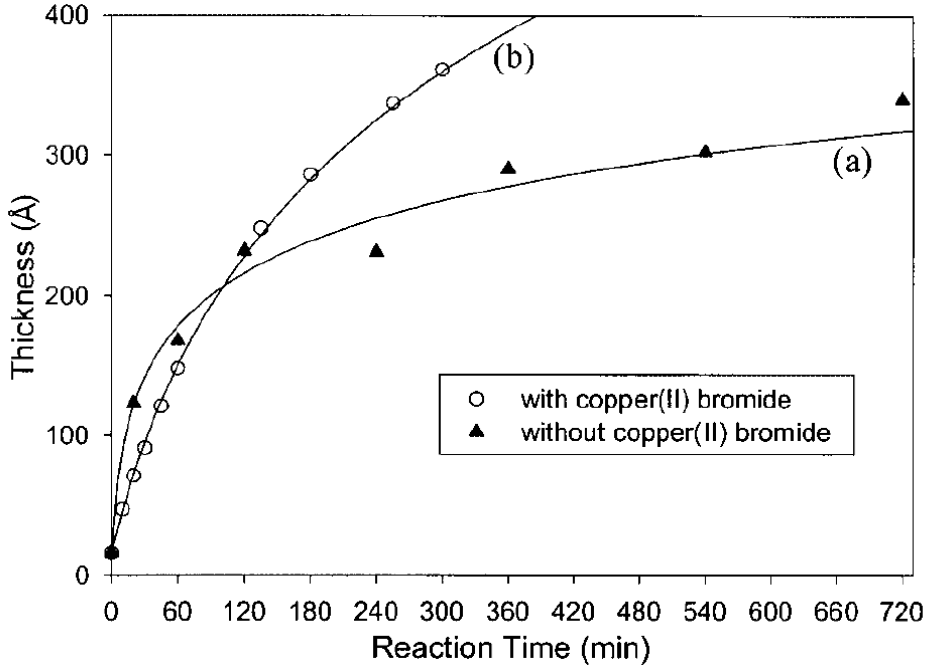

Figure 1.7 Results from Kim et al. [38] demonstrate that a) surface-initiated ATRP (SI-ATRP) of methyl methacrylate, when performed without adding the Cu(II) bromide deactivator results in fast initial growth followed by a plateau in the thickness, suggesting significant irreversible termination. Curve b) suggests that there is a decrease in the extent of irreversible termination reactions, and the growth rate is more constant growth when Cu(II) bromide was added. Reprinted with permission from Ref. [38] (*J. Poly. Sci.:Part A: Poly. Chem.* **2003**, *41*, 386; Copyright (2003) Wiley Interscience).

In the studies related to SI-ATRP of styrene, Matyaszweski et al. [34] demonstrate that polystyrene (PS) layer, when synthesized in presence of deactivating species, Cu(II) bromide, could be reinitiated with MMA to create surface-tethered polystyrene-*block*-poly(methyl methacrylate) and polystyrene-*block*-poly(t-butyl

acrylate) layers. However, the PS layers synthesized at same reaction conditions but without added Cu(II) bromide could not be chain-extended. Thus, preaddition of deactivating species is an effective strategy for not only reducing or eliminating irreversible termination reactions, but also for imparting or improving the reinitiation ability of the layers by preserving the active end groups.

This strategy of adding deactivating species has been used previously in SI-PMP by Otsu et al. [55] to grow surface-tethered multiblock copolymers from PS beads using SI-PMP. In that work they use tetraethylthiuram disulfide (TED) as the source of deactivating radicals. However, SI-PMP in presence of TED has not been used previously to synthesize multiblock copolymer layers from the flat surfaces. As discussed earlier, addition of deactivating species keeps the concentration of active free radicals low. Consequently, the concentration of added deactivating species becomes a critical parameter that affects the kinetics of SI-PMP. To the best of my knowledge, impact of added deactivating species on the kinetics of surface-tethered chain growth has not been investigated previously. Thus, it is necessary to understand the impact of monomer concentration, initial photoiniferter concentration, light intensity and concentration of deactivating species on layer growth kinetics and ability of to make block copolymers. This line of research on the impact of photopolymerization conditions on layer growth and reinitiation ability is crucial if one desires to precisely design surface-tethered multiblock copolymer layers.

1.4 Stimuli-Responsive Polymer Layers

As discussed in previous sections, tuning the interfacial properties of materials for particular applications demands special attention. One way to tune the material interface is to decorate it with the elements that can exhibit a controlled and predictable response under different conditions [66]. Further specialized applications may require the surface to have dual or conflicting properties: depending upon the environmental conditions, a given surface may be hydrophobic or hydrophilic, acidic or basic, conductive or nonconductive, adhesive or repellent, or be able to release or absorb some species. This requirement of adaptive properties requires surfaces to have the capability to undergo reversible changes in response to changes in environmental conditions. These surfaces are often referred to as the “smart” or “intelligent surfaces” [66].

One way to create smart surfaces is to graft responsive (macro)molecules to surfaces via chemical/physical treatment. Significant efforts have been made to prepare and characterize the responsive surface-attached polymer layers [66,67]. Depending upon the chemical nature, the responsive grafted polymer layers can respond to various stimuli such as pH, temperature, ionic strength, solvent quality, light, electric and magnetic fields [68,69]. Owing to these responsive capabilities, the smart surfaces are proposed as suitable platforms for chemical gates on membranes [11,12] or in microfluidic devices [13], vehicles for pulsatile/stealth drug delivery [70,71], biosensors [69,72] and molecular motors [73]. However, to-date besides the coatings synthesized by Xia et al. [74], the fabrication of the responsive coatings is limited to the ones that respond to only one stimulus at a time.

Of particular interest to me were polymer brushes of polyelectrolytes and thermoresponsive poly(*N*-isopropylacrylamide) PNIPAM. Polyelectrolytes have an array of technological applications: they are used as processing aids such as flocculants [75] and drag reduction agents [76]; as additives in detergents and cosmetics [77]; and in the fabrication of membranes [78], ion exchange resins, gels, and modified plastics. On the other hand, the temperature-dependent solubility change of PNIPAM can be exploited in a number of applications such as drug delivery [71,79], creation of non-fouling surfaces [80,81], and creation of artificial organs [82]. My interest in these two polymeric materials was particularly motivated because of applications in the area of drug delivery and biosensors.

The response characteristics of either polyacid or PNIPAM brushes have been studied thoroughly. Polyacids are long chain molecules with ionizable groups that can dissociate in water, yielding charged groups along the backbone. However, the degree of dissociation and, in turn, the charge along the backbone of polyacid chains is a function of the pH and/or ionic strength. As the net charge of the polyacid changes, there is a corresponding change in its hydrodynamic volume. The effect of pH, ionic strength and valency on the swelling of polyacids (especially weak polyacids) has been studied by various groups [83-89].

Increasing pH of the contacting solution increases degree of dissociation of carboxylate groups. Consequently, the concentration of charged groups along the polyacid chain and, in turn, the repulsive electrostatic forces increase stretching of the polyacid brush. The effect of ionic strength (or salt concentration) is more complex: depending upon whether the counterion concentration outside of the layer is greater or

less than that within the brush, the thickness of the polyacid layer may decrease or increase as a function of salt concentration. At low ionic strengths (often referred to as the “osmotic brush regime”), the concentration of counterions inside the brush is greater than the external salt concentration in solution. The osmotic pressure of the confined counterions causes the stretching of the brush. At high ionic strength (often referred to as the “salted brush regime”), the concentration of the counterions inside the brush is lower than the external salt concentration, which screens the electrostatic interactions between the chain segments resulting in the collapse of the polyacid brush.

PNIPAM is one of the most widely studied thermo-responsive polymers. In deionized water, it exhibits lower critical solution temperature (LCST) behavior. At ~32 ºC, PNIPAM undergoes a solubility change: at temperatures higher than 32 ºC, PNIPAM chains are well-solvated in water, whereas water is a poor solvent at temperatures below 32 ºC [90]. This sharp LCST of PNIPAM springs from its chemical nature. PNIPAM has a hydrophobic backbone, which carries a strong hydrophilic amide group ($–CONH_2$) substituted with a hydrophobic isopropyl group. While the amide group likes water due to its hydrogen-bonding ability with water molecules, the hydrophobic isopropyl groups tend to stay away from water. These counteracting, but temperature-dependent hydrophilic and hydrophobic interactions cause PNIPAM chains to exhibit LCST behavior in aqueous solutions.

Though the thermoresponsive behavior of PNIPAM coils and hydrogels in aqueous solution has been investigated extensively, the behavior of surface-grafted PNIPAM brushes to the changes in temperature has been studied only in recent years. Through surface plasmon resonance measurements, Lopez et al. [91] demonstrate that

PNIPAM brushes undergo solubility transition over a broad temperature range centered around 32 ºC. Through neutron reflectivity studies, Kent and coworkers similarly observe a broad transition of PNIPAM brushes. Additionally, Kent et al. [92] and Leckband et al. [93] investigated the effect of grafting density and molecular weight of PNIPAM chains on phase behavior. Their studies indicate that the molecular weight and grafting density of chains are critical parameters that influence the LCST behavior of PNIPAM brushes: the solubility transition of PNIPAM brushes is more pronounced at higher molecular weight and grafting density. Further investigations of the LCST behavior of PNIPAM brushes by Genzer et al. [94] indicate that the LCST decreases with increasing bulk salt concentration (ionic strength). Despite the fact that homo-PMAA and homo-PNIPAM brushes have been synthesized and characterized by several groups, merits of combining PMAA and PNIPAM in the form of block copolymers layers have not been explored to-date. These multicomponent layers can potentially respond to a suite of stimuli as compared to a layer that responds to only one stimulus at a time.

1.5 Major Research Objectives

In view of the previous discussions, the major objectives of the present work were to:

i) characterize the kinetics of SI-PMP through experimental studies and modeling;

ii) understand the irreversible termination mechanisms prevalent in SI-PMP;

iii) explore the possibility of improving the reinitiation ability of polymer layers formed using SI-PMP via preaddition of TED;

iv) explore the potential of SI-PMP for synthesizing PMAA-*block*-PNIPAM (PMAA-*b*-PNIPAM) layers; and

v) investigate the responsive characteristics of PMAA-*b*-PNIPAM layers to changes in pH, temperature and ionic strength.

In this dissertation, Chapter 2 is focused on understanding the irreversible termination mechanisms involved in SI-PMP (Objectives **i** and **ii**). As discussed earlier, preaddition of TED can overcome the problem of irreversible termination reaction. Chapters 3 and 4 discuss the impact of preaddition of TED and other photopolymerization conditions such as light intensity and initial photopolymerization conditions on kinetics of polymer layer growth and ability to make block copolymer layers (Objective **iii**). Strategies learned to make block copolymer layers in Chapter 3 and 4 are applied to synthesize block copolymer layers of PMAA and PNIPAM. Chapter 5 reports the synthesis and multiresponsive behavior of these PMAA-b-PNIPAM layers (Objectives **iv** and **v**). Finally Chapter 6 summarizes and concludes this thesis work with recommendations for future studies related to synthesis of stimuli-responsive polymer layers.

1.6 References

1. Milner, S. T. “Polymer Brushes”, *Science* **1991**, *251*, 905-914.

2. Zhao, B.; Brittain, W. J. “Polymer Brushes: Surface-Immobilized Macromolecules”, *Prog. Poly. Sci.* **2000**, *25*, 677-710.

3. Halperin, A.; Tirrell, M.; Lodge, T. P. “Tethered Chains in Polymer Microstructures”, *Adv. Poly. Sci.* **1992**, *100*, 31-71.

4. Currie, E. P. K.; Norde, W.; Cohen Stuart, M. A. “Tethered Polymer Chains: Surface Chemistry and Their Impact on Colloidal and Surface Properties”, *Adv. Colloid Interf. Sci.* **2003**, *100*, 205-265.

5. Raphaël, E.; de Gennes, P. G. “Rubber-Rubber Adhesion with Connector Molecules”, *J. Phys. Chem.* **1992**, *96*, 4002-4007.

6. Ji, H.; de Gennes, P. G. “Adhesion *via* Connector Molecules: The Many Stitch Problem”, *Macromolecules* **1993**, *26*, 520-525.

7. Tirrell, M.; Kokkoli, E.; Biesalski, M. “The Role of Surface Science in Bioengineered Materials”, *Surf. Sci.* **2002**, *500*, 61-83.

8. van Zanten, J. H. “Terminally Anchored Chain Interphases: Their Chromatographic Properties”, *Macromolecules* **1994**, *27*, 6797-6807.

9. Joanny, J.–F. “Lubrication by Molten Polymer Brushes”, *Langmuir* **1992**, *8*, 989-995.

10. Gupta, S. A.; Cochran, H. D.; Cummings, P. T. “Shear Behavior of Squalane and Tetracosane under Extreme Confinement. I. Model, Simulation Method, and Interfacial Slip”, *J. Chem. Phys.* **1997**, *107*, 10316-10326.

11. Ito, Y.; Ochiai, Y.; Park, Y. S.; Imanishi, Y. “pH-Sensitive Gating by Conformational Change of a Polypeptide Brush Grafted onto a Porous Polymer Membrane”, *J. Am. Chem. Soc.* **1997**, *119*, 1619-1623.

12. Zhang, H.; Ito, Y. “pH Control of Transport through a Porous Membrane Self-Assembled with a Poly(acrylic acid) Loop Brush”, *Langmuir* **2001**, *17*, 8336-8340.

13. Barker, S. L. R.; Ross, D.; Tarlov, M. J.; Gaitan, M.; Locascio, L. E. “Control of Flow Direction in Microfluidic Devices with Polyelectrolyte Multilayers”, *Anal. Chem.* **2000**, *72*, 5925-5929.

14. Edmondson, S.; Osborne, V. L.; Huck, W. T. S. "Polymer Brushes *via* Surface-Initiated Polymerizations", *Chem. Soc. Rev.* **2004**, *33*, 14-22.

15. Kilbey, S. M., II; Watanabe, H.; Tirrell, M. "Structure and Scaling of Polymer Brushes Near the Θ Condition", *Macromolecules* **2001**, *34*, 5249-5259.

16. Toomey, R.; Mays, J.; Tirrell, M. "*In-Situ* Thickness Determination of Adsorbed Layers of Poly(2-Vinylpyridine)-Polystyrene Diblock Copolymers by Ellipsometry", *Macromolecules* **2004**, *37*, 905-911.

17. Karim, A.; Satija, S. K.; Douglas, J. F.; Anker, J. F.; Fetters, L. J. **"**Neutron Reflectivity Study of the Density Profile of a Model End-Grafted Polymer Brush: Influence of Solvent Quality", *Phys. Rev. Lett*. **1994**, *73*, 3407-3410.

18. Kreer, T.; Müser, M. H.; Binder, K.; Klein, J. "Frictional Drag Mechanisms between Polymer-Bearing Surfaces", *Langmuir* **2001**, *17*, 7804-7813.

19. Lemieux, M.; Usov, D.; Minko, S.; Stamm, M.; Shulha, H.; Tsukruk, V. V. "Reorganization of Binary Polymer Brushes: Reversible Switching of Surface Microstructures and Nanomechanical Properties", *Macromolecules* **2003**, *36*, 7244-7255.

20. Munch, M. R.; Gast, A. P. "Kinetics of Block Copolymer Adsorption on Dielectric Surface from a Selective Solvent", *Macromolecules* **1990**, *23*, 2313-2320.

21. Dhinojwala, A.; Granick, S. "Surface Forces in the Tapping Mode: Solvent Permeability and Hydrodynamic Thickness of Adsorbed Polymer Brushes", *Macromolecules* **1997**, *30*, 1079-1085.

22. Tian, P.; Uhrig, D.; Mays, J.; Watanabe, H.; Kilbey, S. M., II "Role of Branching on the Structure of Polymer Brushes Formed from Comb Copolymers", *Macromolecules* **2005**, *38*, 2524-2529.

23. Alonzo, J.; Huang, Z.; Liu, M.; Mays, J. W.; Dadmun, M.; Kilbey, S. M., II "Looped Polymer Brushes Formed by Self-assembly of Poly(2-vinylpyridine)-Polystyrene-Poly(2-vinylpyridine) Triblock Copolymers at the Solid-Fluid Interface. Kinetics of Preferential Adsorption", *Macromolecules* **2006**, *39*, 8434-8439.

24. Karim, A.; Satija, S. K.; Douglas, J. F.; Anker, J. F.; Fetter, L. J. "Neutron Reflectivity Study of the Density Profile of a Model End-Grafted Polymer Brush: Influence of Solvent Quality", *Phys. Rev. Lett.* **1994**, *73*, 3407-3410.

25. Luzinov, I.; Julthongpiput, D.; Malz, H.; Pionteck, J.; Tsukruk, V. V. "Polystyrene Layers Grafted to Epoxy-Modified Silicon Surfaces", *Macromolecules* **2000**, *33*, 1043-1048.

26. Penn, L. S.; Hunter, T. F.; Lee, Y.; Quirk, R. P. “Grafting Rates of Amine-Functionalized Polystyrenes onto Epoxidized Silica Surfaces”, *Macromolecules* **2000**, *33*, 1105-1107.

27. Prucker, O.; Rühe, J. “Polymer Layers through Self-Assembled Monolayers of Initiators”, *Langmuir* **1998**, *14*, 6893-6898.

28. Prucker, O.; Rühe, J. “Synthesis of Poly(styrene) Monolayers Attached to High Surface Area Silica Gels through Self-Assembled Monolayers of Azo Initiators”, *Macromolecules* **1998**, *31*, 592-601.

29. Schmidt, R.; Zhao, T.; Green, J. B.; Dyer, D. J. “Photoinitiated Polymerization of Styrene from Self-Assembled Monolayers on Gold”, *Langmuir* **2002**, *18*, 1281-1287.

30. Paul, R.; Schmidt, R.; Dyer, D. J. “Synthesis of Ultrathin Films of Polyacrylonitrile by Photoinitiated Polymerization from Self-Assembled Monolayers on Gold”, *Langmuir* **2002**, *18*, 8719-8723.

31. Dyer, D. J. “Photoinitiated Synthesis of Grafted Polymers”, *Adv. Poly. Sci.* **2006**, *197*, 47-66.

32. Advincula, R. “Polymer Brushes by Anionic and Cationic Surface-Initiated Polymerization (SIP)”, *Adv. Poly. Sci.* **2006**, *197*, 107-136.

33. Ejaz, M.; Yamamoto, S.; Ohno, K.; Tsujii, Y.; Fukuda, T. “Controlled Graft Polymerization of Methyl Methacrylate on Silicon Substrate by the Combined Use of the Langmuir-Blodgett and Atom Transfer Radical Polymerization Techniques”, *Macromolecules* **1998**, *31*, 5934-5936.

34. Matyjaszewski, K.; Miller, P. J.; Shukla, N.; Immaraporn, B.; Gelman, A.; Luokala, B. B.; Siclovan, T. M.; Kickelbick, G.; Vallant, T.; Hoffmann, H.; Pakula, T. “Polymers at Interfaces: Using Atom Transfer Radical Polymerization in the Controlled Growth of Homopolymers and Block Copolymers from Silicon Surfaces in the Absence of Untethered Sacrificial Initiator”, *Macromolecules* **1999**, *32*, 8716-8724.

35. Zhao, B.; Brittain, W. J. “Synthesis, Characterization, and Properties of Tethered Polystyrene-*b*-Polyacrylate Brushes on Flat Silicate Substrates”, *Macromolecules* **2000**, *33*, 8813-8820.

36. Shah, R. R.; Merreceyes, D.; Husemann, M.; Rees, I.; Abbott, N. L.; Hawker, C. J.; Hedrick, J. L. “Using Atom Transfer Radical Polymerization to Amplify Monolayers of Initiators Patterned by Microcontact Printing into Polymer Brushes for Pattern Transfer”, *Macromolecules* **2000**, *33*, 597-605.

37. Ejaz, M.; Tsujii, Y.; Fukuda, T. “Controlled Grafting of a Well-defined Polymer on a Porous Glass Filter by Surface-Initiated Atom Transfer Radical Polymerization”, *Polymer* **2001**, *42,* 6811-6815.

38. Kim, J. B.; Huang, W.; Miller, M. D.; Baker, G. L.; Bruening, M. L. “Kinetics of Surface-Initiated Atom Transfer Radical Polymerization”, *J. Poly. Sci.:Part A: Poly. Chem.* **2003**, *41*, 386-394.

39. Boyes, S. G.; Granville, A. M.; Baum, M.; Akgun, B.; Mirous, B. K.; Brittain, W. J. “Polymer Brushes–Surface Immobilized Polymers”, *Surf. Sci.* **2004**, *570*, 1-12.

40. Husseman, M.; Malmström, E. E.; McNamara, M.; Mate, M.; Mecerreyes, D.; Benoit, D. G.; Hedrik, J. L.; Mansky, P.; Huang, E.; Russell, T. P.; Hawker, C. J. “Controlled Synthesis of Polymer Brushes by "Living" Free Radical Polymerization Techniques”, *Macromolecules* **1999**, *32*, 1424-1431.

41. Husemann, M.; Morrison, M.; Benoit, D.; Frommer, J.; Mate, C. M.; Hingsberg, W. D.; Hedrik, J. L.; Hawker, C. J. “Manipulation of Surface Properties by Patterning of Covalently Bound Polymer Brushes”, *J. Am. Chem. Soc.* **2000**, *122*, 1844-1845.

42. Bartholome, C.; Beyou, E.; Bourgeat-Lami, E.; Chaumont, P.; Zydowicz, N. “Nitroxide-Mediated Polymerizations from Silica Nanoparticle Surfaces: "Graft from" Polymerization of Styrene Using a Triethoxysilyl-Terminated Alkoxyamine Initiator”, *Macromolecules* **2003**, *36*, 7946-7952.

43. Tsujii, Y.; Ejaz, M.; Sato, K.; Goto, A.; Fukuda, T. “Mechanism and Kinetics of RAFT-Mediated Graft Polymerization of Styrene on a Solid Surface. 1. Experimental Evidence of Surface Radical Migration”, *Macromolecules* **2001**, *34,* 8872-8878.

44. Baum, M.; Brittain, W. J. “Synthesis of Polymer Brushes on Silicate Substrates Reversible Addition Fragmentation Chain Transfer Technique”, *Macromolecules* **2002**, *35*, 610-615.

45. Nakayama, Y.; Matsuda, T. “Surface Macromolecular Architectural Designs Using Photo-Graft Copolymerization Based on Photochemistry of Benzyl *N*,*N*-Diethyldithiocarbamate”, *Macromolecules* **1996**, *29*, 8622-8630.

46. Luo, N.; Metters, A. T.; Hutchison, J. B.; Bowman, C. N.; Anseth, K. S. “A Methacrylated Photoiniferter as a Chemical Basis for Microlithography: Micropatterning Based on Photografting Polymerization”, *Macromolecules* **2003**, *36*, 6739-6745.

47. Higashi, J.; Nakayama, Y.; Marchant, R. E.; Matsuda, T. " High-Spatioresolved Microarchitectural Surface Prepared by Photograft Copolymerization Using Dithiocarbamate: Surface Preparation and Cellular Responses", *Langmuir* **1999**, *15*, 2080-2088.

48. Kobayashi, T.; Takahashi, S.; Fujii, N. "Silane Coupling Agent Having Dithiocarbamate Group for Photografting of Sodium Styrene Sulfonate on Glass Surface", *J. App. Polym. Sci.* **1993**, *49*, 417-423.

49. de Boer, B.; Simon, H. K.; Werts, M. P. L.; van der Vegte, E. W.; Hadziioannou, G. ""Living" Free Radical Photopolymerization Initiated from Surface-Grafted Iniferter Monolayers", *Macromolecules* **2000**, *33*, 349-356.

50. Qin, S. H.; Qiu, K. Y. "A New Polymerizable Photoiniferter for Preparing Poly(methyl methacrylate) Macromonomer", *Eur. Poly. J.* **2001**, *37*, 711-717.

51. Nakayama, Y.; Matsuda, T. "*In-Situ* Observation of Dithiocarbamate-Based Surface Photograft Copolymerization Using Quartz Crystal Microbalance", *Macromolecules* **1999**, *32*, 5405-5410.

52. Otsu, T.; Yoshida, M.; Tazaki, T. "A Model for Living Radical Polymerization", *Macromol. Chem. Rapid Commun.* **1982**, *3*, 133-140.

53. Lambrinos, P.; Tardi, M.; Polton, A.; Sigwalt, P. "The Mechanism of the Polymerization of n-Butyl Acrylate Initiated with *N*,*N*-diethyl Dithiocarbamate Derivatives", *Eur. Polym. J.* **1990**, *26*, 1125-1135.

54. Kazmaier, P. M.; Moffat, K. A.; Georges, M. K.; Veregin, R. P. N.; Hamer, G. K. "Free-Radical Polymerization for Narrow-Polydispersity Resins. Semiempirical Molecular Orbital Calculations as a Criterion for Selecting Stable Free-Radical Reversible Terminators", *Macromolecules* **1995**, *28*, 1841-1846.

55. Otsu, T.; Ogawa, T.; Yamamoto, T. "Solid Phase Block Copolymer Synthesis by the Iniferter Technique", *Macromolecules* **1986**, *19*, 2087-2089.

56. Turner, S. R.; Blevins, R. W. "Photoinitiated Block Copolymer Formation Using Dithiocarbamate Fee Radical Chemistry", *Macromolecules* **1990**, *23*, 1856-1859.

57. Otsu, T.; Matsunaga, T.; Doi, T.; Matsumoto, A. "Features of Living Radical Polymerization of Vinyl Monomers in Homogeneous System Using *N*,*N*-diethyldithiocarbamate Derivatives as Photoiniferters", *Eur. Poly. J.* **1995**, *31*, 67-78.

58. Kannurpatti, A. R.; Lu, S.; Bunker, G. M.; Bowman, C. N. "Kinetic and Mechanistic Studies of Iniferter Photopolymerizations", *Macromolecules* **1996**, *29*, 7310-7315.

59. Ward, J. H.; Shahar, A.; Peppas, N. A. “Kinetics of ‘Living’ Radical Polymerizations of Multifunctional Monomer”, *Polymer* **2002**, *43*, 1745-1752.

60. Gopireddy, D.; Husson, S. M. “Room Temperature Growth of Surface-Confined Poly(acrylamide) from Self-Assembled Monolayers Using Atom Transfer Radical Polymerization”, *Macromolecules* **2002**, *35*, 4218-4221.

61. Xiao, D.; Wirth, M. J. “Kinetics of Surface-Initiated Atom Transfer Radical Polymerization of Acrylamide on Silica”, *Macromolecules* **2002**, *35*, 2919-2925.

62. Ejaz, M.; Ohno, K.; Tsujii, Y.; Fukuda, T. “Controlled Grafting of a Well-Defined Glycopolymer on a Solid Surface by Surface-Initiated Atom Transfer Radical Polymerization”, *Macromolecules* **2000**, *33*, 2870-2874.

63. Jeyaprakash, J. D.; Samuel, S.; Dhamodharan, R.; Rühe, J. “Polymer Brushes *via* ATRP: Role of Activator and Deactivator in the Surface-Initiated ATRP of Styrene on Planar Substrates”, *Macromol. Rapid. Commun.* **2002**, *23*, 277-281.

64. Huang, X.; Wirth, M. J. “Surface Initiation of Living Radical Polymerization for Growth of Tethered Chains of Low Polydispersity”, *Macromolecules* **1999**, *32*, 1694-1696.

65. Kim, J. B.; Huang, W.; Miller, M. D.; Baker, G. L.; Bruening, M. L. “Synthesis of Triblock Copolymer Brushes by Surface-Initiated Atom Transfer Radical Polymerization”, *Macromolecules* **2002**, *35*, 5410-5416.

66. Luzinov, I.; Minko, S.; Tsukruk, V. V. “Adaptive and Responsive Surfaces through Controlled Reorganization of Interfacial Polymer Layers”, *Prog. Poly. Sci.* **2004**, *29*, 635-698.

67. Russell, T. P. “Surface-responsive Materials”, *Science* 2002, 297, 964-967.

68. Gil, E. S.; Hudson, S. M. “Stimuli-responsive Polymers and their Bioconjugates”, *Prog. Poly. Sci.* **2004**, *29*, 1173-1222.

69. Roy, I.; Gupta, M. N. “Smart Polymeric Materials: Emerging Biochemical Applications”, *Chem. Biol.* **2003**, *10*, 1161-1171.

70. Kikuchi, A.; Okano, T. “Pulsatile Drug Release Control Using Hydrogels”, *Adv. Drug Delivery Rev.* **2002**, *54*, 53-77.

71. Kost, J.; Langer, R. “Responsive Polymeric Delivery Systems”, *Adv. Drug Delivery Rev.* **2001**, *46*, 125-148.

72. Yang, C. C.; Tian, Y.; Jen, A. K.-Y.; Chen, W. C. "New Environmentally Responsive Fluorescent *N*-isopropylacrylamide Copolymer and Its Application to DNA Sensing", *J. Polym. Sci., Part A.: Polym. Chem*. **2006**, *44*, 5495-5504.

73. Santer, S.; Rühe, J. "Motion of Nano-Objects on Polymer Brushes", *Polymer* **2004**, *45*, 8279-8297.

74. Xia, F.; Feng, L. Wang, S.; Sun, T.; Song, W.; Jiang, W.; Jiang, L. "Dual-Responsive Surfaces that Switch between Superhydrophilicity and Superhydrophobicity", *Adv. Mater.* **2006**, *18*, 432-436.

75. Reis, E. A.; Caraschi, J. C.; Carmona-Ribeiro, A. M.; Petri, D. F. "Polyelectrolytes at Charged Particles: Particle Number Density, Molecular Weight, and Charge Ratio Effects", *J. Phys. Chem. B* **2003**, *107*, 7993-7997.

76. Ohsedo, Y.; Takashina, R.; Gong, J. P.; Osada, Y. "Surface Friction of Hydrogels with Well-defined Polyelectrolyte Brushes", *Langmuir* **2004**, *20*, 6549-6555.

77. Noble, P. F.; Cayre, O. J.; Alargova, R. G.; Velev, O. D.; Paunov, V. N. "Fabrication of "Hairy" Colloidosomes with Shells of Polymeric Microrods", *J. Am. Chem. Soc.* **2004**, *126*, 8092-8093.

78. Ding, J.; Chuy, C.; Holdcroft, S. "A Self-organized Network of Nanochannels Enhances Ion Conductivity through Polymer Films", *Chem. Mater.* **2001**, *13*, 2231-2233.

79. Neradovic, D.; Hinrichs, W. L. J.; Kettenes-van den Bosch, J. J.; van Nostrum, W. E.; Hennink, W. E. "Poly(*N*-isopropylacrylamide) with Hydrolyzable Lactic Acid Ester Side Groups: A New Type of Thermosensitive Polymer Suitable for Drug Delivery Purposes", *J. Controlled Release* **2001**, *72*, 252-253.

80. Yamada, N.; Okano, T.; Sakai, H.; Karikusa, F.; Sawasaki, Y.; Sakurai, Y. "Thermo-responsive Polymeric Surfaces; Control of Attachment and Detachment of Cultured Cells", *Makromol. Chem. Rapid Commun.* **1990**, *11*, 571-576.

81. Cunliffe, D.; Alarcón, C. D.; Peters, V.; Smith, J. R.; Alexander, C. "Thermoresponsive Surface-Grafted Poly(*N*-isopropylacrylamide) Copolymers: Effect of Phase Transitions on Protein and Bacterial Attachment", *Langmuir* **2003**, *19*, 2888-2899.

82. Angelova, N.; Hunkeler, D. "Rationalizing the Design of Polymeric Biomaterials", *Trends Biotechnol.* **1999**, *17*, 409-421.

83. Rühe, J.; Ballauff, M.; Biesalski, M.; Dziezok, P.; Grohn, F.; Johannsmann, D.; Houbenov, N.; Hugenberg, N.; Konradi, R.; Minko, S.; Motornov, M.; Netz, R. R.; Schmidt, M.; Seidel, C.; Stamm, M.; Stephan, T.; Usov, D.; Zhang, H. "Polyelectrolyte Brushes", *Adv. Poly. Sci*. **2004**, *165*, 79-150.

84. Biesalski, M.; Johannsmann, D.; Rühe, J. "Synthesis and Swelling Behavior of a Weak Polyacid Brush", *J. Chem. Phys.* **2002**, *117*, 4988-4994.

85. Konradi, R.; Rühe, J. "Binding of Oppositely Charged Surfactants to Poly(methacrylic acid) Brushes", *Macromolecules* **2005**, *38*, 6140-6151.

86. Ayres, N.; Boyes, S. G.; Brittain, W. J. "Stimuli-Responsive Polyelectrolyte Polymer Brushes Prepared *via* Atom-Transfer Radical Polymerization", *Langmuir* **2007**, *23*, 182-189.

87. Biesalski, M.; Johannsmann, D.; Rühe, J. "Electrolyte-induced Collapse of a Polyelectrolyte Brush", *J. Chem. Phys.* **2004**, *120*, 8807-8814.

88. Zhang, H. N.; Rühe, J. "Swelling of Poly(methacrylic acid) Brushes: Influence of Monovalent Salts in the Environment", *Macromolecules* **2005**, *38*, 4855-4860.

89. Currie, E. P. K.; Sieval, A. B.; Fleer, G. J.; Cohen Stuart, M. A. "Polyacrylic Acid Brushes: Surface Pressure and Salt-Induced Swelling", *Langmuir* **2000**, *16*, 8324-8333.

90. Dhara, D.; Chatterji, P. R. "Phase Transition in Linear and Cross-Linked Poly(*N*-Isopropylacrylamide) in Water: Effect of Various Types of Additives", *J. Macromol. Sci.: Rev. Macromol. Chem. Phys*. **2000**, *40*, 51-68.

91. Balamurugan, S.; Mendez, S.; Balamurugan, S. S.; O'Brien, M. J., II, Lopez, G. P. "Thermal Response of Poly(*N*-isopropylacrylamide) Brushes Probed by Surface Plasmon Resonance", *Langmuir* **2003**, *19*, 2545-2549.

92. Yim, H.; Kent, M. S.; Mendez, S.; Balamurugan, S. S.; Balamurugan, S.; Lopez, G. P.; Satija, S. "Temperature-Dependent Conformational Change of PNIPAM Grafted Chains at High Surface Density in Water", *Macromolecules* **2004**, *37*, 1994-1997.

93. Plunkett, K. N.; Zhu, X.; Moore, J. S.; Leckband, D. E. " PNIPAM Chain Collapse Depends on the Molecular Weight and Grafting Density", *Langmuir* **2006**, *22*, 4259-4166.

94. Jhon, Y. K.; Bhat, R. R.; Jeong, C.; Rojas, O. J.; Szleifer, I.; Genzer, J. "Salt-Induced Depression of Lower Critical Solution Temperature in a Surface-Grafted Neutral Thermoresponsive Polymer", *Macromol. Rapid Commun*. **2006**, *27*, 697-701.

CHAPTER 2

KINETICS OF SURFACE-INITIATED PHOTOINIFERTER-MEDIATED PHOTOPOLYMERIZATION

[As published in *Macromolecules* **2005**, *38*, 8202-8210 with minor changes]

Surface-tethered poly(methyl methacrylate) films were synthesized by surface-initiated photoiniferter-mediated photopolymerization (SI-PMP), and the kinetics of film growth were followed by measuring layer thickness as a function of reaction time, monomer concentration, and light intensity using variable angle ellipsometry. The initial rate of photopolymerization had approximate first-order dependence on monomer concentration. However, the rate of photopolymerization decreased with reaction time, indicating the presence of termination reactions. To determine which termination reactions are prevalent, kinetic models accounting for bimolecular termination as well as chain transfer to monomer were developed for the photoiniferter-mediated photopolymerization reactions and used to analyze the experimental data. Comparisons of model predictions to experimental data as functions of reaction time and light intensity suggest that bimolecular termination is the dominant termination mechanism in these systems for the range of reaction conditions investigated.

2.1 Introduction

Interfacial properties such as biocompatibility, wettability, corrosion resistance, and friction can be controlled by modifying a surface with polymeric materials. Owing to these capabilities, surface modification can be employed in the fields of food packaging, microelectronics, lithography, and biomaterials. Many applications in these fields require the surface to have specific structure and properties. As an example, the surface chemistry [1], hydrophobicity [2], or topography [3] of traditional biomaterials are often modified with polymers to direct cellular adhesion and growth. Frequently used methods of modifying surfaces with polymers are classified as either "grafting to" or "grafting from" approaches.

In grafting to, premade chains are tethered to the surface either by physisorption or via chemical bond formation between reactive groups on a surface and reactive end groups of polymer chains [4-9]. This approach is often preferred for fundamental studies because the chain size, composition, and architecture can be rigorously controlled and characterized prior to assembly. However, it is difficult to achieve high grafting densities [10] with grafting to approaches because as the layer assembles it becomes more efficient at preventing subsequent chains from diffusing through the layer and reaching the tethering surface [6]. Also, layers made by physisorption can be disengaged from the surface if the solvent condition that enabled layer formation is reversed.

The "grafting from" technique, which involves growing chains from a surface, overcomes limitations of the grafting to approach. In this technique, initiators are immobilized onto the substrate and surface-initiated polymerization is used to generate

surface-tethered polymer chains. A variety of polymerization methods, including thermally [11,12] and photoinitiated [13,14] free-radical polymerizations and "living" free-radical polymerization techniques, such as atom transfer radical polymerization (ATRP) [15-21], nitroxide-mediated free-radical polymerization [22-24], and reversible addition fragmentation transfer (RAFT) [25,26], have been used to produce surface-tethered polymer layers using the "grafting from" approach. In the current work, we used a "living" free-radical photopolymerization technique based on a dithiocarbamate photoiniferter chemistry first discovered by Otsu et al. [27] to produce surface-tethered poly(methyl methacrylate) layers. Photoiniferter-mediated polymerizations are advantageous because they enable spatial and temporal control over polymerization by controlling the location, intensity, and duration of light exposure. Hence, compared to other living free-radical polymerization techniques, photoiniferter-mediated polymerizations can be used readily for micropatterning surfaces with grafted polymer chains of defined thickness [28-30].

Photoiniferters are usually dithiocarbamate derivatives that can initiate, terminate, and act as transfer agents during the polymerization [27]. The UV photolysis of a photoiniferter yields a carbon radical and a dithiocarbamyl radical. The carbon radical can react with vinyl monomer to initiate radical polymerization and then propagate by addition of more monomer. The dithiocarbamyl radical is stable and reacts weakly or not at all with vinyl monomers [31,32]. Instead, it acts as a transfer agent or terminates the growing chain reversibly by reacting with propagating polymer chains [31]. This reversible capping allows dithiocarbamate derivatives to be used as living free radical initiators. Otsu et al. [33] confirmed the living nature of photoiniferter polymerizations in

bulk and in solution, and studied the effect of different reaction conditions on the polymerization rate.

More recent kinetic studies of photoiniferter-mediated photopolymerizations of mono- and multifunctional methacrylates in bulk performed by Kannurpatti et al. [34] and Ward et al. [35] confirmed the previously observed living-radical reaction mechanism [31,32]. Kannurpatti et al. [34] and Ward et al. [35] also observed that the normal autoacceleration effect seen in polymerizations of highly crosslinked systems initiated by conventional initiators can be reduced or eliminated by using iniferters. However, the situation of surface-initiated photopolymerization is quite different from bulk or solution polymerizations and the kinetic behaviors need to be studied separately.

Several groups [28,29,36-40] have used photoiniferter-mediated photopolymerizations from surface-immobilized photoiniferters to modify surface properties of various organic and inorganic substrates. Luo et al. [29] studied the photopolymerization of poly(ethylene glycol) monomethacrylate from a dithiocarbamate-functionalized polymer substrate. A significant amount of gelation was observed in this system, presumably due to significant chain transfer to the poly(ethylene glycol) monomethacrylate macromer. Therefore, polymer layer growth in this system resulted not only from propagation of surface-tethered polymer chains but also from crosslinking between surface-tethered chains and polymer chains or networks in the bulk.

A study to confirm the living nature of surface-initiated photoiniferter-mediated photopolymerization (SI-PMP) was carried out by Nakayama et al. [28] in which dithiocarbamate-modified polystyrene films were used as the substrate. Micropatterned surfaces were obtained by graft-copolymerization of styrene using a lattice-patterned

projection mask. The thickness of the polystyrene graft was estimated by measuring the height difference between the graft-copolymerized and nontreated surface. A linear dependence of dry polymer layer thickness on exposure time was observed, and they attributed this pattern of behavior as suggesting living radical polymerization. However, these measurements were made only during the early stages of polymerization.

de Boer et al. [38] also studied the kinetics of photoiniferter-mediated photopolymerizations from glass and silicon substrates. Micropatterned polystyrene layers were synthesized and thicknesses of the polymer layers were estimated by measuring the height differences between polymerized and unpolymerized regions of the same substrate using atomic force microscopy (AFM). The authors also observed a linear increase in the measured thickness of the dried polystyrene films with polymerization time.

To date, detailed kinetic studies of SI-PMP as a function of reaction conditions such as monomer concentration and light intensity have only been conducted by Nakayama et al. [40]. Their study of dithiocarbamate-based surface photograft copolymerization of various vinyl monomers, including acrylamides and acrylates, using quartz crystal microbalance (QCM) measurements revealed a linear increase in the rate of polymerization with monomer concentration and intensity. However, this study was again limited to short exposure times.

The question of how surface-initiated photoiniferter-mediated photo-polymerizations behave over long reaction times and at various intensities remains unresolved. Yet this question is extremely important if one wishes to fully understand how to utilize photoiniferter-mediated photopolymerizations to design surface-tethered

polymer layers. It is therefore essential to investigate whether the system retains its "living" characteristics at longer times. It should be emphasized that a linear increase in the polymer layer thickness does not necessarily indicate that the polymerization is living. Previously, it has been shown that surface-initiated polymerizations via thermally initiated, free-radical polymerization can also lead to linear growth of polymer films [11]. By definition, living radical polymerizations are those in which the molar mass of polymer chains increases linearly with polymerization time because the irreversible termination reactions are absent. Living radical polymerizations initiated from flat substrates often show "pseudo-living" characteristics. These pseudo-living characteristics arise due to the loss of radicals by various termination reactions that occur in the absence of a sufficient concentration of persistent deactivating radicals, and often, the effect of losing radicals does not manifest until longer times. Such a phenomenon has been observed by various groups [16,20,41,42] in their studies of surface-initiated ATRP.

To fully understand the kinetic behavior of SI-PMP, I have studied the effect of reaction time, monomer concentration, and light intensity on the polymerization rate and thickness of surface-tethered poly(methyl methacrylate) (PMMA) layers. Kinetic models that explore the impact of different termination reactions on the growth of surface-tethered polymer layers were developed and used to analyze the experimental results to determine which termination mechanisms are significant.

2.2 Experimental

Materials. Sodium diethyldithiocarbamate (Fluka, 97%) was recrystallized from methanol (Fisher Scientific, 99.9%), and *p*-chlorotrimethoxysilane (Gelest Inc., 95%) was used as received. Methyl methacrylate (MMA, Aldrich, 99%) was dehibited by washing with sodium hydroxide (Alfa Aesar, 97%) solution and water and then distilled under vacuum from CaH_2 (Aldrich, 90-95%) prior to use. Anhydrous toluene (Alfa Aesar, 99.8%) and anhydrous tetrahydrofuran (Acros, 99.9%) were used as received. Sulfuric acid (EMD Chemicals Inc., 95-98%) and hydrogen peroxide (Sigma, 30% v/v in water) were also used as received.

Synthesis of the Photoiniferter, *N,N*-(Diethylamino)dithiocarbamoylbenzyl-(trimethoxy)silane (SBDC). SBDC was synthesized and purified by a previously developed protocol [38]; the synthesis scheme and procedure is described in Appendix A. The final product, SBDC, was confirmed with ^{1}H NMR spectroscopy performed using a Bruker AC300 Fourier transform NMR spectrometer. ^{1}H NMR (300 MHz, $CDCl_3$): δ_H 7.68-7.48 (dd, 4H, C_6H_4), 4.62 (s, 2H, CH_2S), 4.13 (q, 2H, NCH_2), 3.83 (q, 2H, NCH_2), 3.70 (s, 9H, $Si(OCH_3)_3$), 1.35 (t, 6H, CH_3).

Formation of Self-Assembled Monolayers (SAMs) of Photoiniferter on Silicon Wafers. Silicon wafers of size 1 cm × 1.2 cm were cleaned by treating with freshly made piranha solution (H_2SO_4:H_2O_2 (30%); 3:1) for 30-45 min at room temperature. The surfaces were then washed with copious amounts of water. *Caution! Piranha solution should be handled with extreme care, as it reacts violently with most organic materials. Do not store piranha solution in a closed vessel*. These freshly

pretreated wafers were dried with a stream of dry nitrogen and placed individually in oven-dried test tubes. Each test tube containing a silicon wafer was flame-dried. A 2 mM deposition solution comprising 30 μL of SBDC in 48 mL of anhydrous toluene was prepared in a separate cleaned, dry flask. Aliquots (4 mL) of the deposition solution were transferred to each flame-dried test tube containing a silicon wafer, and depositions were allowed to proceed for ~12 h at room temperature under a nitrogen blanket. After the deposition period, the SAM-covered silicon wafers were rinsed and sonicated in pure toluene and dried with a stream of N_2.

Photopolymerization. MMA solutions (5 mL) in anhydrous toluene were prepared in air-free Schlenk tubes. The concentrations used were 1.17, 2.34, and 4.68 M, which correspond to 12.5, 25, and 50% v/v, respectively. The monomer solution was degassed by 4-5 freeze-pump-thaw cycles. Up to four SAM-modified silicon wafers were placed in a reaction cell made of Teflon. The volume of the cell is ~4 mL. The cell was covered with a soda lime glass plate and sealed using a screw-tightened clamping ring that seals the glass against a seated O-ring. The degassed monomer solution was then transferred *via* syringe to the reaction cell containing the SAM-modified silicon wafers. The assembly of the reaction cell and transfer of degassed monomer solution were all carried out in a glovebox where the oxygen level was kept below 1 ppm. The assembled reaction cell was removed from the glovebox and then exposed to collimated 365 nm light (EXFO 100WActicure ultraviolet/visible spot-curing system with 365 nm optical filter) at fixed intensities. The light intensity was measured at 365 nm with a radiometer (OAI 306 UV powermeter). After photopolymerization, the PMMA-modified silicon wafers were sonicated in toluene for 30-45 min to remove any nonbonded polymer. To

ensure that there were no nonbonded PMMA chains entangled within the grafted polymer layer, the polymer-modified silicon wafers were extracted in a Soxhlet extraction apparatus with toluene as the solvent for 24 h (~100 extraction cycles). There was no significant change in ellipsometric thickness of the PMMA layers measured before and after extraction. Therefore, it was concluded that sonication for 30-45 min was sufficient to remove any nonbonded polymer chains.

Characterization. The formation of the SBDC SAMs was confirmed by measuring the ellipsometric thickness using a Beaglehole Instruments phase-modulated Picometer™ ellipsometer that employs a photoelastic birefringence modulator to modulate the polarization of the incident light beam. A single wavelength (λ = 632.8 nm) laser beam was used as a probe, and the ellipsometric angles ψ and Δ were measured by changing the angle of incidence from 80° to 35°. The ellipsometric angles as a function of incident angle were fitted using a Cauchy model (Igor Pro. software package) to determine the thickness. A refractive index of 1.45 was assigned to the SAM. Thickness measurements were taken at five different points on every sample. The SAMs were also characterized by measuring static water contact angle. These measurements were performed using a Krüss DSA10-static contact angle instrument. At least three measurements were taken per sample at room temperature.

The PMMA layers were characterized by transmission-Fourier transform infrared spectroscopy (transmission-FTIR), ellipsometry, and contact angle goniometry. Transmission-FTIR experiments were performed using a Nicolet Nexus 870 FTIR spectrometer equipped with a Nicolet-OMNI transmission accessory and liquid nitrogen cooled MCT-A detector. A Whatman laboratory gas generator (model 75-45) was used to

purge the sample compartment with dry, CO_2-free air. A total of 2000 scans were collected for the absorbance spectra at a resolution of 8 cm^{-1}. For PMMA layer thickness calculations, the refractive index of PMMA was taken to be 1.48.

2.3 Results and Discussion

Characterization of Photoiniferter SAM. The formation of self-assembled monolayers of SBDC was confirmed using variable angle ellipsometry and contact angle goniometry. The thickness of the SAM was found to be 1.4 ± 0.2 nm, and the static water contact angle was measured to be 64 ± 3°. Thickness values were consistent with previously observed values [38] and values predicted by bond length calculations (1.3 nm). The values for static water contact angle for SAMs of SBDC have not been previously reported.

Growth of Poly(methyl methacrylate) (PMMA) Layers. Figure 2.1 shows the idealized process for the formation of a tethered PMMA chain by SI-PMP of MMA. Several such chains grow simultaneously along the surface to form a surface-tethered PMMA brush. The growth rate of the PMMA brush depends on various parameters such as monomer concentration and light intensity. The presence of the PMMA layer was confirmed by transmission-FTIR spectroscopy. Figure 2.2 shows the infrared spectrum for a representative surface-tethered PMMA layer: peaks at 1730 and 2990 cm^{-1} correspond to the carbonyl group (C=O) of methacrylate ester and asymmetric C-H stretching (C-CH_3), respectively. The peak at 1490 cm^{-1} is due to C-CH_3 deformation.

Static water contact angles of PMMA layers were measured to be 76 ± 5°, which is consistent with previously reported value of 80° [43].

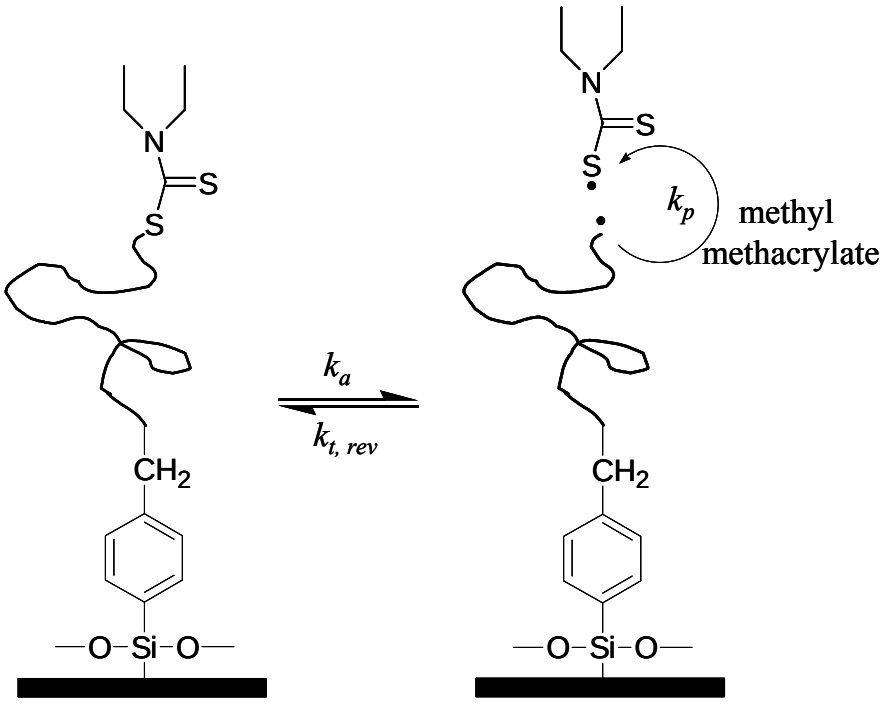

Figure 2.1 Idealized scheme for the growth of surface-tethered PMMA by surface-initiated photoiniferter-mediated photopolymerization of MMA to form a tethered PMMA chain. The stable DTC radical reversibly terminates the active carbon radical to produce the dormant species. The surface-bound carbon radical, when active, propagates by the addition of monomer to form a polymer chain. Several densely packed chains grow simultaneously to form a surface-tethered polymer layer.

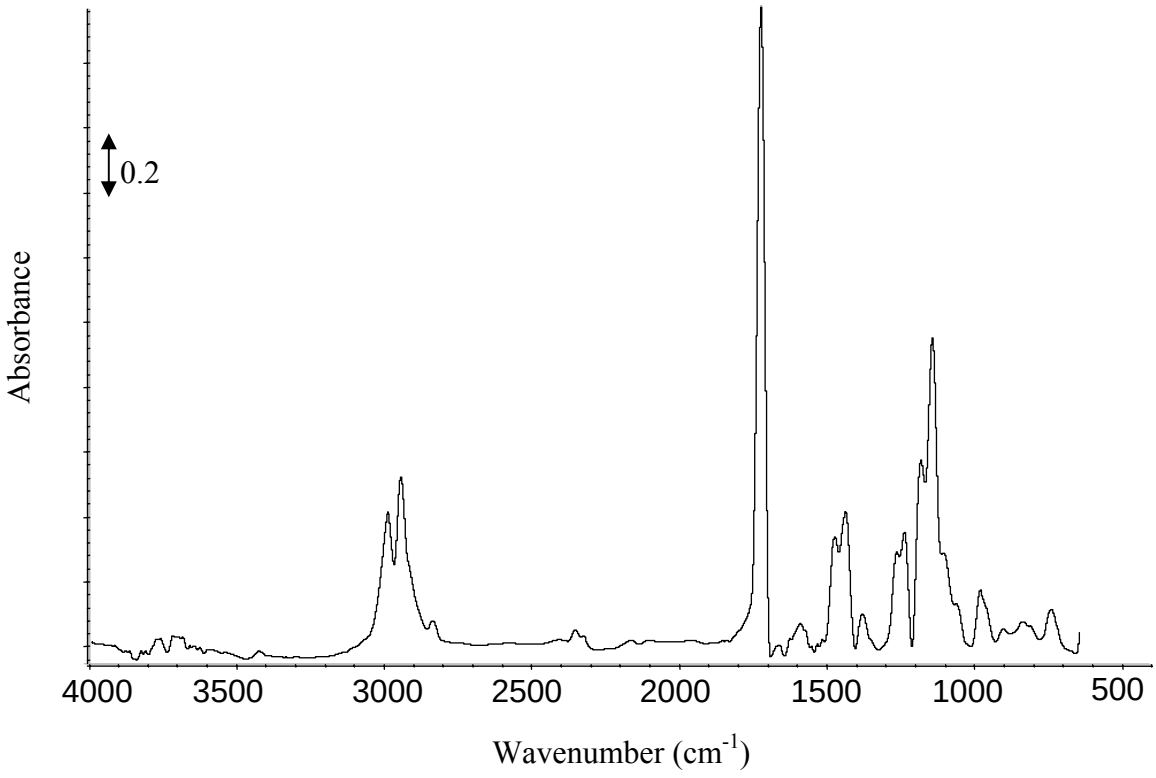

Figure 2.2 Transmission-Fourier transform infrared spectrum of poly(methyl methacrylate) layer. The sample layer thickness was 153 nm.

Kinetic Analysis of Polymer Layer Growth. Before analyzing experimental results of kinetic studies, it is first instructive to examine the kinetic model for surface-initiated chain growth *via* a reversible, light-mediated radical capping mechanism. The rate of SI-PMP should be proportional to the monomer concentration and the concentration of surface-attached free radicals, as shown in eq 1.

$$R_p = k_p[STR\bullet][M] \tag{1}$$

In this equation, R_p is the rate of polymerization, k_p is the propagation rate constant, [*M*] is the monomer (here, MMA) concentration, and $[STR\bullet]$ is the concentration of surface-tethered radicals. Because the rate of photopolymerization is proportional to the rate of increase in molecular weight of surface-tethered polymer chains [44] eq 1 can be recast as

$$\frac{d(MW)}{dt} = k_1 k_p [STR\bullet][M] \tag{2}$$

where *t* is the polymerization time, *MW* is the molecular weight of a polymer chain, and k_1 is a proportionality constant between the rate of polymerization and the rate of increase in the chain molecular weight. Furthermore, in the "brush" regime, the polymer layer thickness scales linearly with molecular weight of a chain [45]. Therefore, eq 2 can be rewritten as

$$\frac{dT}{dt} = k[STR\bullet][M] \tag{3}$$

where the constant $k = k_1 k_2 k_p$, T is the ellipsometric thickness of the dry polymer layer, and k_2 is a proportionality constant that relates the molecular weight of a polymer chain in the brush regime to its observed thickness.

Photoiniferter-mediated photopolymerization is described as a living-radical polymerization [27,33,35,38,39,46]. For a living-radical polymerization, irreversible termination reactions that decrease active free-radical concentration are absent so that the

concentration of free radicals remains constant during the course of polymerization [44]. Additionally, in the case of surface-initiated polymerizations, the concentration of monomer remains constant because of low monomer conversion, which can be attributed to the fact that a very low number of initiator molecules ($<10^{15}/cm^2$) are present on the surface to initiate polymerization [41]. Therefore, according to eqs 2 and 3, the absence of termination reactions should produce a constant rate of polymerization as well as a linear increase in molecular weight and thickness of a grafted polymer layer with polymerization time.

Figure 2.3 shows how the measured dry layer thicknesses of grafted PMMA layers vary with polymerization time for three different monomer concentrations. The data show a slow initial increase in thickness followed by a rapid increase. Since all polymerization inhibitors have been previously removed from the system (discussed in Appendix C) and because it is known that when this photoiniferter is used for polymerizations in bulk solution the molar mass of the polymer chains increases with polymerization time [47], these two regimes of kinetic behavior are attributed to the configurations of the surface-tethered chains. At early times, when the thickness is increasing slowly, we hypothesize that the chains, due to their small molecular weights, are in the "mushroom" regime. As the chains continue to grow, they begin to interact with one another and transition from the coiled "mushroom" regime to the extended "brush" regime [48,49]. Another possible reason behind the initial lag period could be an autoacceleration effect, in which surface-tethered radicals terminate predominantly as compared to initiating polymer chains (within the initial lag period) due to close proximity, followed by a situation where PMMA layer grows fast because the surface-

tethered radicals are far apart to terminate. The possibility of this situation of autoacceleration is discussed in Appendix D in detail.

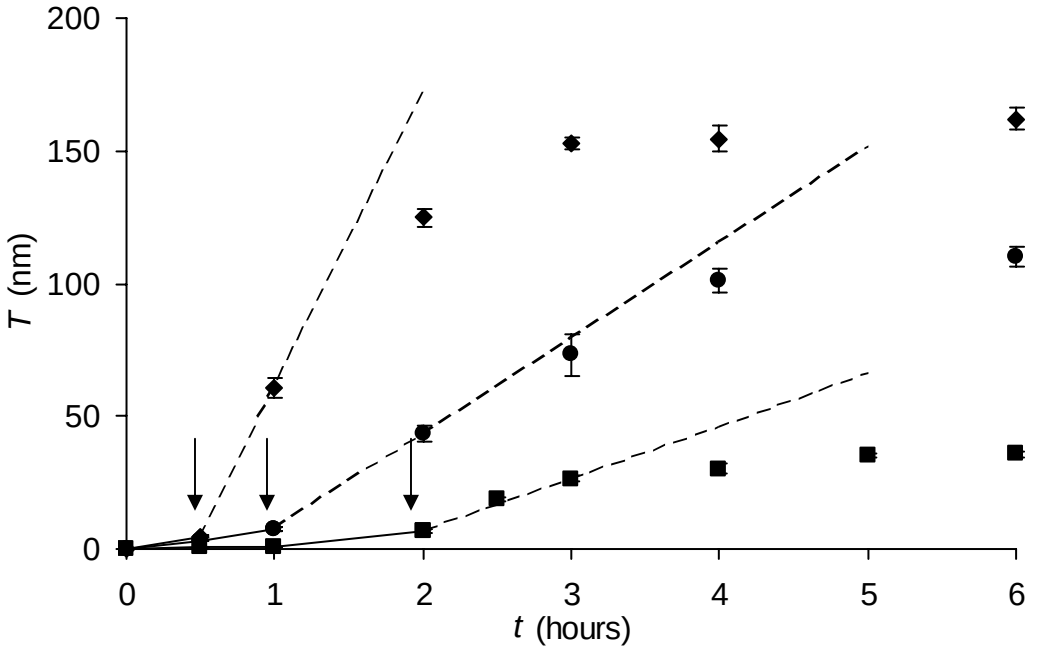

Figure 2.3 Dry poly(methyl methacrylate) layer thickness as a function of exposure time at a light intensity of 5mW/cm^2. Methyl methacrylate concentrations in toluene are (■) 1.17, (●) 2.34, and (♦) 4.68 M. Arrows indicate the apparent mushroom-to-brush transition for the concentrations studied, and the dotted lines show the behavior of an idealized living photopolymerization. The slopes of these lines also represent the initial growth rates of the PMMA layer.

The apparent transition for each monomer concentration is marked by an arrow in Figure 2.3. The polymerization time at which the transition occurs, t_{brush}, decreases as monomer concentration (and therefore R_p) increases. The PMMA layer thicknesses at this transition are consistently observed to be between 4 and 6 nm. The rate of growth of the PMMA layer once it enters the brush regime can be used to test the dependence of the

photopolymerization rate on monomer concentration. Shown in Figure 2.4, the initial growth rates, defined by the slopes of the dashed lines in Figure 2.3, display a nearly first-order (1.25 ± 0.20) dependence on monomer concentration. Considering that the discrete data give rise to imprecision in identifying the exact location of the mushroom-to-brush transition, the agreement between the data and the model (eq 3) is quite good and confirms that the reaction rate is approximately first-order with respect to monomer concentration in the brush regime.

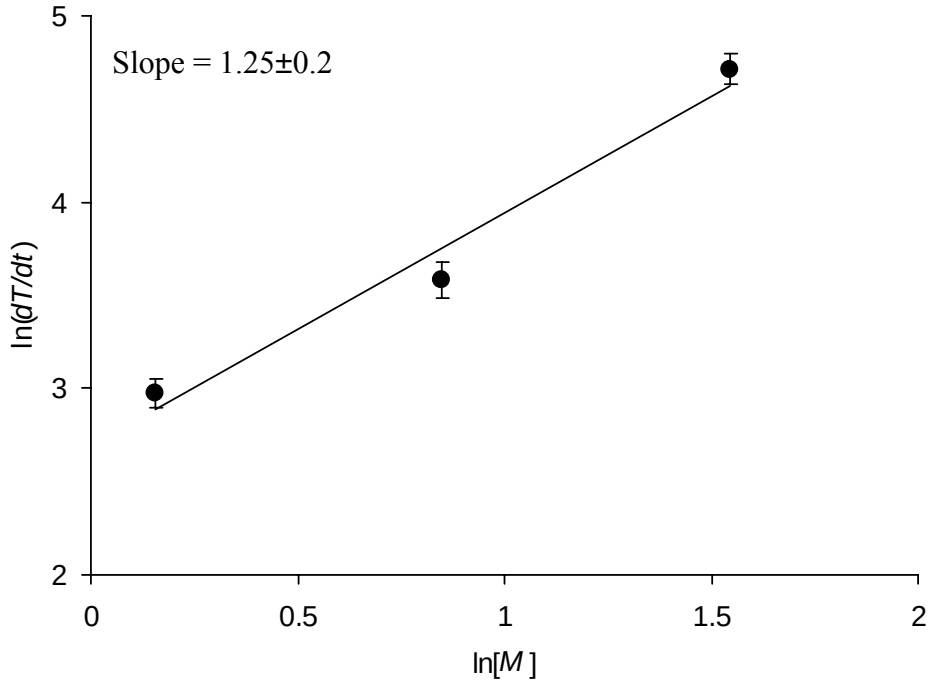

Figure 2.4 Rate of growth of PMMA layer as a function of monomer concentration at irradiation intensity of 5 mW/cm^2.

As can be seen from Figure 2.3, the growth of the PMMA layer in the brush regime is nonlinear with exposure time, indicating that SI-PMP of MMA under the described conditions does not proceed via a living free radical polymerization mechanism. As argued for surface-initiated ATRP systems exhibiting pseudo-living behavior [16,41,42], the observed pseudo-living nature of SI-PMP of MMA at the current reaction conditions most likely stems from the fact that very few initiator molecules are present on the surface to produce a sufficient concentration of deactivating dithiocarbamyl radicals in solution that reversibly terminate the surface-tethered radicals. In the absence of sufficient deactivator to establish and keep the equilibrium depicted in Figure 2.1 shifted toward the "dormant" species, irreversible termination reactions such as bimolecular termination or chain transfer of the radical from the surface will occur to a significant extent.

Consequently, in consideration of eq 3, a continuous decrease in $[STR\bullet]$ leads to a continuous decrease in the growth rate, as manifest in the decreasing rate of change in layer thickness with time during photopolymerization. This behavior also has been seen in studies of brush formation by surface-confined ATRP, and bimolecular termination has been identified as the primary cause of the decreasing growth rate (nonliving character) [16,20,41]. In the case of SI-PMP, possible reasons for the permanent loss of surface-tethered radicals include (a) bimolecular termination, (b) chain transfer to monomer, (c) chain transfer to dithiocarbamyl radical, (d) chain transfer to an adjacent polymer chain, and (e) chain transfer to solvent.

Kinetic Analysis of Termination Mechanisms. To provide insight into the mechanisms responsible for loss of surface-tethered radicals in SI-PMP, we begin by writing a general expression (eq 4) for the rate of decrease in surface-attached radical concentration.

$$-\frac{d[STR\bullet]}{dt} = -k_a[STR-DTC] + k_{t,rev}[STR\bullet][DTC\bullet] + k_{bt}[STR\bullet]^2 + k_{ct}[STR\bullet][M]$$
$$+ k_{ct-S}[STR\bullet][S] + k_{ct-DTC}[STR\bullet][DTC\bullet] + k_{ct-P}[STR\bullet][P] \quad (4)$$

In this equation, k_a is the kinetic constant for activation of surface-tethered photoiniferter, $[STR-DTC]$ is the concentration of surface-tethered photoiniferter, $[DTC\bullet]$ is the concentration of dithiocarbamyl radicals, $k_{t,rev}$ is the kinetic constant for reversible termination of surface-tethered carbon radical by dithiocarbamyl radical, k_{bt} is the kinetic constant for bimolecular termination, k_{ct} is the kinetic constant for chain transfer to monomer, k_{ct-DTC} is the kinetic constant for chain transfer to dithiocarbamyl radical, k_{ct-S} is the kinetic constant for chain transfer to solvent, $[S]$ is the concentration of solvent, k_{ct-P} is the kinetic constant for chain transfer to free polymer chains in solution, and $[P]$ is the concentration of free polymer.

The first two terms on the right side of eq 4 represent the activation and deactivation of surface-tethered photoiniferters (Figure 2.1). Though the deactivation by dithiocarbamyl radicals does not result in permanent loss of surface-tethered radicals, it certainly reduces $[STR\bullet]$. However, as discussed earlier, the reversible termination of

surface-tethered radicals by dithiocarbamyl radicals is insignificant because $[DTC\bullet]$ is low. Accordingly, the first two terms on the right side of eq 4 can be neglected at long exposure times where decreasing rates of chain growth are observed. Also, because very few initiator molecules (~10^{15} molecules/cm^2) are present on the surface, the concentration of dithiocarbamyl radicals generated from the surface is orders of magnitude lower (~10^{-7} M, as estimated by Matyjaszewski et al. [16] in an ATRP system) than the monomer and solvent concentrations. Additionally, because all of the surface-tethered radicals are restricted to the vicinity of the surface but DTC radicals are untethered and free to diffuse away from the surface, $[STR\bullet]$ is estimated to be orders of magnitude (0.01-1 M, according to Kim et al. [20]) higher than $[DTC\bullet]$. The concentration of free polymer in solution is also lower as compared to $[STR\bullet]$, $[M]$, or $[S]$. Therefore, as a first approximation, the last two terms in eq 4 can also be neglected, leaving bimolecular termination and chain transfer to monomer and to solvent as the most probable mechanisms responsible for the irreversible termination of the surface-attached radicals.

Bimolecular termination involves the reaction of two extremely reactive radicals while chain transfer to monomer or solvent requires the reaction of an active free radical with a stable C-H bond [50]. The values of k_{bt} reported for free-radical polymerization (~10^6 L/(mol s)) of MMA in a toluene solution are orders of magnitudes higher than k_{ct} (~10^{-4} L/(mol s)) and k_{ct-S} (~10^{-5} L/(mol s)) [51]. However, for surface-initiated polymerizations, these values can be significantly different, and therefore the possibility of chain transfer to monomer and solvent cannot be discarded. However, because k_{ct} is

an order of magnitude higher than k_{ct-S}, only chain transfer to monomer will be considered at this stage. With all these assumptions, eq 4 can be simplified to yield eq 5.

$$-\frac{d[STR\bullet]}{dt} = k_{bt}[STR\bullet]^2 + k_{ct}[STR\bullet][M] \tag{5}$$

Equation 5 suggests that loss of radicals by chain transfer to monomer should become more significant as monomer concentration increases while bimolecular termination should become more significant as $[STR\bullet]$ increases. To determine the prevailing termination mechanism in SI-PMP over a broad range of relevant reaction conditions, experimental film thickness data were fit to kinetic models that incorporate the termination mechanisms individually. Thus, simplified forms of eq 5 were solved by considering either bimolecular termination or chain transfer to monomer to be the only significant termination mechanism. These two solutions provide two independent expressions for $[STR\bullet]$ as a function of exposure time that can be combined with eq 3 to obtain expressions for polymer layer thickness as a function of time.

Integration of eq 5 considering bimolecular termination as the only significant termination mechanism yields the following time-dependent expression for concentration of surface-attached radicals:

$$[STR\bullet] = \frac{[STR\bullet]_0}{1 + k_{bt}[STR\bullet]_0 t} \tag{6}$$

where $[STR\bullet]_0$ is initial concentration of surface-attached radicals. Substituting this expression for $[STR\bullet]$ into eq 3 and solving for $T(t)$ yields the following expression for PMMA brush thickness as a function of exposure time, *t*.

$$T = \frac{k}{k_{bt}}[M]\ln\{1 + k_{bt}[STR\bullet]_0(t - t_{brush})\} + T_{brush} \tag{7}$$

where T_{brush} is the thickness of the PMMA layer at t_{brush}. This model is valid only for $t \geq t_{brush}$ because the assumption that bimolecular termination does not occur in the mushroom regime has been made. In essence, until the layer is sufficiently crowded such that neighboring chains have lateral interactions (that cause the chains to swell away from the surface and adopt the characteristic stretched structure of a brush), the chains behave as if they are isolated and therefore unable to terminate by bimolecular coupling.

Integrating eq 5 when considering chain transfer to monomer as the only significant termination mechanism yields eq 8 for $[STR\bullet]$.

$$[STR\bullet] = [STR\bullet]_0 \exp(-k_{ct}[M]t) \tag{8}$$

Substituting this expression for $[STR\bullet]$ into eq 3 and then integrating yields the following time-dependent expression for polymer layer thickness:

$$T = \frac{k}{k_{ct}}[STR\bullet]_0\{\exp(-k_{ct}[M]t_{brush}) - \exp(-k_{ct}[M]t)\} + T_{brush} \tag{9}$$

Because chain transfer to monomer does not require direct interaction between two surface-tethered chains, this termination is assumed to occur in the mushroom and brush regimes (i.e., from $t = 0$) for all data sets.

Figure 2.5a and 2.5b shows predicted PMMA layer thicknesses as a function of time for three different monomer concentrations. The curves in Figure 2.5a, which represent the bimolecular termination model only, are produced using eq 7. The curves shown in Figure 2.5b show the pattern of behavior assuming chain transfer to monomer as the dominant termination mechanism (eq 9). The shapes of the curves in each figure illustrate how each termination mechanism affects the time-dependent evolution of the grafted films. Both termination results in a decreasing growth rate and limits the film thickness, but the patterns of PMMA layer growth are unmistakably different.

As shown in Figure 2.5a, when bimolecular termination is the dominant termination mechanism the initial growth rate and maximum layer thickness are functions of monomer concentration. Furthermore, the relative decrease in polymerization rate is independent of monomer concentration and only depends on exposure time. In contrast, when chain transfer to monomer concentration is dominant, the maximum film thickness is independent of monomer concentration (Figure 2.5b). Equation 9 predicts that the limiting film thickness under these termination conditions is equal to the value of $k[STR\bullet]_0/k_{ct}$. As observed from Figure 2.5b, the time at which this limiting thickness is reached decreases as monomer concentration increases.

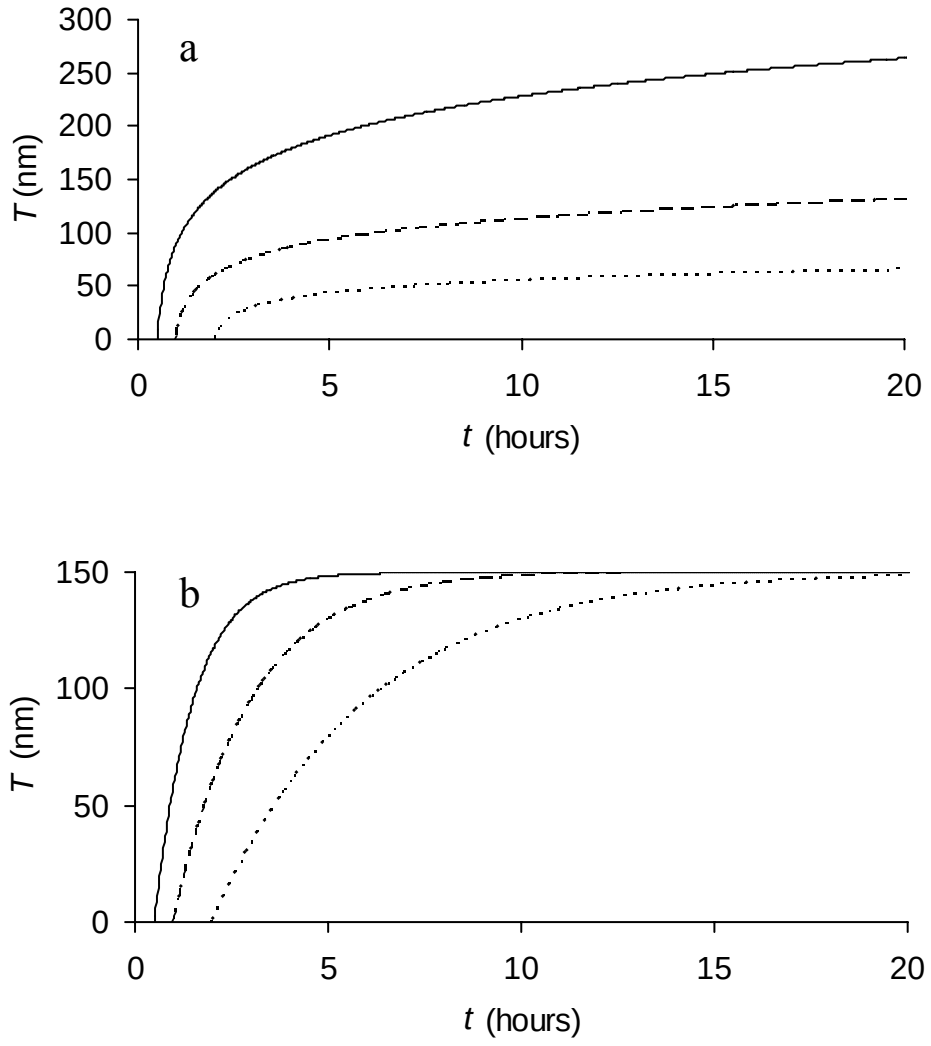

Figure 2.5 Effect of exposure time on the thickness of the PMMA layer predicted using kinetic models that consider a) bimolecular termination and b) chain transfer to monomer as irreversible termination mechanisms. The model equations are a) $T = 10.68[M]\ln(1+10t)$ for bimolecular termination and b) $T = 250\{\exp(-0.213[M]t_{brush}) - \exp(-0.213[M]t)\}$ for chain transfer to monomer. The [*M*] values used to obtain the model predictions are 4.68 (50% v/v; thin line), 2.34 (25% v/v; broken line) and 1.17 M (12.5% v/v; dotted line).

To determine which termination mechanism is dominant for the PMMA system investigated here, the experimentally obtained thickness data from Figure 2.2 were compared with predictions from both termination models. These results are shown in Figure 2.6. The values of the constants k/k_{bt} and $k_{bt}[STR\bullet]_0$ in eq 7 and the constants $k[STR\bullet]_0/k_{ct}$ and k_{ct} in eq 9 were obtained by fitting the respective termination models to the 4.68 M monomer concentration data. These kinetic constants were then used to predict film thickness as a function of time for the 1.17 and 2.34 M monomer concentration data sets because these constants, by definition, are independent of monomer concentration.

Figure 2.6a compares the measured film thicknesses to the predictions of the bimolecular termination model. As can be seen from this figure, the model predictions provide a reasonably good fit to all experimental data sets including those obtained at 1.17 and 2.34 M monomer concentrations. Also, the essential features predicted by this model are exhibited by the experimental data. For example, the maximum thickness of the PMMA layer obtained is observed to increase with monomer concentration.

Figure 2.6b compares the experimental data with film thickness values predicted using the chain-transfer termination model. While the 4.68 M data are fit very well by the model, the growth of the polymer layers at monomer concentrations of 1.17 and 2.34 M are significantly overpredicted. The deviation between the experimental data and the model predictions increases as monomer concentration decreases. In addition, contrary to model predictions, it is clear that the same PMMA layer thickness is not achieved at different monomer concentrations. These observations support the conclusion that chain

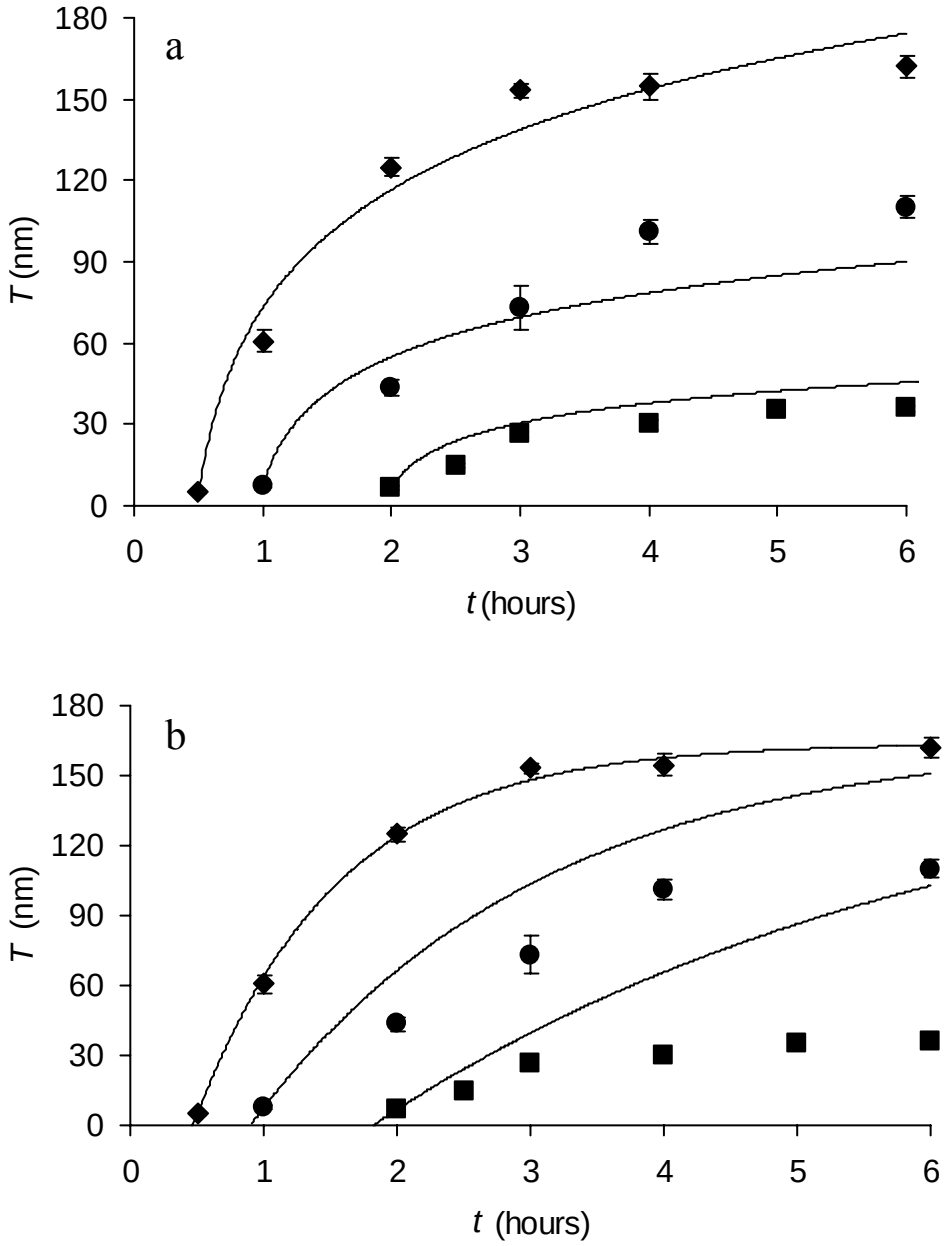

Figure 2.6 Comparison of the PMMA layer thicknesses measured using variable angle ellipsometry as a function of exposure time with model predictions (thin lines) for a) bimolecular termination and b) chain transfer to monomer. Irradiation intensity is 5 mW/cm^2 and methyl methacrylate concentrations in toluene are (■) 1.17, (●) 2.34, and (♦) 4.68 M.

transfer to monomer is not the dominant termination mechanism for the PMMA system at the lower monomer concentrations and irradiation conditions studied. Comparison of the experimentally obtained PMMA layer thicknesses with the predictions of models that consider chain transfer to solvent alone and chain transfer to monomer and solvent together as the only termination mechanisms also indicated that chain transfer is not the dominant termination mechanism. However, for the sake of brevity, the development and analysis of the models considering chain transfer to solvent alone and chain transfer to monomer and solvent together are not presented in this chapter. For development and analysis of these models, please refer to Appendix E.

Figure 2.6 shows that there is reasonable agreement between the predictions of both termination models and the actual PMMA layer growth at the monomer concentration of 4.68 M. This is expected since the parameters needed in both models were obtained from best fits of these data. To clarify the termination mechanism(s) at work at this relatively high monomer concentration, additional measurements were performed where the surface-attached free radical concentration was varied via irradiation intensity and the monomer concentration held constant at 4.68 M.

Effect of Light Intensity on Polymer Layer Growth. As shown in Figure 2.1, activation of the photoiniferter produces a surface-tethered carbon radical and a dithiocarbamyl radical in solution. The dithiocarbamyl radical can recombine with the tethered carbon radical to form the dormant species, which can then be re-activated or reinitiated as part of the living-radical photopolymerization mechanism. By performing a mass balance on the surface-attached carbon radicals and dithiocarbamyl radicals and assuming pseudo-steady state for the surface-tethered radical concentration, as previously

done by Kannurpatti et al. [34], it can be shown that $[STR\bullet]$ prior to any irreversible termination events is proportional to the square root of the irradiation intensity.

$$[STR\bullet]_0 = \left(\frac{\phi\varepsilon[STR-DTC]_0}{k_{t,rev}} \right)^{0.5} I_0^{0.5} \tag{10}$$

In this equation, ϕ is the photoiniferter initiation efficiency, ε is extinction coefficient of the photoiniferter, $[STR-DTC]_0$ is the initial photoiniferter concentration, and I_0 is the irradiation intensity. By substituting eq 10 into eqs 7 and 9, time-dependent expressions for film thickness as a function of light intensity (I_0) can be obtained; eqs 11 and 12 consider bimolecular termination or chain transfer to monomer as the sole termination mechanism, respectively:

$$T = \frac{k}{k_{bt}}[M]\ln\left\{1 + k_{bt}\left(t - t_{brush}\right)\left(\frac{\phi\varepsilon[STR-DTC]_0}{k_{t,rev}} \right)^{0.5} I_0^{0.5}\right\} + T_{brush} \tag{11}$$

$$T = \frac{k}{k_{ct}}\left(\frac{\phi\varepsilon[STR-DTC]_0}{k_{t,rev}} \right)^{0.5} I_0^{0.5}\left\{\exp\left(-k_{ct}[M]t_{brush}\right) - \exp\left(-k_{ct}[M]t\right)\right\} + T_{brush} \tag{12}$$

Values for the lumped kinetic constants and reaction parameters in eq 11 (k/k_{bt}, k_{bt}, and $\left(\phi\varepsilon[STR-DTC]_0/k_{t,rev}\right)^{1/2}$) and eq 12 ($k/k_{ct}\left(\phi\varepsilon[STR-DTC]_0/k_{t,rev}\right)^{1/2}$ and k_{ct}) were obtained from the previous best-fit analysis of thickness as a function of exposure time at

an intensity of 5 mW/cm^2 (Figure 2.6) and application of eq 10. Finally, with the assumption that the mushroom-to-brush transition occurs at similar thicknesses regardless of intensity, it can be shown that t_{brush} varies inversely with $I_0^{0.5}$. Therefore, approximate values of t_{brush} for different intensities can be calculated with the knowledge of t_{brush} at a single intensity. These assumptions allow the influence of irradiation intensity on polymer graft thickness to be predicted.

Figure 2.7 shows how the experimentally measured and predicted PMMA layer thicknesses depend on light intensity for irradiation times of 0.5, 1, and 2 h. In Figure 2.7a, the lines correspond to model predictions for bimolecular termination, (eq 11) while the lines in Figure 2.7b result from the model predictions for chain transfer to monomer (eq 12). It should be emphasized that no fitting of the intensity data was performed to obtain parameters and construct the model curves. All necessary model parameters were obtained from previous fits of thickness versus exposure time data at 5 mW/cm^2. As shown by the model curves in Figure 2.7a, for a fixed exposure time, the thickness of the PMMA layer plateaus at high-intensity values when bimolecular termination is the prevailing termination mechanism. However, the chain transfer model (Figure 2.7b) predicts a continuous increase in the layer thickness as intensity is increased and exposure time is held constant.

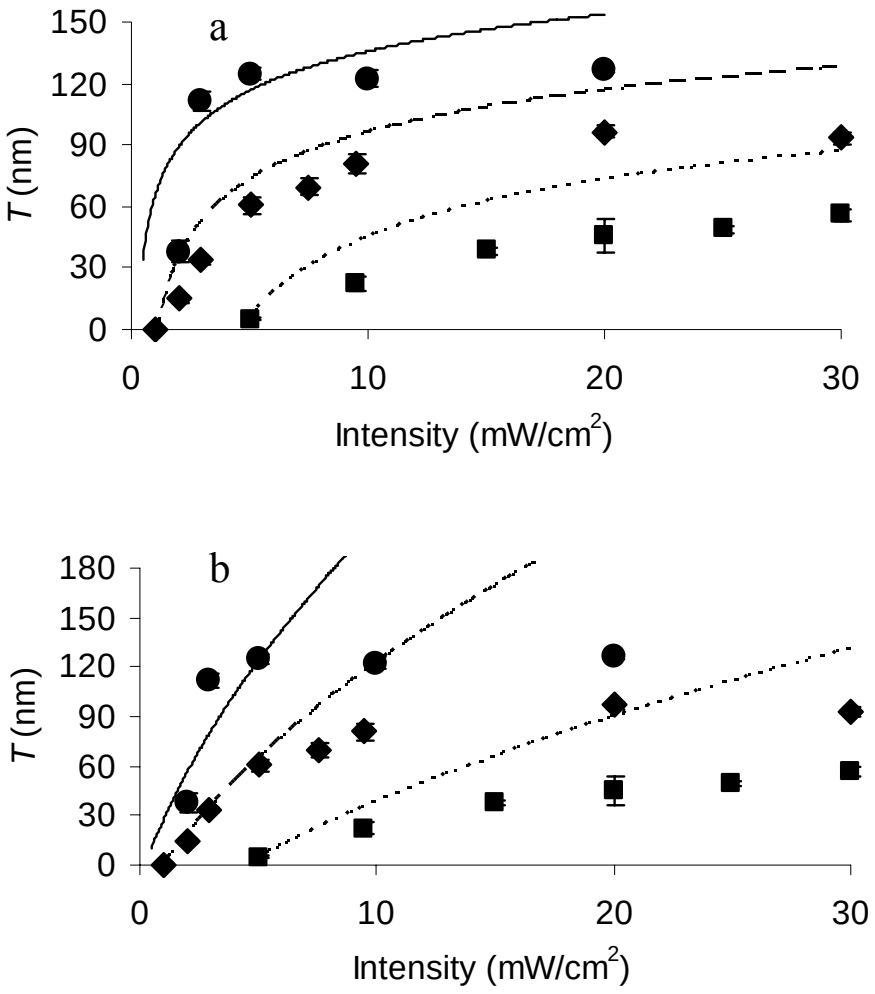

Figure 2.7 Comparison of the measured PMMA layer thicknesses as a function of intensity with model predictions (lines) considering a) bimolecular termination and b) chain transfer to monomer. The model equations are a) $T = 10.68[M]\ln\left[1 + 4.472\left(t - 1.118/I_0^{0.5}\right)I_0^{0.5}\right]$ for bimolecular termination and b) $T = 111.8I_0^{0.5}\left\{\exp\left(-0.213[M]\left(1.118/I_0^{0.5}\right)\right) - \exp\left(-0.213[M]t\right)\right\}$ for chain transfer to monomer. [*M*] = 4.68 M. The *t* values used to obtain the model predictions are 2 (thin line), 1 (broken line) and 0.5 (dotted line) hours. The factor $\left(1.118/I_0^{0.5}\right)$ is used to empirically predict t_{brush} at different intensities from the 4.68 M data at $I_0 = 5mW/cm^2$. The polymerizations were carried out for (■) 0.5, (♦) 1, and (●) 2 hours at [*M*] = 4.68 M.

As can be seen in Figure 2.7a, the experimental data follow a trend similar to that predicted by the bimolecular termination, with the layer thickness becoming independent of irradiation intensity at high intensities. The intensity at which this "saturation effect" occurs decreases as exposure time increases. The large deviation observed in Figure 2.7a between the experimental data and the model predictions at shorter exposure times is most likely due to inaccuracy in predicting t_{brush} as a function of intensity with a limited number of data points. This variability becomes more significant at shorter exposure times because the percent error in $(t - t_{brush})$ is greater. The experimental intensity data were also compared with thickness predictions based on the chain transfer $[STR\bullet]_0$ model (Figure 2.7b). The pattern of behavior displayed by the data as intensity is increased is significantly different than the trends predicted by this model. The model predicts a continuous increase in the thickness of the PMMA layer with increasing intensity, while the experimentally measured layer thickness is observed to level off as previously noted. The chain transfer model predictions match the experimental data only at lower intensities. This is reasonable given that when the intensity is decreased, $[STR\bullet]_0$ is also decreased. Under such conditions it may be that chain transfer to monomer becomes a more significant termination mechanism; however, a detailed study at low intensities is necessary to verify this argument.

The fact that the agreement between the predicted and measured PMMA layer thickness is better in Figure 2.7a compared to Figure 2.7b further supports the conclusion that bimolecular termination is the dominant termination mechanism for the majority of reaction conditions studied. Although both termination mechanisms are likely occurring, and chain transfer to monomer may play a significant role at low irradiation intensities

(<5 mW/cm^2) and high monomer concentrations (>4.68 M), the bimolecular termination model clearly is better able to reproduce the characteristics of PMMA layer growth via SI-PMP seen at high intensities and across a spectrum of monomer concentrations.

2.4 Conclusions

Poly(methyl methacrylate) layers were synthesized successfully on silicon substrates using SI-PMP. The initial rate of PMMA layer growth is observed to have first-order dependence on monomer concentration. Nonlinear growth of the PMMA layer with the exposure time indicates that irreversible termination reactions are present in the system, leading to the loss of surface-tethered free radicals. Therefore, the photoiniferter-mediated surface-initiated photopolymerization is nonliving. We hypothesize that irreversible termination of surface-tethered radicals occurs due to insufficient concentration of deactivating species (dithiocarbamyl radicals) at the surface. Kinetic models developed and applied to probe the prevalence of bimolecular termination and chain transfer to monomer indicate that bimolecular termination is the dominant termination mechanism for the range of reaction conditions investigated in this study. The model framework developed in this study can be used to predict the SI-PMP behavior of a variety of monomer systems including those with higher chain transfer coefficients than MMA. These systems are expected to exhibit the characteristics of chain-transfer dominant termination at lower monomer concentrations and at higher intensities than those observed with MMA. Lastly, on the basis of previous studies of photoiniferter-mediated photopolymerizations in bulk solution [52], it is hypothesized

that the irreversible termination by either mechanism can be suppressed, and the "living" characteristics of any SI-PMP system can be improved by the presence of additional deactivating species. These studies of impact of added deactivating species on PMMA layer growth are described in the following chapter.

2.5 References

1. Lee, J. H.; Jung, H. W.; Kang, I.; Lee, H. B. "Cell Behaviour on Polymer Surfaces with Different Functional Groups" *Biomaterials* **1994**, *15*, 705– 711.

2. van Kooten, T. G.; Schakenraad, J. M.; van der Mei, H. C.; Busscher, H. J. "Influence of Substratum Wettability on the Strength of Adhesion of Human Fibroblasts", *Biomaterials* **1992**, *13*, 897–904.

3. Walboomers, X. F.; Monaghan, W.; Curtis, A. S. G.; Jansen, C. "Attachment of Fibroblasts on Smooth and Microgrooved Polystyrene", *J. Biomed. Mat. Res.* **1999**, *46*, 212-220.

4. Edmondson, S.; Osborne, V. L.; Huck, W. T. S. "Polymer Brushes *via* Surface-initiated Polymerizations", *Chem. Soc. Rev.* **2004**, *33*, 14-22.

5. Kilbey II, S.M.; Watanabe, H.; Tirrell, M. "Structure and Scaling of Polymer Brushes Near the θ Condition", *Macromolecules* **2001**, *34*, 5249-5259.

6. Toomey, R.; Mays, J.; Tirrell, M. "In-Situ Thickness Determination of Adsorbed Layers of Poly(2-Vinylpyridine)-Polystyrene Diblock Copolymers by Ellipsometry", *Macromolecules* **2004**, *37*, 905-911.

7. Karim, A.; Satija, S. K.; Douglas, J. F.; Anker, J. F.; Fetters, L. J. **"**Neutron Reflectivity Study of the Density Profile of a Model End-Grafted Polymer Brush: Influence of Solvent Quality", *Phys. Rev. Lett*. **1994**, *73*, 3407-3410.

8. Kreer, T.; Müser, M. H.; Binder, K.; Klein, J. "Frictional Drag Mechanisms between Polymer-Bearing Surfaces", *Langmuir* **2001**, *17*, 7804-7813.

9. Lemieux, M.; Usov, D.; Minko, S.; Stamm, M.; Shulha, H.; Tsukruk, V. V. "Reorganization of Binary Polymer Brushes: Reversible Switching of Surface Microstructures and Nanomechanical Properties", *Macromolecules* **2003**, *36*, 7244-7255.

10. Zhao, B.; Brittain, W. J. "Polymer Brushes: Surface-Immobilized Macromolecules", *Prog. Poly. Sci.* **2000**, *25*, 677-710.

11. Prucker, O.; Rühe, J. "Polymer Layers through Self-Assembled Monolayers of Initiators", *Langmuir* **1998**, *14*, 6893-6898.

12. Prucker, O.; Rühe, J. "Synthesis of Poly(styrene) Monolayers Attached to High Surface Area Silica Gels through Self-Assembled Monolayers of Azo Initiators", *Macromolecules* **1998**, *31*, 592-601.

13. Schmidt, R.; Zhao, T.; Green, J. B.; Dyer, D. J. "Photoinitiated Polymerization of Styrene from Self-Assembled Monolayers on Gold", *Langmuir* **2002**, *18*, 1281-1287.

14. Paul, R.; Schmidt, R.; Dyer, D. J. "Synthesis of Ultrathin Films of Polyacrylonitrile by Photoinitiated Polymerization from Self-Assembled Monolayers on Gold", *Langmuir* **2002**, *18*, 8719-8723.

15. Ejaz, M.; Yamamoto, S.; Ohno, K.; Tsujii, Y.; Fukuda, T. "Controlled Graft Polymerization of Methyl Methacrylate on Silicon Substrate by the Combined Use of the Langmuir-Blodgett and Atom Transfer Radical Polymerization Techniques", *Macromolecules* **1998**, *31*, 5934-5936.

16. Matyjaszewski, K.; Miller, P. J.; Shukla, N.; Immaraporn, B.; Gelman, A.; Luokala, B. B.; Siclovan, T. M.; Kickelbick, G.; Vallant, T.; Hoffmann, H.; Pakula, T. "Polymers at Interfaces: Using Atom Transfer Radical Polymerization in the Controlled Growth of Homopolymers and Block Copolymers from Silicon Surfaces in the Absence of Untethered Sacrificial Initiator", *Macromolecules* **1999**, *32*, 8716-8724.

17. Zhao, B.; Brittain, W. J. "Synthesis, Characterization, and Properties of Tethered Polystyrene-*b*-polyacrylate Brushes on Flat Silicate Substrates", *Macromolecules* **2000**, *33*, 8813-8820.

18. Shah, R. R.; Merreceyes, D.; Husemann, M.; Rees, I.; Abbott, N. L.; Hawker, C. J.; Hedrick, J. L. "Using Atom Transfer Radical Polymerization to Amplify Monolayers of Initiators Patterned by Microcontact Printing into Polymer Brushes for Pattern Transfer", *Macromolecules* **2000**, *33*, 597-605.

19. Ejaz, M.; Tsujii, Y.; Fukuda, T. "Controlled Grafting of a Well-defined Polymer on a Porous Glass Filter by Surface-Initiated Atom Transfer Radical Polymerization", *Polymer* **2001**, *42*, 6811-6815.

20. Kim, J. B.; Huang, W.; Miller, M. D.; Baker, G. L.; Bruening, M. L. "Kinetics of Surface-Initiated Atom Transfer Radical Polymerization", *J. Poly. Sci.:Part A: Poly. Chem.* **2003**, *41*, 386-394.

21. Boyes, S. G.; Granville, A. M.; Baum, M.; Akgun, B.; Mirous, B. K.; Brittain, W. J. "Polymer Brushes–Surface Immobilized Polymers", *Surf. Sci.* **2004**, *570*, 1-12.

22. Husseman, M.; Malmström, E. E.; McNamara, M.; Mate, M.; Mecerreyes, D.; Benoit, D. G.; Hedrik, J. L.; Mansky, P.; Huang, E.; Russell, T. P.; Hawker, C. J. "Controlled Synthesis of Polymer Brushes by "Living" Free Radical Polymerization Techniques", *Macromolecules* **1999**, *32*, 1424-1431.

23. Husemann, M.; Morrison, M.; Benoit, D.; Frommer, J.; Mate, C. M.; Hingsberg, W. D.; Hedrik, J. L.; Hawker, C. J. "Manipulation of Surface Properties by Patterning of Covalently Bound Polymer Brushes", *J. Am. Chem. Soc.* **2000**, *122*, 1844-1845.

24. Bartholome, C.; Beyou, E.; Bourgeat-Lami, E.; Chaumont, P.; Zydowicz, N. "Nitroxide-Mediated Polymerizations from Silica Nanoparticle Surfaces: "Graft from" Polymerization of Styrene Using a Triethoxysilyl-Terminated Alkoxyamine Initiator", *Macromolecules* **2003**, *36*, 7946-7952.

25. Tsujii, Y.; Ejaz, M.; Sato, K.; Goto, A.; Fukuda, T. "Mechanism and Kinetics of RAFT-Mediated Graft Polymerization of Styrene on a Solid Surface. 1. Experimental Evidence of Surface Radical Migration", *Macromolecules* **2001**, *34,* 8872-8878.

26. Baum, M.; Brittain, W. J. "Synthesis of Polymer Brushes on Silicate Substrates via Reversible Addition Fragmentation Chain Transfer Technique", *Macromolecules* **2002**, *35*, 610-615.

27. Otsu, T.; Yoshida, M.; Tazaki, T. "A Model for Living Radical Polymerization", *Macromol. Chem. Rapid Commun.* **1982**, *3*, 133-140.

28. Nakayama, Y.; Matsuda, T. "Surface Macromolecular Architectural Designs Using Photo-Graft Copolymerization Based on Photochemistry of Benzyl *N*,*N*-Diethyldithiocarbamate", *Macromolecules* **1996**, *29*, 8622-8630.

29. Luo, N.; Metters, A. T.; Hutchison, J. B.; Bowman, C. N.; Anseth, K. S. "A Methacrylated Photoiniferter as a Chemical Basis for Microlithography: Micropatterning Based on Photografting Polymerization", *Macromolecules* **2003**, *36*, 6739-6745.

30. Peppas, N. A.; Ward, J. H. "Biomimetic Materials and Micropatterned Structures Using Iniferters", *Adv. Drug Delivery Rev.* **2004**, *56*, 1587-1597.

31. Lambrinos, P.; Tardi, M.; Polton, A.; Sigwalt, P. "The Mechanism of the Polymerization of n-Butyl Acrylate Initiated with *N*,*N*-diethyl Dithiocarbamate Derivatives", *Eur. Polym. J.* **1990**, *26*, 1125-1135.

32. Kazmaier, P. M.; Moffat, K. A.; Georges, M. K.; Veregin, R. P. N.; Hamer, G. K. "Free-Radical Polymerization for Narrow-Polydispersity Resins. Semiempirical Molecular Orbital Calculations as a Criterion for Selecting Stable Free-Radical Reversible Terminators", *Macromolecules* **1995**, *28*, 1841-1846.

33. Otsu, T.; Matsunaga, T.; Doi, T.; Matsumoto, A. "Features of Living Radical Polymerization of Vinyl Monomers in Homogeneous System Using *N*,*N*-diethyldithiocarbamate Derivatives as Photoiniferters", *Eur. Poly. J.* **1995**, *31*, 67-78.

34. Kannurpatti, A. R.; Lu, S.; Bunker, G. M.; Bowman, C. N. "Kinetic and Mechanistic Studies of Iniferter Photopolymerizations", *Macromolecules* **1996**, *29*, 7310-7315.

35. Ward, J. H.; Shahar, A.; Peppas, N. A. "Kinetics of 'Living' Radical Polymerizations of Multifunctional Monomer", *Polymer* **2002**, *43*, 1745-1752.

36. Higashi, J.; Nakayama, Y.; Marchant, R. E.; Matsuda, T. "High-Spatioresolved Microarchitectural Surface Prepared by Photograft Copolymerization Using Dithiocarbamate: Surface Preparation and Cellular Responses", *Langmuir* **1999**, *15*, 2080-2088.

37. Kobayashi, T.; Takahashi, S.; Fujii, N. "Silane Coupling Agent Having Dithiocarbamate Group for Photografting of Sodium Styrene Sulfonate on Glass Surface", *J. App. Polym. Sci.* **1993**, *49*, 417-423.

38. de Boer, B.; Simon, H. K.; Werts, M. P. L.; van der Vegte, E. W.; Hadziioannou, G. ""Living" Free Radical Photopolymerization Initiated from Surface-Grafted Iniferter Monolayers", *Macromolecules* **2000**, *33*, 349-356.

39. Qin, S. H.; Qiu, K. Y. "A New Polymerizable Photoiniferter for Preparing Poly(methyl methacrylate) Macromonomer", *Eur. Poly. J.* **2001**, *37*, 711-717.

40. Nakayama, Y.; Matsuda, T. "In-Situ Observation of Dithiocarbamate-Based Surface Photograft Copolymerization Using Quartz Crystal Microbalance", *Macromolecules* **1999**, *32*, 5405-5410.

41. Gopireddy, D.; Husson, S. M. "Room Temperature Growth of Surface-Confined Poly(acrylamide) from Self-Assembled Monolayers Using Atom Transfer Radical Polymerization", *Macromolecules* **2002**, *35*, 4218-4221.

42. Xiao, D.; Wirth, M. J. "Kinetics of Surface-Initiated Atom Transfer Radical Polymerization of Acrylamide on Silica", *Macromolecules* **2002**, *35*, 2919-2925.

43. Wu, S. In *Polymer Interface and Adhesion*, 1st ed.; Marcel Dekker, Inc.: New York, 1982; p 162-163.

44. Huang, X.; Wirth, M. J. "Surface Initiation of Living Radical Polymerization for Growth of Tethered Chains of Low Polydispersity", *Macromolecules* **1999**, *32*, 1694-1696.

45. Halperin, A.; Tirrell, M.; Lodge, T.P. "Tethered Chains in Polymer Microstructures", *Adv. Poly. Sci.* **1992**, *100*, 31-71.

46. Otsu, T. "Iniferter Concept and Living Radical Polymerization", *J. Poly. Sci.:Part A: Poly. Chem.* **2000**, *38*, 2121-2136.

47. Otsu, T.; Matsunaga, T.; Doi, T.; Matsumoto, A. "Features of Living Radical Polymerization of Vinyl Monomers in Homogeneous System Using *N*,*N*-diethyldithiocarbamate Derivatives as Photoiniferters", *Eur. Poly. J.* **1995**, *31*, 67-78.

48. Marques, C. M.; Joanny, J.–F. "Block Copolymer Adsorption in a Nonselective Solvent", *Macromolecules* **1989**, *22*, 1454-1458.

49. Douglas, J. F.; Karim, A.; Kent, M. S.; Satija, S. K. In "Encyclopedia of Materials: Science and Technology", Buschow, K. H. J., Cahn, R. W., Flemings, M. C., Ilschner, B., Kramer, E. J., Mahajan, S., Eds.; Pergamon Press: New York, **2001**; Vol. 8, pp 7218-7223.

50. Odian, G. In "Principles of Polymerization", 4th ed.; Wiley-Interscience: New Jersey, **2004**; p 198-350.

51. Ueda, A.; Nagai, S. In "Polymer Handbook", 4th ed.; Brandup, J., Immergut, E. H., Grulke, E. A., Eds.; Wiley-Interscience: New Jersey, 1999; Vol. 1, p II/97.

52. Doi, T.; Matsumoto, A.; Otsu, T. "Radical Polymerization of Methyl Acrylate by Use of Benzyl *N*,*N*-Diethyldithiocarbamate in Combination with Tetraethylthiuram Disulfide as a Two-Component Iniferter", *J. Poly. Sci.:Part A: Poly. Chem.* **1994**, *32*, 2911-2918.

CHAPTER 3

IMPACT OF ADDED TETRAETHYLTHIURAM DISULFIDE DEACTIVATOR ON THE KINETICS OF GROWTH AND REINITIATION OF POLY(METHYL METHACRYLATE) BRUSHES MADE BY SURFACE-INITIATED PHOTOINIFERTER-MEDIATED PHOTOPOLYMERIZATION

[As published in *Macromolecules* **2006**, *39*, 8987-8991 with minor additions]

Without intervention, it has been found that surface-initiated photoiniferter-mediated photopolymerization (SI-PMP) of methyl methacrylate suffers from irreversible termination, which leads to cessation of polymerization. These irreversible termination reactions were successfully reduced by preaddition of tetraethylthiuram disulfide (TED). The poly(methyl methacrylate) layers were also reinitiated using styrene as a monomer to investigate the effect of TED concentration on the extent of irreversible termination. The reinitiation efficiency increased as [TED] was increased, indicating that extent of irreversible termination reactions can be reduced by increasing [TED]. It was also observed that dithiocarbamyl radicals generated from TED can initiate polymerization in solution, resulting in significant monomer consumption.

3.1 Introduction

Polymer brushes [1] grafted covalently to solid substrates are of great importance owing to their potential applications in food packaging, lithography, microelectronics and

design of corrosion resistant and biocompatible materials to name a few. Of the various methods by which polymer brushes can be made, the "grafting from" approach using controlled (free) radical polymerizations has become perhaps the most widely practiced [2]. Techniques such as atom transfer radical polymerization (ATRP) [3-9], nitroxide-mediated free-radical polymerization (NMP) [10-12] and reversible addition fragmentation transfer (RAFT) [13,14] have been used to produce polymer brushes. While the grafting-from approaches in general allow surface densities and molecular weights of the tethered chains to be manipulated independently, thereby allowing interfacial structure to be tailored, the controlled-polymerization methods have the additional advantage of being amenable to the synthesis of multiblock copolymers. The creation of such multifunctional layers springs from the preservation of the active end groups during the polymerization, brought about by establishing and maintaining an equilibrium between capped, dormant chains and active, free-radical species. Most often, this is accomplished by the addition of a deactivating species that reacts reversibly with the radical [4,8,10,15-21], thereby allowing another block(s) to be added subsequently [4,10,15,16,21].

In previous chapters and a recent publication [22], I described interest in using surface initiated, photoiniferter-mediated photopolymerization (SI-PMP) to create polymer brushes [22]. SI-PMP is advantageous for the fabrication of these interfacial layers because it is mediated by light, which permits polymerization to be carried out at room temperature and readily allows spatial and temporal control over layer growth. Photoiniferter-mediated photopolymerization was first discovered by Otsu et al. [23] and has been extensively used by several groups [24-30] to modify surface properties of

various organic and inorganic substrates. Ideally, photoiniferter-mediated photopolymerization involves a dynamic equilibrium between growing chains with active free radicals and chains that exist in a "dormant" state, temporarily capped with the deactivating dithiocarbamyl radicals [23] as depicted in Figure 3.1. As predicted by persistent radical effect and mentioned previously, a sufficient concentration of these deactivating species must be present to provide reversible deactivation of chains during propagation to create an equilibrium between active and dormant chains that favors a low yet persistent concentration of free-radicals leading to controlled-radical polymerization behavior [31,32]. However, the extremely low concentration of deactivating radicals produced by surface-initiated photoiniferter-mediated photopolymerization (SI-PMP) from flat surfaces leads to irreversible termination, primarily by bimolecular termination and cessation of layer growth [22]. Analogous "non-living" behavior is also observed in the synthesis of polymer brushes by surface-initiated ATRP [4,8,33-35] and NMP [10-12] from low area substrates.

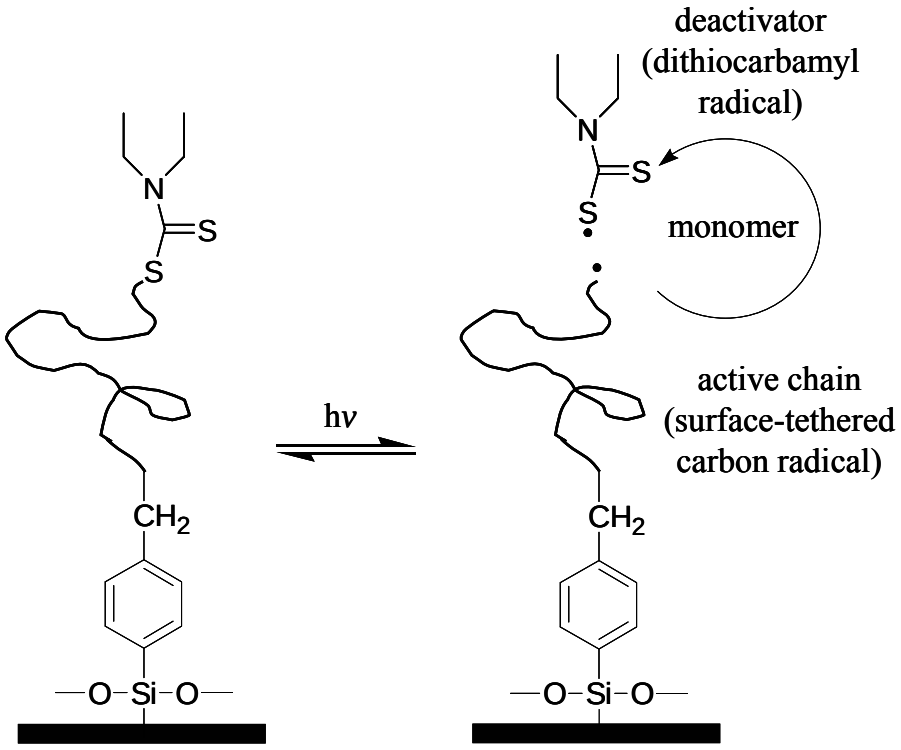

Figure 3.1 Idealized scheme for the growth of surface-tethered PMMA chain by surface-initiated photoiniferter-mediated photopolymerization of MMA.

Because of the problem of cessation of layer growth brought about by bimolecular termination, in this work I investigate the impact of adding a source of deactivating species, tetraethylthiuram disulfide (TED), to the reaction mixture. As shown in Figure 3.2, when irradiated with UV light, TED undergoes a homolytic cleavage, yielding two dithiocarbamyl (DTC) radicals. Previously, TED has been used by Doi et al. [36] to prevent bimolecular termination during photoiniferter-mediated photopolymerization of methyl acrylate in bulk or in benzene. Lovell et al. [37] used TED in combination with conventional initiator, 2,2-dimethoxy-2-2-phenylacetophenone to create crosslinked polymers without trapped radicals. Similarly, in studies of SI-PMP of poly(ethylene

glycol) methyl ether methacrylate from diethyldithiocarbamate-modified polymer substrates, Luo et al. [38] inferred that chain transfer to poly(ethylene glycol) units can be suppressed by addition of TED to the reaction mixture. Otsu et al. [39] were able to synthesize di- and triblock copolymers of polystyrene (PS) and poly(methyl methacrylate) (PMMA) layers using surface-initiated photopolymerization from photoiniferter-modified PS beads in presence of TED.

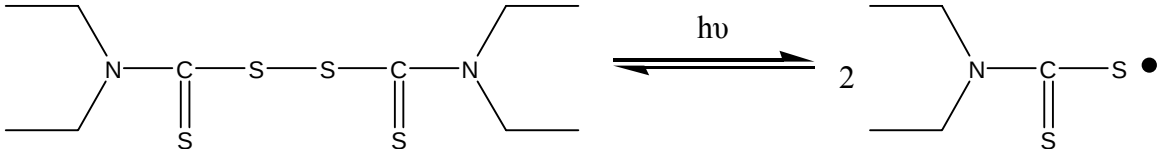

Figure 3.2 Formation of two identical dithiocarbamyl radicals by homolytic cleavage of tetraethylthiuram disulfide (TED) mediated by ultraviolet (UV) light.

However, to date, synthesis of block copolymer brushes from flat surfaces using SI-PMP in presence of TED has not been reported. Additionally, the impact of added TED on the kinetics of surface-tethered chain growth and the ability of this strategy to preserve active ends during brush formation to allow block copolymers to be created has not been investigated adequately. To better understand the kinetics of SI-PMP in presence of TED, I have studied the impact of TED concentration on the growth of surface-tethered PMMA layers by SI-PMP. Additionally, reinitiation experiments were conducted using PMMA layers photopolymerized in the presence of varying concentrations of TED. These studies provide additional insight into the reinitiation efficiency (ability of PMMA layers to restart growth) and, therefore, the extent of

irreversible termination reactions occurring during SI-PMP of MMA in the presence of TED.

3.2 Experimental

Materials. Purities and preparations of methyl methacrylate (MMA), solvents and reagents are described in detail in Chapter 2 and a previous publication [22]. Additional compounds used here were styrene (Acros; 99%), which was dehibited by passing it through a neutral alumina column prior to use, and tetraethylthiuram disulfide (TED) (Sigma; 97%), which was used as received. The synthesis and characterization [22,28] of the photoiniferter, N,N-(diethylamino)dithiocarbamoylbenzyl(trimethoxy)silane (SBDC) and procedures used to make self-assembled monolayers (SAMs) of this iniferter on silicon surfaces are discussed in Chapter 2 and therefore not repeated here.

Photopolymerization. The protocols used in these photopolymerization studies, including solution preparation, assembly of the reaction cell, photopolymerization, and post-photopolymerization treatments, were also described in Chapter 2 and a previous paper [22] and therefore are not repeated here. The only significant change in these studies is the addition of TED to the photopolymerization solutions. Solutions of MMA and TED in anhydrous toluene were prepared in airfree Schlenk tubes. MMA concentration of 4.68 M in toluene was used for all experiments. The concentrations of TED (based on the volume of the solution of MMA in toluene) used were 0.02, 0.2, 1, 2 mM. The reinitiation of the PMMA layers synthesized at various photopolymerization conditions used styrene as a monomer. Styrene concentration of 4.34 M in toluene was

used for all reinitiation experiments, and for all of these reinitiation studies, the preparations, photopolymerization and post-polymerization treatment were analogous to those followed for MMA photopolymerizations.

Characterization. A Beaglehole Instruments Phase-Modulated Picometer^{TM} Ellipsometer (He-Ne laser, $\lambda = 632.8$ nm) was used to measure the dry layer thicknesses of the SBDC SAMs, PMMA layers and PMMA-PS block-copolymer layers. Refractive indices of 1.45, 1.48 and 1.59 were used for the SAMs of SBDC, PMMA and PS, respectively. The ellipsometric angles ψ and Δ, measured by changing the angle of incidence from 80° to 35°, were fitted using a Cauchy model (Igor Pro. software package) to determine the thickness. Thickness measurements were taken at five different points on every sample in ambient air. The SAMs, PMMA layers and PMMA-PS block-copolymers were also characterized by measuring the static water contact angle. The details of contact angle instrument and measurement method are discussed in Chapter 2 and therefore not repeated here. Monomer conversions were estimated from the ^{1}H nuclear magnetic resonance (NMR) spectra of aliquots of reaction cell solutions before and after photopolymerization. These ^{1}H NMR spectra were recorded on a Bruker AC300 Fourier transform NMR spectrometer. Monomer conversion was calculated as the ratio of the peak integral corresponding to the double bond proton (CH_2=C) of MMA after SI-PMP to the peak integral corresponding to the double bond proton of MMA before SI-PMP. For the comparison of peak integrals, peaks corresponding to the constant concentration of solvent (toluene) protons were used as internal controls.

3.3 Results and Discussion

Growth of the PMMA Layers. Figure 3.3 shows how the dry layer thicknesses of grafted PMMA layers measured using variable-angle ellipsometry increase with polymerization time for various TED concentrations, [TED]. All data sets show an initial period of slow increase in thickness followed by a rapid increase. This initial lag has been previously attributed to the "mushroom-to-brush" transition [22] (indicated by the arrow). Therefore, the kinetic analysis of the variation of PMMA layer thickness with time at all [TED] is done after this initial lag period (after the exposure time marked by the arrow). As seen by the curve labeled **a** in Figure 3.3, when no TED is added to the polymerization solution, the thickness of the PMMA layer increases rapidly after the initial lag period, but is followed by a sharp decline in the growth rate. Through complementary kinetic modeling studies, this cessation of layer growth has been primarily attributed to loss of active ends by bimolecular termination [22].

The data sets labeled **b**, **c**, **d** and **e** in Figure 3.3 show the effect of increasing [TED] on the growth of the grafted PMMA layers. As seen in Figure 3.3, when [TED] = 0.02 mM (data set **b**), the maximum growth rate (observed between 30 min and 1 hr exposure time) is slower than when no TED is added; however, the thickness of this PMMA layer after 6 hours of exposure (209 ± 5 nm) exceeds that of the sample polymerized without TED (162 ± 4 nm). The presence of a thicker layer suggests that the extent of irreversible termination is lower in the presence of TED. At a [TED] of 0.2 mM (data set labeled **c** in Figure 3.3), a non-linear increase in PMMA layer thickness is still observed. However, at [TED] of 1 and 2 mM (data sets **d** and **e**, respectively), the

measured thicknesses of PMMA layers increase linearly throughout the experiment, albeit the layers grow more slowly compared to the other three cases. A linear increase in PMMA layer thickness throughout the photopolymerization provides evidence that the extent of irreversible termination is less than at the lower TED concentrations studied. These simultaneous decreases in extent of irreversible termination and PMMA layer growth rate are consistent with a shift in the equilibrium of the surface-tethered radicals towards the dormant state.

Thus, based on the behaviors exhibited in Figure 3.3, I conclude that TED decreases the extent of irreversible termination reactions that occur during SI-PMP; however, I also observed that at long times when [TED] = 2 mM, the viscosity of the bulk solution increased. In comparison, I observed no thickening of the solution in control experiments in which a bare silicon substrate was immersed in monomer solution without TED and irradiated for 6 hours. These pieces of information suggest that monomer consumption caused by propagation of dithiocarbamyl radicals occurs in solution. This dithiocarbamyl-initiated photopolymerization of MMA has been previously observed by Otsu et al. [23], Lambrinos et al. [40] and Turner et al. [41] in their studies of photoiniferter-mediated photopolymerization. NMR analysis was used to quantify the consumption of monomer in solution as a function of exposure time and [TED]. Figure 3.4 shows monomer conversion as a function of exposure time when no TED was added and at [TED] = 2 mM. As can be seen, monomer conversion becomes significant when TED is added to the system. In the presence of TED, monomer conversion increases with exposure time. Increased monomer conversion, in addition to irreversible termination, reduces the rate of PMMA layer growth at long exposure times.

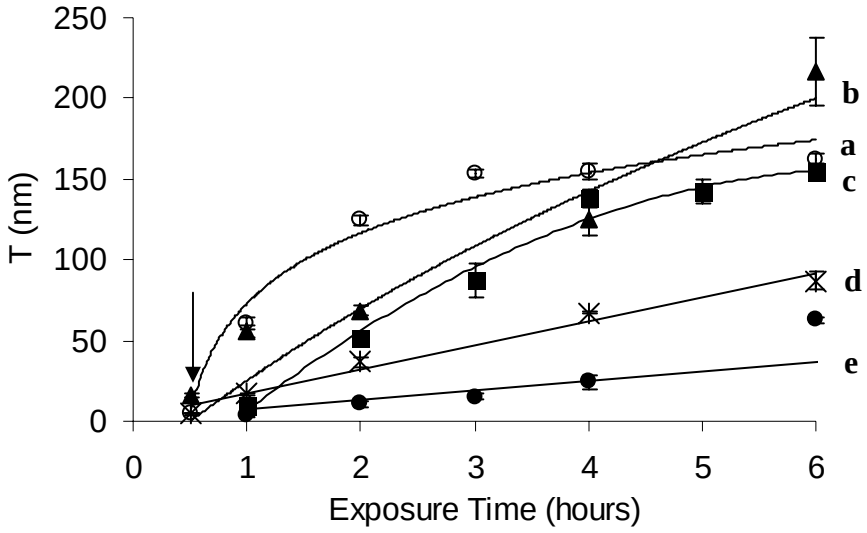

Figure 3.3 Dry PMMA layer thicknesses at TED concentrations of (a) 0 mM, (b) 0.02 mM, (c) 0.2 mM, (d) 1 mM and (e) 2 mM. The thin lines are only to guide the eye. In these experiments, MMA concentration of 4.68 M and light intensity of 5 mW/cm^2 were used. Error bars represent the standard deviation calculated from repeat measurements using three identical samples (and five thickness measurements per sample).

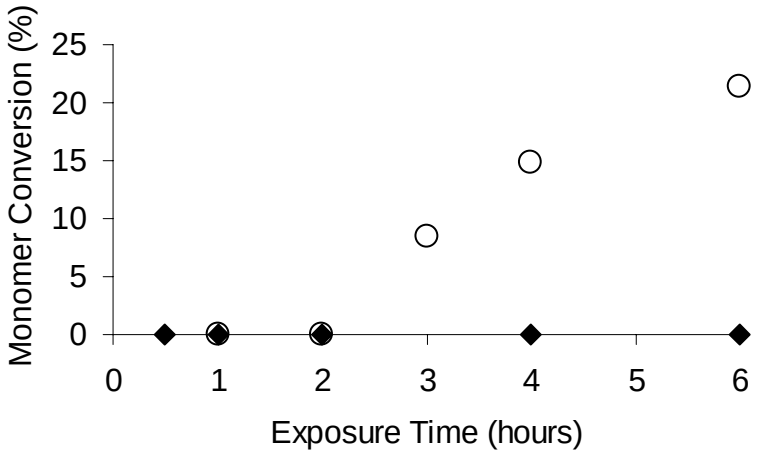

Figure 3.4 Effect of exposure time on the conversion of MMA when no TED was added (filled diamonds; ♦) and at a TED concentration of 2 mM (hollow circles; ○).

Because monomer conversion is not significant at short exposure times, even at high TED concentrations, the shift in the equilibrium of the surface-tethered radicals towards the dormant state as a function of increasing [TED] can be inferred by comparing the maximum PMMA layer growth rates obtained during early stages of photopolymerization. As can be seen from Figure 3.5a, the maximum rate of PMMA layer growth decreases with increasing [TED], implying that the instantaneous concentration of active, surface-tethered radicals decreases as [TED] is increased. As a result, because of the shift in the equilibrium of the surface-tethered radicals towards the dormant state, propagation and extent of irreversible termination are both decreased.

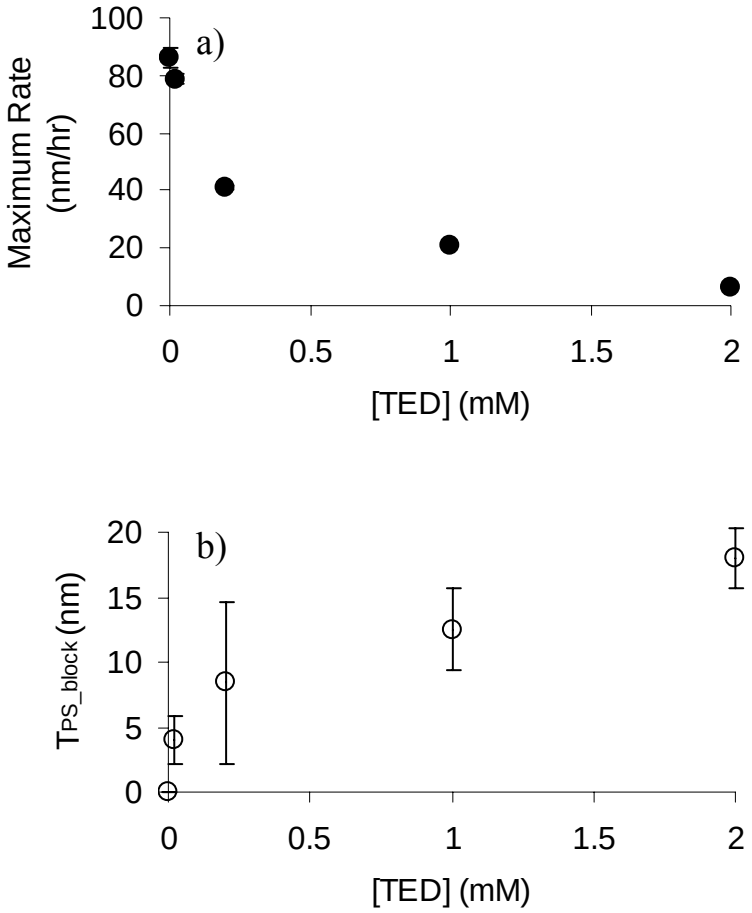

Figure 3.5 Effect of TED concentration on (a) maximum rate of PMMA layer growth and (b) the thickness of poly(styrene) blocks synthesized by reinitiating the PMMA layers that were synthesized at various TED concentrations. The maximum rates were obtained by plotting a straight line through the first two data points for thickness of PMMA layers after the initial lag period (after the exposure time marked by the arrow) for each TED concentration. Error bars in the maximum rates represent the standard error obtained using linear regression of the multiple measurements. Reinitiation of the PMMA layers (synthesized at light intensity of 5 mW/cm^2, [MMA] = 4.68 M and exposure time = 6 hours) was conducted at intensity of 5 mW/cm^2, [styrene] = 4.34 M and exposure time = 4 hours.

To support the inference that the extent of irreversible termination decreases upon preaddition of TED, PMMA layers synthesized with 6 hours of UV exposure in the presence of TED were reinitiated using styrene as a monomer. All the reinitiation polymerizations were conducted for 4 hours in toluene using a light intensity of 5 mW/cm^2 (λ = 365 nm) and a styrene concentration of 4.34 M without preaddition of TED. Also, a control experiment in which synthesis of a PS layer directly tethered to photoiniferter-modified silicon wafer at the reinitiation conditions was carried out. The thickness of this control PS layer was found to be 76 ± 2 nm. Because all of the reinitiation experiments were conducted under exactly the same conditions, the molecular weights of the PS chains grown during reinitiation of PMMA layers should be approximately constant. Therefore, owing to steric crowding effects, the ellipsometric thickness of the PS block formed will be a function of the number of PS chains per unit area, which in turn depends on the number of PMMA chains per unit area capable of reinitiating.

Figure 3.5b shows how the PS-block thickness (dry layer) increases as a function of [TED] used during formation of the initial PMMA layer. When no TED was added to the polymerization solution, the PMMA layer could not be reinitiated, indicating the complete loss of active chain ends via irreversible termination reactions during the initial 6 hour MMA polymerization. As [TED] increases, the PS-block thickness increases, suggesting that the extent of irreversible termination reactions during PMMA layer formation decreases with increasing [TED]. Even at [TED] = 2 mM, however, a significant degree of termination is still believed to occur since the PS-block thickness of the sample polymerized under these conditions (18 ± 2 nm) is still significantly less than

that of the PS control layer (76 ± 2 nm). These results suggest that TED, which provides deactivating DTC radicals, helps to at least partially preserve DTC-capped PMMA chains that are capable of reinitiation in the presence of PS.

Contact angle measurements were made to confirm that the observed thickness increases seen after reinitiation with styrene are due to the formation of surface-tethered PMMA-PS block copolymers and not due to the formation of PS chains tethered directly to photoiniferter-modified silicon wafer. If surface-tethered PS chains instead of PMMA-PS block copolymers are created, a mixed polymer brush containing individual PMMA and PS chains tethered to the surface would be formed. In this case, because static water contact angles of PMMA and PS are significantly different [42], a mixed PMMA-PS brush contact angle will reflect the presence of i) a PMMA surface if PMMA chain length is greater than PS chain length; ii) a PS surface if PS chain length is greater than PMMA chain length; or iii) a mixed PMMA-PS surface if PMMA and PS chains are of approximately equal length. Alternatively, a PMMA-PS block copolymer exposed to toluene, which is a better solvent for PS than PMMA, will exhibit contact angle that corresponds to PS.

Table 3.1 lists the water contact angle of the photopolymerized PMMA-PS layers along with the individual thicknesses of PMMA and PS layers. All measurements were taken after the layers were sonicated in toluene and vacuum-dried. As can be seen from Table 3.1, a water contact angle of 74.3 ± 1.9°, which corresponds to that of PMMA [42], was observed when no TED was added to the polymerization solution. This result is expected because no increase in the PMMA layer thickness was observed upon reinitiation with styrene. For TED concentrations of 0.02 mM, 0.2 mM, 1 mM and 2 mM,

static water contact angles of 90.6 ± 0.3°, 92.3 ± 2.2°, 91.3 ± 3.2° and 95.2 ± 0.6°, respectively, were measured. These contact angles correspond to the static water contact angle of PS [42]. At [TED] of 0.02, 0.2 mM and 1mM, the PMMA thicknesses are greater than the thickness of PS layer synthesized at reinitiation conditions, suggesting that the PMMA chain lengths at these [TED] are greater than the length of PS chains formed upon reinitiation. As hypothesized earlier, this comparison of chain lengths and contact angle data indicate that the PMMA layers synthesized at [TED] = 0.02, 0.2 mM and 1 mM, when reinitiated in presence of styrene produce PMMA-PS block copolymer, rather than a mixed brush of individual PMMA and PS chains. I note that at [TED] = 2 mM the thickness of the initial PMMA layer is smaller than that of the PS layer grown under control conditions. Nevertheless, based on the behaviors observed in the reinitiation studies of PMMA layers made at lower TED concentrations, I believe that reinitiation of PMMA layers grown at [TED] = 2 mM also produce a PMMA-PS block copolymer.

[TED] (mM)	PMMA block thickness (nm)	PS block thickness (nm)	static water contact angle (°)
0	162 ± 4	0	74.3 ± 1.9
0.02	216 ± 21	4 ± 2	90.6 ± 0.3
0.2	154 ± 5	8 ± 6	92.3 ± 2.2
1	87 ± 5	13 ± 3	91.3 ± 3.2
2	63 ± 1	18 ± 2	95.2 ± 0.6

Table 3.1 Static water contact angle of PMMA-PS layers along with the individual thicknesses of PMMA and PS layers as a function of TED concentrations used for the synthesis of PMMA layers. Uncertainties in the reported contact angles represent the standard deviation calculated from three identical samples with three repeat measurements per sample.

It should be noted that these studies to quantify the impact of TED on PMMA layer growth kinetics and reinitiation capability only prove that preaddition of TED helps reduce the extent of irreversible termination reactions. This decrease in irreversible termination reactions, however, is not sufficient to conclude that preaddition of TED improves the control over SI-PMP. Such a contention requires additional information about the molecular weight (MW) and molecular weight distribution (MWD) of the surface-tethered PMMA chains. To obtain these MW and MWD data, it is necessary to first degraft the PMMA chains from the surface and subsequently characterize them with gel permeation chromatography (GPC) or an analogous technique. Unfortunately, application of any degrafting strategy to low-area substrates is rather impractical because of the insufficient amount of polymer synthesized. Previous efforts to degraft polymer chains synthesized by surface-initiated polymerizations have involved the use of high area substrates such as silica gel [10,43-44]. However, a uniform SI-PMP from photoiniferter-modified silica gel is difficult to achieve because of high solution opacities that can lead to non-uniform exposure of all initiating sites. In addition, molecular weight data obtained from such systems may not accurately reflect the molecular weight distribution of chains grown from flat substrates due to important differences in surface geometry, chain conformation, and ratio of surface to bulk radical concentrations. Therefore, degrafting of PMMA chains to obtain MW and MWD data was not included in this work.

3.4 Conclusions

These studies of the impact of TED, a source of deactivating dithiocarbamyl radicals, on the growth of PMMA by SI-PMP reveal interesting trade-offs: As expected, TED reduces the rate of growth of the layers and decreases the extent of irreversible termination reactions that lead to cessation of polymerization; however, at long times the DTC radicals generated from TED can initiate polymerization in solution, resulting in monomer consumption, which can further retard the rate of propagation. Reinitiation studies using styrene support the contention that preaddition of TED helps to preserve the active ends, leading to an increase in reinitiation efficiency and block copolymer formation, as manifest by increasing PS-block thicknesses with increasing [TED]. These studies show that it is necessary to supply a source of deactivating radicals to decrease the extent of irreversible termination reactions during SI-PMP, but this benefit comes at the cost of reducing the rate of polymerization and layer growth. These insights into the kinetic behavior and reinitiation efficiency of SI-PMP in the presence of an added deactivating species highlight the impact and importance of reaction conditions, including amount of TED, on the engineering of soft material interfaces by SI-PMP.

3.5 References

1. Halperin, A.; Tirrell, M.; Lodge, T.P. "Tethered Chains in Polymer Microstructures", *Adv. Poly. Sci.* **1992**, *100*, 31-71.

2. Zhao, B.; Brittain, W. J. "Polymer Brushes: Surface-Immobilized Macromolecules", *Prog. Poly. Sci.* **2000**, *25*, 677-710.

3. Ejaz, M.; Yamamoto, S.; Ohno, K.; Tsujii, Y.; Fukuda, T. "Controlled Graft Polymerization of Methyl Methacrylate on Silicon Substrate by the Combined Use of the Langmuir-Blodgett and Atom Transfer Radical Polymerization Techniques", *Macromolecules* **1998**, *31*, 5934-5936.

4. Matyjaszewski, K.; Miller, P. J.; Shukla, N.; Immaraporn, B.; Gelman, A.; Luokala, B. B.; Siclovan, T. M.; Kickelbick, G.; Vallant, T.; Hoffmann, H.; Pakula, T. "Polymers at Interfaces: Using Atom Transfer Radical Polymerization in the Controlled Growth of Homopolymers and Block Copolymers from Silicon Surfaces in the Absence of Untethered Sacrificial Initiator", *Macromolecules* **1999**, *32*, 8716-8724.

5. Zhao, B.; Brittain, W. J. "Synthesis, Characterization, and Properties of Tethered Polystyrene-*b*-Polyacrylate Brushes on Flat Silicate Substrates", *Macromolecules* **2000**, *33*, 8813-8820.

6. Shah, R. R.; Merreceyes, D.; Husemann, M.; Rees, I.; Abbott, N. L.; Hawker, C. J.; Hedrick, J. L. "Using Atom Transfer Radical Polymerization to Amplify Monolayers of Initiators Patterned by Microcontact Printing into Polymer Brushes for Pattern Transfer", *Macromolecules* **2000**, *33*, 597-605.

7. Ejaz, M.; Tsujii, Y.; Fukuda, T. "Controlled Grafting of a Well-defined Polymer on a Porous Glass Filter by Surface-Initiated Atom Transfer Radical Polymerization", *Polymer* **2001**, *42*, 6811-6815.

8. Kim, J. B.; Huang, W.; Miller, M. D.; Baker, G. L.; Bruening, M. L. "Kinetics of Surface-Initiated Atom Transfer Radical Polymerization", *J. Poly. Sci.:Part A: Poly. Chem.* **2003**, *41*, 386-394.

9. Boyes, S. G.; Granville, A. M.; Baum, M.; Akgun, B.; Mirous, B. K.; Brittain, W. J. "Polymer Brushes–Surface Immobilized Polymers", *Surf. Sci.* **2004**, *570*, 1-12.

10. Husseman, M.; Malmström, E. E.; McNamara, M.; Mate, M.; Mecerreyes, D.; Benoit, D. G.; Hedrik, J. L.; Mansky, P.; Huang, E.; Russell, T. P.; Hawker, C. J. "Controlled Synthesis of Polymer Brushes by "Living" Free Radical Polymerization Techniques", *Macromolecules* **1999**, *32*, 1424-1431.

11. Husemann, M.; Morrison, M.; Benoit, D.; Frommer, J.; Mate, C. M.; Hingsberg, W. D.; Hedrik, J. L.; Hawker, C. J. "Manipulation of Surface Properties by Patterning of Covalently Bound Polymer Brushes", *J. Am. Chem. Soc.* **2000**, *122*, 1844-1845.

12. Bartholome, C.; Beyou, E.; Bourgeat-Lami, E.; Chaumont, P.; Zydowicz, N. "Nitroxide-Mediated Polymerizations from Silica Nanoparticle Surfaces: "Graft From" Polymerization of Styrene Using a Triethoxysilyl-Terminated Alkoxyamine Initiator", *Macromolecules* **2003**, *36*, 7946-7952.

13. Tsujii, Y.; Ejaz, M.; Sato, K.; Goto, A.; Fukuda, T. "Mechanism and Kinetics of RAFT-Mediated Graft Polymerization of Styrene on a Solid Surface. 1. Experimental Evidence of Surface Radical Migration", *Macromolecules* **2001**, *34*, 8872-8878.

14. Baum, M.; Brittain, W. J. "Synthesis of Polymer Brushes on Silicate Substrates via Reversible Addition Fragmentation Chain Transfer Technique", *Macromolecules* **2002**, *35*, 610-615.

15. Zhao, B.; Brittain, W. J. "Synthesis, Characterization, and Properties of Tethered Polystyrene-*b*-Polyacrylate Brushes on Flat Silicate Substrates", *Macromolecules* **2000**, *33*, 8813-8820.

16. Boyes, S. G.; Granville, A. M.; Baum, M.; Akgun, B.; Mirous, B. K.; Brittain, W. J. "Polymer Brushes-Surface Immobilized Polymers", *Surf. Sci.* **2004**, *570*, 1-12.

17. Ejaz, M.; Tsujii, Y.; Fukuda, T. "Controlled Grafting of a Well-defined Polymer on a Porous Glass Filter by Surface-Initiated Atom Transfer Radical Polymerization", *Polymer* **2001**, *42*, 6811-6815.

18. Ejaz, M.; Ohno, K.; Tsujii, Y.; Fukuda, T. "Controlled Grafting of a Well-Defined Glycopolymer on a Solid Surface by Surface-Initiated Atom Transfer Radical Polymerization", *Macromolecules* **2000**, *33*, 2870-2874.

19. Jeyaprakash, J. D.; Samuel, S.; Dhamodharan, R.; Rühe, J. "Polymer Brushes via ATRP: Role of Activator and Deactivator in the Surface-Initiated ATRP of Styrene on Planar Substrates", *Macromol. Rapid. Commun.* **2002**, *23*, 277-281.

20. Huang, X.; Wirth, M. J. "Surface Initiation of Living Radical Polymerization for Growth of Tethered Chains of Low Polydispersity", *Macromolecules* **1999**, *32*, 1694-1696.

21. Kim, J. B.; Huang, W.; Miller, M. D.; Baker, G. L.; Bruening, M. L. "Synthesis of Triblock Copolymer Brushes by Surface-Initiated Atom Transfer Radical Polymerization", *Macromolecules* **2002**, *35*, 5410-5416.

22. Rahane, S. B.; Kilbey, S. M., II; Metters, A. T. "Kinetics of Surface-Initiated Photoiniferter-Mediated Photopolymerization", *Macromolecules* **2005**, *38*, 8202-8210.

23. Otsu, T.; Yoshida, M.; Tazaki, T. "A Model for Living Radical Polymerization", *Macromol. Chem. Rapid Commun.* **1982**, *3*, 133-140.

24. Nakayama, Y.; Matsuda, T. "Surface Macromolecular Architectural Designs Using Photo-Graft Copolymerization Based on Photochemistry of Benzyl *N*,*N*-Diethyldithiocarbamate", *Macromolecules* **1996**, *29*, 8622-8630.

25. Luo, N.; Metters, A. T.; Hutchison, J. B.; Bowman, C. N.; Anseth, K. S. "A Methacrylated Photoiniferter as a Chemical Basis for Microlithography: Micropatterning Based on Photografting Polymerization", *Macromolecules* **2003**, *36*, 6739-6745.

26. Higashi, J.; Nakayama, Y.; Marchant, R. E.; Matsuda, T. "High-Spatioresolved Microarchitectural Surface Prepared by Photograft Copolymerization Using Dithiocarbamate: Surface Preparation and Cellular Responses", *Langmuir* **1999**, *15*, 2080-2088.

27. Kobayashi, T.; Takahashi, S.; Fujii, N. "Silane Coupling Agent Having Dithiocarbamate Group for Photografting of Sodium Styrene Sulfonate on Glass Surface", *J. App. Polym. Sci.* **1993**, *49*, 417-423.

28. de Boer, B.; Simon, H. K.; Werts, M. P. L.; van der Vegte, E. W.; Hadziioannou, G. ""Living" Free Radical Photopolymerization Initiated from Surface-Grafted Iniferter Monolayers", *Macromolecules* **2000**, *33*, 349-356.

29. Qin, S. H.; Qiu, K. Y. "A New Polymerizable Photoiniferter for Preparing Poly(methyl methacrylate) Macromonomer ", *Eur. Poly. J.* **2001**, *37*, 711-717.

30. Nakayama, Y.; Matsuda, T. "In-Situ Observation of Dithiocarbamate-Based Surface Photograft Copolymerization Using Quartz Crystal Microbalance", *Macromolecules* **1999**, *32*, 5405-5410.

31. Fischer, H. "The Persistent Radical Effect: A Principle for Selective Radical Reactions and Living Radical Polymerizations", *Chem. Rev.* **2001**, *101*, 3581-3610.

32. Fischer, H. "The Persistent Radical Effect in "Living" Radical Polymerization", *Macromolecules* **1997**, *30*, 5666-5672.

33. Gopireddy, D.; Husson, S. M. "Room Temperature Growth of Surface-Confined Poly(acrylamide) from Self-Assembled Monolayers Using Atom Transfer Radical Polymerization", *Macromolecules* **2002**, *35*, 4218-4221.

34. Xiao, D.; Wirth, M. J. "Kinetics of Surface-Initiated Atom Transfer Radical Polymerization of Acrylamide on Silica", *Macromolecules* **2002**, *35*, 2919-2925.

35. Sankhe, A. Y.; Husson, S. M.; Kilbey, S. M., II "Effect of Catalyst Deactivation on Polymerization of Electrolytes by Surface-Confined Atom Transfer Radical Polymerization in Aqueous Solutions", *Macromolecules* **2006**, *39*, 1376-1383.

36. Doi, T.; Matsumoto, A.; Otsu, T. "Radical Polymerization of Methyl Acrylate by Use of Benzyl *N*,*N*-Diethyldithiocarbamate in Combination with Tetraethylthiuram Disulfide as a Two-Component Iniferter", *J. Poly. Sci.:Part A: Poly. Chem.* **1994**, *32*, 2911-2918.

37. Lovell, L. G.; Elliott, B. J.; Brown, J. R.; Bowman, C. N. "The Effect of Wavelength on the Polymerization of Multi(meth)acrylates with Disulfide/Benzilketal Combinations", *Polymer* **2001**, *42*, 421-429.

38. Luo, N.; Hutchinson, J. B.; Anseth, K. S.; Bowman, C. N. "Surface-Initiated Photopolymerization of Poly(ethylene glycol) Methyl Ether Methacrylate on a Diethyldithiocarbamate-Mediated Polymer Substrate", *Macromolecules* **2002**, *35*, 2487-2493.

39. Otsu, T.; Ogawa, T.; Yamamoto, T. "Solid-phase Block Copolymer Synthesis by the Iniferter Technique", *Macromolecules* **1986**, *19*, 2087-2089.

40. Lambrinos, P.; Tardi, M.; Polton, A.; Sigwalt, P. "The Mechanism of the Polymerization of n-Butyl Acrylate Initiated with *N*,*N*-diethyl Dithiocarbamate Derivatives", *Eur. Polym. J.* **1990**, *26*, 1125-1135.

41. Turner, S. R.; Blevins, R. W. "Photoinitiated Block Copolymer Formation Using Dithiocarbamate Fee Radical Chemistry", *Macromolecules* **1990**, *23*, 1856-1859.

42. Wu, S. In *Polymer Interface and Adhesion*, Marcel Dekker, Inc.: New York, 1982; p 162-163.

43. Prucker, O.; Rühe, J. "Synthesis of Poly(styrene) Monolayers Attached to High Surface Area Silica Gels through Self-Assembled Monolayers of Azo Initiators", *Macromolecules* **1998**, *31*, 592-601.

44. Prucker, O.; Rühe, J. "Mechanism of Radical Chain Polymerizations Initiated by Azo Compounds Covalently Bound to the Surface of Spherical Particles", *Macromolecules* **1998**, *31*, 602-613.

CHAPTER 4

KINETIC MODELING OF SURFACE-INITIATED PHOTOINIFERTER-MEDIATED PHOTOPOLYMERIZATION IN PRESENCE OF TETRAETHYLTHIURAM DISULFIDE

A kinetic model was developed to investigate the effect of various reaction parameters on surface-initiated photoiniferter-mediated photopolymerization (SI-PMP) of methyl methacrylate. In particular, the effect of photopolymerization conditions such as light intensity, concentration of the added deactivating species - tetraethylthiuram disulfide (TED), and initial photoiniferter concentration on the growth kinetics and reinitiation ability of poly(methyl methacrylate) (PMMA) layers was studied in detail. In accord with experimental results, model predictions suggest that maximum rates of PMMA layer growth observed during the initial stages of SI-PMP increase as the ratio of TED concentration ([TED]) to initial photoiniferter concentration ([PI]) is decreased and as light intensity is increased. Conversely, the maximum thickness of the PMMA layers, which is defined as the thickness at which 99% of the chains are irreversibly terminated, increases as [TED]/[PI] increases and as light intensity decreases. Though increases in [TED]/[PI] and decreases in light intensity affect PMMA layer growth in similar fashion, their effect on reinitiation ability of PMMA layers is significantly different: reinitiation ability increases with increasing [TED]/[PI] but is not improved by decreasing the light intensity. Simulations also suggest that PMMA layers synthesized in the presence of TED

have a greater tendency to form a surface-tethered block copolymer upon reinitiation compared to PMMA layers synthesized without TED and at lower light intensity.

4.1 Introduction

Controlled radical polymerization (CRP) processes are attractive mainly due to their ability to control polymer molecular weight and synthesize multi-block copolymer architectures [1]. Combining CRP techniques with surface-tethered initiators enables dense homopolymer and block copolymer brushes to be synthesized [2]. CRP techniques such as atom transfer radical polymerization (ATRP) [3-9], nitroxide-mediated free-radical polymerization (NMP) [10-12], reversible addition fragmentation transfer (RAFT) [13,14] and photoiniferter-mediated photopolymerization (PMP) [15-21] all have been used to produce polymer brushes. The ability of these CRP techniques to form multi-block copolymer architectures is a consequence of an equilibrium between active radicals and dormant polymer chains being established and maintained during polymer layer growth. This equilibrium keeps the radical concentration low, minimizing irreversible termination and, in turn, preserving the active chain ends necessary for the formation of multi-block copolymers.

Owing to certain advantages (for example, ease of achieving spatial and temporal control over layer growth) over other living-radical polymerization techniques, surface-initiated photoiniferter-mediated photopolymerization (SI-PMP) [22-23] was chosen as a means of synthesizing poly(methyl methacrylate) (PMMA) brushes. Previously, I showed that without intervention, SI-PMP of methyl methacrylate (MMA) suffers from

irreversible termination, leading to cessation of polymerization [22]. As a result, these PMMA layers lack the ability of subsequent reinitiation to create multi-block architectures. Knowing that reinitiation is enabled by preservation of active ends during polymerization, a source of deactivating species, tetraethylthiuram disulfide (TED), was added to the reaction mixture. It was found that the ability to reinitiate layer growth and add a second block improves as the concentration of TED is increased [23]. However, to-date, the dependence of reinitiation ability and layer growth kinetics on various photopolymerization conditions such as light intensity and photoiniferter concentration in presence or absence of a deactivator like TED has not been investigated. In this work, I augment and support experimental findings reported in Chapter 3 with predictions of a kinetic model developed for the SI-PMP system, thereby gaining a deeper insight into the SI-PMP process.

While there is an abundance of studies pertaining to modeling CRP processes in bulk or solution [24-31], adaptation and application of these models to surface-initiated CRP (SI-CRP) is scarce. The efforts that aim to simulate SI-CRP processes are limited to the Monte Carlo simulations developed by Genzer [32] and the simulations using rate-based models of Kim et al. [8]. The simulations of Genzer used to investigate SI-CRP (specifically surface-initiated ATRP, or SI-ATRP) rely on the probabilities of reaction and motion of polymer chains, and the approach utilizes experimentally available kinetic rate constants obtained for solution-phase ATRP. On the other hand, the simulations developed by Kim et al. take a more traditional approach of simultaneously solving rate equations that describe the individual processes (initiation, propagation and termination) occurring in SI-ATRP.

The model developed in the present work is specific to SI-PMP by virtue of describing the effects of parameters specific to SI-PMP (for example, light intensity); however, the approach is similar to that of Kim et al. [8] in that it uses rate equations written to describe individual processes. Additionally, because some of the kinetic rate constants (for example, termination rate constants) can be affected significantly by confinement of polymer chains to surface, analogous to the approach of Kim et al. [8], the rate constants were obtained by the fitting of the experimental results to the model predictions rather than specifying the values *a priori*. As a result, while the approach is qualitatively general, the model developed in this work and used to investigate the effect of TED concentration, light intensity and initial photoiniferter concentration on the kinetics of growth and reinitiation ability, is quantitatively specific to the formation of PMMA brushes.

In addition to predicting the effect of various reaction parameters on PMMA layer growth kinetics and reinitiation ability, the model is used to reveal how photopolymerization conditions can be manipulated to increase PMMA layer thicknesses while maintaining a significant reinitiation ability. As discussed earlier, one requirement for maintaining significant reinitiation ability is the maintenance of a low concentration of propagating radicals during photopolymerization, which can be achieved by either adding TED to reaction mixture or decreasing light intensity. Predictions of the rate-based model provided in this chapter demonstrate how TED preaddition and decreased light intensity differ in their effect on reinitiation ability of PMMA brushes and how either mixed or multi-block copolymer brush architectures can be targeted through intelligent choice of these reactions conditions.

4.2 Model Development and Methods

Formulation of the Model. The overall SI-PMP process that occurs in the presence of TED can be broken down into four individual processes. The particular chemistries used when carrying out SI-PMP of MMA have been described in detail in Chapter 2 and previous publications [22,23]. Briefly, SI-PMP of MMA in the presence of TED involves

i) reversible activation (termination) of surface-tethered photoiniferter molecule, forming (recombining) a surface-tethered carbon radical, STR●, and a free dithiocarbamyl radical, DTC●;
ii) reversible cleavage (termination) of TED to yield two free DTC●;
iii) irreversible termination of a surface-tethered radical via bimolecular termination; and
iv) propagation via reaction of a STR● with monomer (MMA) to grow a surface-tethered PMMA chain.

I emphasize here that previous experimental work on the MMA system suggests that bimolecular termination, rather than chain transfer, is the dominant irreversible termination event [22], and therefore this irreversible termination mechanism is included exclusively.

Mathematically, first three reactions can be represented by eqs 1-4, which result from writing a mole balance for each species involved in the individual processes just described:

$$\frac{d[STR\bullet]}{dt} = k_a^{'}[STR-DTC] - k_{t,rev}[STR\bullet][DTC\bullet] - k_t[STR\bullet]^2 \qquad (1)$$

$$\frac{d[STR-DTC]}{dt} = -k_a^{'}[STR-DTC] + k_{t,rev}[STR\bullet][DTC\bullet] \quad (2)$$

$$\frac{d[DTC\bullet]}{dt} = k_{a,TED}^{'}[TED] - k_{t,TED}[DTC\bullet]^2 + k_a^{'}[STR-DTC] - k_{t,rev}[STR\bullet][DTC\bullet] \quad (3)$$

$$\frac{d[TED]}{dt} = -k_{a,TED}^{'}[TED] + k_{t,TED}[DTC\bullet]^2 \quad (4)$$

The propagation reaction is represented in terms of the evolution of PMMA layer thickness, T as a function of exposure time, t:

$$\frac{dT}{dt} = k^{'}k_p[STR\bullet][M] \quad (5)$$

In these equations, $[STR\bullet]$ is the concentration of surface-tethered radicals, $[M]$ is the monomer concentration, $[DTC\bullet]$ is the concentration of DTC●, $[STR-DTC]$ is the concentration of surface-tethered radicals in deactivated state (made by reversible capping of STR● with DTC●), $k_a^{'}$ is the effective kinetic constant for (reversible) activation of surface-tethered photoiniferter molecules into surface-tethered carbon radicals, $k_{t,rev}$ is the kinetic constant for deactivation of STR● by reaction with DTC● (which is a reversible termination event), k_t is the kinetic constant for irreversible bimolecular termination of STR●, $k_{a,TED}^{'}$ is the effective kinetic constant for activation (homolytic cleavage) of TED, $k_{t,TED}$ is the kinetic constant for reversible deactivation of

dithiocarbamyl radicals to form TED, and $[TED]$ is the concentration of TED. In eq 5, k_p is the propagation rate constant and k' is a proportionality constant between the rate of polymerization and growth rate (rate of change of thickness) of PMMA layer, which is described and justified previously [33,34].

Taken together, eqs 1 through 5 constitute a comprehensive kinetic model for simulating PMMA layer growth as a function of various photopolymerization conditions. Application of the described model to characterize the kinetics of SI-PMP, however, requires an understanding of its inherent assumptions and limitations, as well as suitable values for the unknown kinetic parameters.

Parameterizing the Model. The values of k_a' and $k_{a,TED}'$ are calculated using eqs 6 and 7 [35], respectively, and are listed in Table 4.1.

$$k_a' = f_1 k_a = \frac{f_1 I_0 \varepsilon_P \lambda}{N_{AV} hc} \tag{6}$$

$$k_{a,TED}' = f_2 k_{a,TED} = \frac{f_2 I_0 \varepsilon_{TED} \lambda}{N_{AV} hc} \tag{7}$$

In these expressions, I_0 is the light intensity (in mW/cm^2), ε_P is the extinction coefficient of photoiniferter molecules, ε_{TED} is the extinction coefficient of TED, λ is the wavelength of incident UV-light (365 nm), N_{AV} is Avogadro's number, h is Planck's constant and c is the speed of light. For the described simulations, ε_P is calculated using UV-Vis absorbance data for photoiniferter molecules (ε_P=100 M^{-1}cm^{-1})

and ε_{TED} = 210 $M^{-1}cm^{-1}$ (obtained from reference 36). It should be noted that initiator efficiencies, f_1 and f_2, are lumped with the kinetic constants for activations of photoiniferter (k_a) and TED ($k_{a,TED}$), respectively. For this reason, and because f_1 and f_2 are unknown, $k_a^{'}$ and $k_{a,TED}^{'}$ are effective activation constants. Close analysis of eqs 1-4 and eqs 6-7 shows that changes in f_1 and f_2 will affect the kinetics of PMMA layer growth in the same fashion as changes in k_a and $k_{a,TED}$, respectively. Therefore, because it is not possible to decouple change in the effective activation constant brought about by changes in the initiator efficiencies or the other parameters in eqs 6 and 7, values of f_1 and f_2 were assumed to be 1. The value of $k_{t,TED}$ was obtained from literature [37]. Because of confinement of the photoiniferter and PMMA chains to the surface, the values of the remaining kinetic constants, $k_{t,rev}$, k_t, $k^{'}$, k_p and the initial concentration of surface-tethered photoiniferter molecules, $[STR-DTC]_0$, may differ significantly from parameter values available in the literature for bulk or solution polymerization. Therefore, as indicated in Table 4.1 and described in detail later, these values were obtained by fitting model predictions with the experimental data.

Model Assumptions and Limitations: The following assumptions were made in developing the kinetic model embodied in eqs 1-5:

1) The chemical structures of photoiniferter and end groups of reversibly deactivated polymer chains are assumed to be the same and initiate/reinitiate with identical kinetics. This assumption has been previously made in modeling of ATRP [24-25,27].

2) The proportionality constant, k' in eq 5 relates photopolymerization rate to the growth of polymer brush layer [33,34]. Although k' depends on the grafting density of the polymer brush, which, ostensibly, is a complex function of photopolymerization conditions, in the current model, k' is assumed to be constant.
3) Monomer concentration is assumed to be constant for SI-PMP. This assumption is often employed when describing SI-CRP from low surface-area substrates [4,8,38,39] and simplifies the model.

Methods. All simulations were carried out on a Dell (Pentium-4) platform using commercially available Polymath (Version 5.0) software. "STIFF" algorithm based on Rosenbrock methods [40] was used to solve the differential equations simultaneously.

4.3 Results and Discussion

Estimation of Unknown Kinetic Parameters and Validation of Kinetic Model. The values of unknown kinetic parameters, $[STR-DTC]_0$, $k_{t,rev}$, k_t, k' and k_p were obtained by fitting the experimental thicknesses as a function of time at $[TED]$ = 0 and 2 $\times$ 10^{-3} M (lowest and highest experimental $[TED]$ investigated in these studies) with the model predictions. This data-fitting procedure involved optimization of unknown kinetic parameters such that the values of sum of square error between the experimental data and model predictions were minimized. The optimum values of fitted kinetic parameters are listed in Table 4.1 along with the values of specified parameters. These parameters were

then used to simulate the growth of PMMA layers as a function of time at $[TED]$ = 0, 2 × 10^{-5}, 2 × 10^{-4} and 2 × 10^{-3} M.

Parameter	Value	Source
$[STR-DTC]_0$	2 × 10^{-5} M	Parameter Estimation
$k_a^{'}$	0.00152 s^{-1} at 5 mW/cm^2	Eq. 6; I_0 = 5 mW/cm^2
$k_{t,rev}$	6.6 × 10^7 M^{-1}.s	Parameter Estimation
k_t	30 × 10^9 M^{-1}.s	Parameter Estimation
$k_{a,TED}^{'}$	0.003198 s^{-1} at 5 mW/cm^2	Eq. 7; I_0 = 5 mW/cm^2
$k_{t,TED}$	2 × 10^5 M^{-1}.s	Plyusnin et al.[37]
$k^{'}k_p$	14.459 × 10^6 nm/M^2.s	Parameter Estimation

Table 4.1 Values of parameters used to simulate the variation of thickness as a function of time.

Figure 4.1 shows experimental results that capture the effect of [*TED*] on the growth of PMMA layers as a function of time and their comparison with the simulated time-dependent PMMA layer thickness profiles. It should be noted that the time axis for each $[TED]$ has been shifted to exclude the experimentally-observed initial lag period, where slow PMMA layer growth is seen. This slow growth/initial lag period has been previously attributed to PMMA layer growth within the "mushroom" regime [22]. Complete thickness profiles that include experimental data within the initial lag period are presented in Chapters 2 and 3 and in previous publications [22,23].

As can be seen from Figure 4.1, though the simulated PMMA layer thickness profiles do not match exactly with the experimental data, the important trends in PMMA layer thickness as a function of time can be predicted correctly using the described model, thereby validating the described simulation strategy. Notably, the model predicts

crossovers that are observed experimentally: at [*TED*] = 2×10^{-5} M, the thickness of the PMMA layer after 6 h of exposure (209 ± 5 nm) exceeds that of the sample polymerized without TED (162 ± 4 nm). Additionally, as shown in Figure 4.2, the model also correctly predicts the experimentally observed decrease in the maximum PMMA layer growth rate with increasing [*TED*].

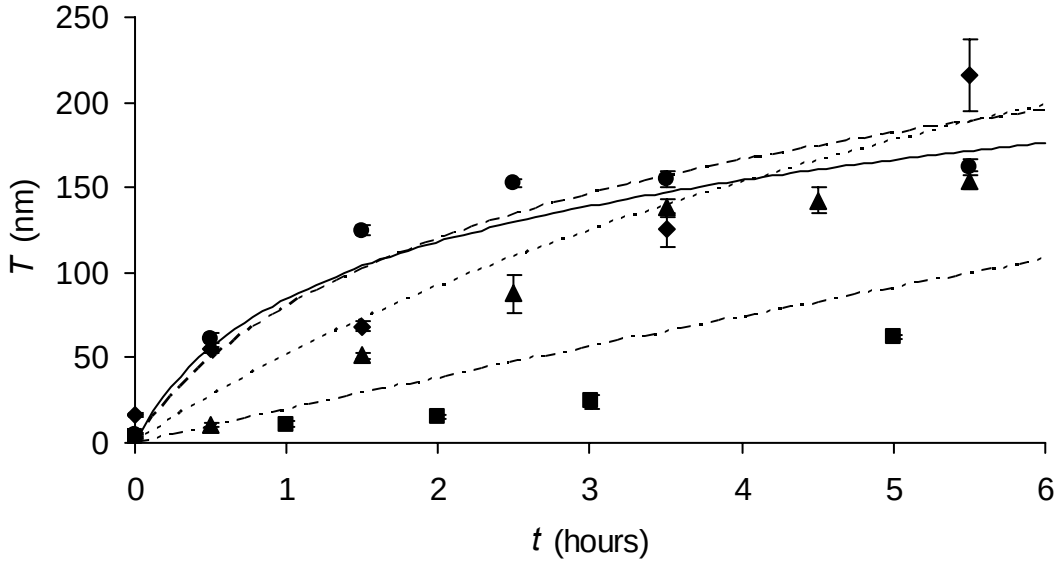

Figure 4.1 Comparison of the PMMA layer thicknesses synthesized at various TED concentrations and measured using variable angle ellipsometry as a function of time with simulated PMMA layer thicknesses. The symbols represent the experimental thicknesses while the lines are simulated thicknesses. Concentrations of TED in toluene were 0 M (●; continuous line), 2×10^{-5} M (♦; dashed line), 2×10^{-4} M (▲; dotted line) and 2×10^{-3} M (■; dashed-dotted line). The concentration of MMA in toluene used in these studies was 4.68 M and the light intensity was 5 mW/cm^2.

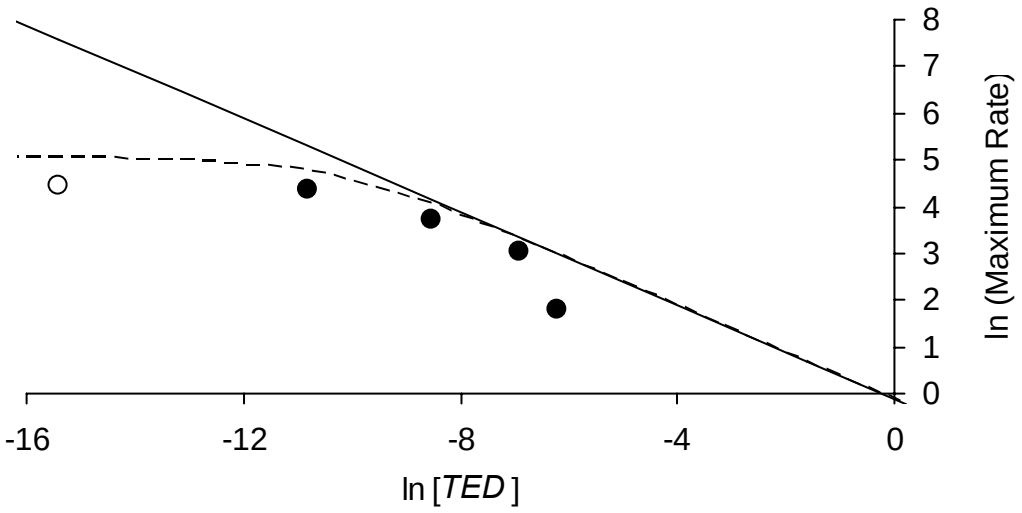

Figure 4.2 Comparison of experimentally observed maximum rates (●) as a function of TED concentration with the simulated maximum rates (broken line) and the predictions of simpler kinetic model that is valid during the initial stages when TED is in excess (thin solid line). The hollow circle represents the limiting case of when there was no TED preadded. On logarithmic scale, for $[TED] \geq 2 \times 10^{-5}$ M, the slope of maximum rate versus [*TED*] is -1/2 indicating that maximum rate decreases inversely with $[TED]^{1/2}$.

The described model and simulation strategy is also validated by comparing predictions of the maximum PMMA layer growth rate of the full model with predictions resulting from a simpler, pseudo-steady state model that is applicable during the initial stages of SI-PMP when PMMA layer growth rate is at its maximum. The pseudo-steady state model (complete derivation provided in Appendix F) is developed by simplifying the comprehensive model (eqs 1-5) according to following assumptions:

1) Irreversible termination reactions are negligible;
2) Pseudo-steady state is assumed for surface-tethered radicals and deactivating, DTC● radicals in solution;

3) [*TED*] is in considerable excess compared to [*STR-DTC*]$_0$ (the initial concentration of surface-tethered photoiniferter molecules);

4) TED activation is small such that $[TED]$ is equal to its initial value, $[TED]_0$.

Applying these assumptions produces the following expression for the concentration of surface-tethered radicals at pseudo-steady state, $[STR\bullet]_s$.

$$[STR\bullet]_s = \frac{k_a^{'}[STR-DTC]_0}{k_a^{'} + \sqrt{\frac{k_{a,TED}^{'}[TED]_0}{k_{t,TED}}}} \tag{8}$$

This expression for $[STR\bullet]_s$ can be substituted into eq 5 to obtain the (maximum) growth rate of the PMMA layers. Eq 8 suggests that $[STR\bullet]_s$ and, therefore, the maximum growth rate of PMMA layers decreases inversely with $[TED]_0^{1/2}$ when TED is in excess and activation is minimal (assumptions 3 and 4). Figure 4.2 compares the experimentally obtained maximum rates with the maximum rates obtained from simulations and predictions of pseudo-steady state model (eq 8) as a function of $[TED]_0$. The maximum rates from experimental results [23] were obtained from the slope of a straight line plotted through the first two data points for thickness of PMMA layers in brush regime. Similarly, to obtain the simulated maximum rates, thicknesses at t = 0 s (0 nm) and t = 0.012 hours were used. As can be seen from Figure 4.2, in the region of excess TED (for experimental system under consideration, $[TED] \geq 2 \times 10^{-5}$ M), the simulated maximum rates and maximum rates predicted using pseudo-steady state model agree with one another and decrease inversely with $[TED]_0^{1/2}$. Additionally, both the

comprehensive and pseudo-steady state model predictions agree reasonably well with the experimentally-obtained maximum PMMA layer growth rates as a function of [*TED*]. This agreement further validates described model and simulation strategy. The deviation seen in Figure 4.2 between the model predictions and the experimental data at [*TED*] = 2 $\times 10^{-3}$ M is likely due to two reasons: i) lower light intensity at the site of polymerization due to significant light absorption by TED in solution, and ii) significant monomer consumption *via* dithiocarbamyl radical-initiated polymerization in solution [23].

Effect of [*TED*] on PMMA Layer Growth. The observed decrease in maximum (initial) growth rate with increasing [*TED*] is a consequence of a decrease in the initial, instantaneous concentration of propagating surface-tethered radicals, which is brought about by a shift in the equilibrium between active, propagating radicals and dormant PMMA chains towards the dormant PMMA chains. In addition to a decrease in propagation rate (growth rate), the decrease in the concentration of propagating radicals also results in a decrease in irreversible termination reactions [24,41]. By virtue of this decrease in irreversible termination reactions with increasing [*TED*], the average lifetime of growing PMMA chains increases with [*TED*]. As a result, the maximum thickness, T_{max}, achievable by SI-PMP should increase with [*TED*]. Figure 4.3a shows the theoretical maximum thickness of PMMA layers as a function of [*TED*]. For the purpose of Figure 4.3a, T_{max} was defined as the thickness at which 99% of the tethered polymer chains are irreversibly terminated. As shown in Figure 4.3a, while T_{max} is approximately independent of [*TED*] at concentrations less than $[STR-DTC]_0$, for $[TED] > [STR-DTC]_0$, T_{max} is proportional to $[TED]^{1/2}$. However, it should be noted that the exposure time required to reach T_{max} also increases with [*TED*]. These increases in

T_{max} and exposure time required to reach T_{max}, both of which occur with increasing [*TED*], are consequences of the previously noted trade-off between continued propagation and increased irreversible termination reactions.

A decrease in the extent of termination with increasing [TED] also explains the crossover observed in experiments and simulations: after certain exposure time, thickness of PMMA layers synthesized in presence of TED exceeds the thickness of PMMA layers synthesized without TED or at lower [*TED*]. This leads to the realization that for a given exposure time, there should be an optimum [*TED*] that maximizes PMMA layer thickness. Figure 4.3b compares the experimentally observed and simulated PMMA layer thicknesses at various [*TED*] after 5.5 hours. As can be seen in Figure 4.3b, both experimental data and simulations suggest that there is an optimum [*TED*] that produces a maximum in PMMA layer thickness at the given polymerization time. This observation of an optimum [*TED*] is analogous to reports of an optimum catalyst concentration that yields maximum polymer layer thickness for surface-initiated ATRP of methyl acrylate [8].

Because the equilibrium between active propagating radicals and dormant polymer chains and, in turn, the trade-off between propagation and irreversible termination reactions is shifted by [*TED*], the optimum [*TED*] that yields maximum PMMA layer thickness should vary with the polymerization time. Figure 4.3c shows the simulated PMMA layer thicknesses as a function of [*TED*] at various polymerization times. As shown in Figure 4.3d, the optimum [*TED*] increases linearly with polymerization time and the slope of $[TED]_{opt}$ versus polymerization time plot is approximately equal to the value of $[STR - DTC]_0$ (2×10^{-5} M) used in the simulations.

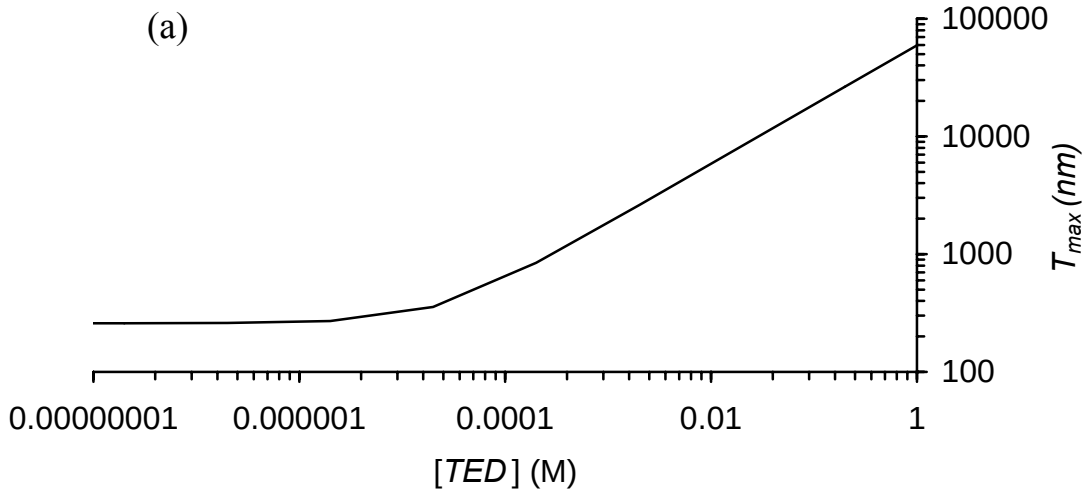
(a)
100000
10000
1000
100
T_{max} (nm)
0.00000001
0.000001
0.0001
0.01
1
[TED] (M)

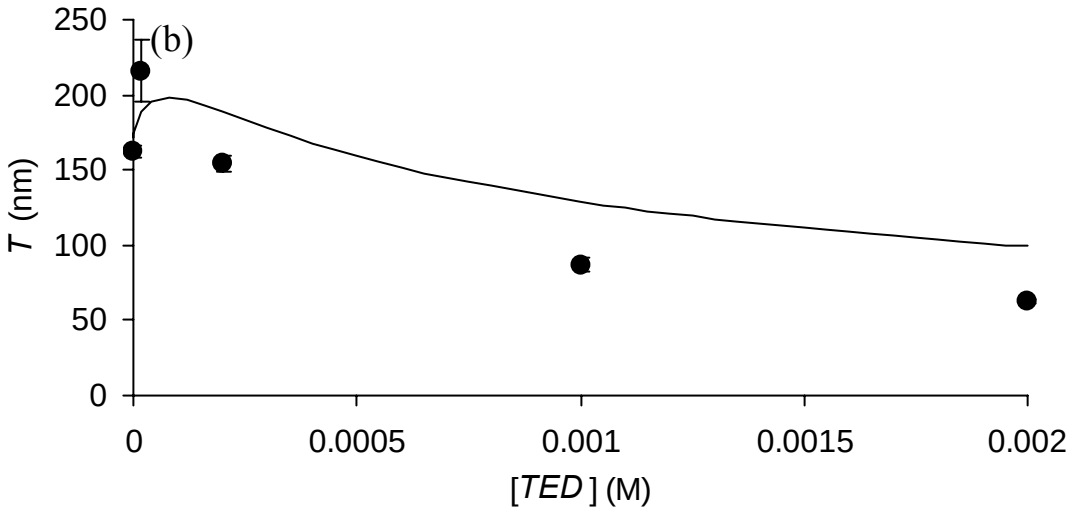
(b)
250
200
150
100
50
0
T (nm)
0
0.0005
0.001
0.0015
0.002
[TED] (M)

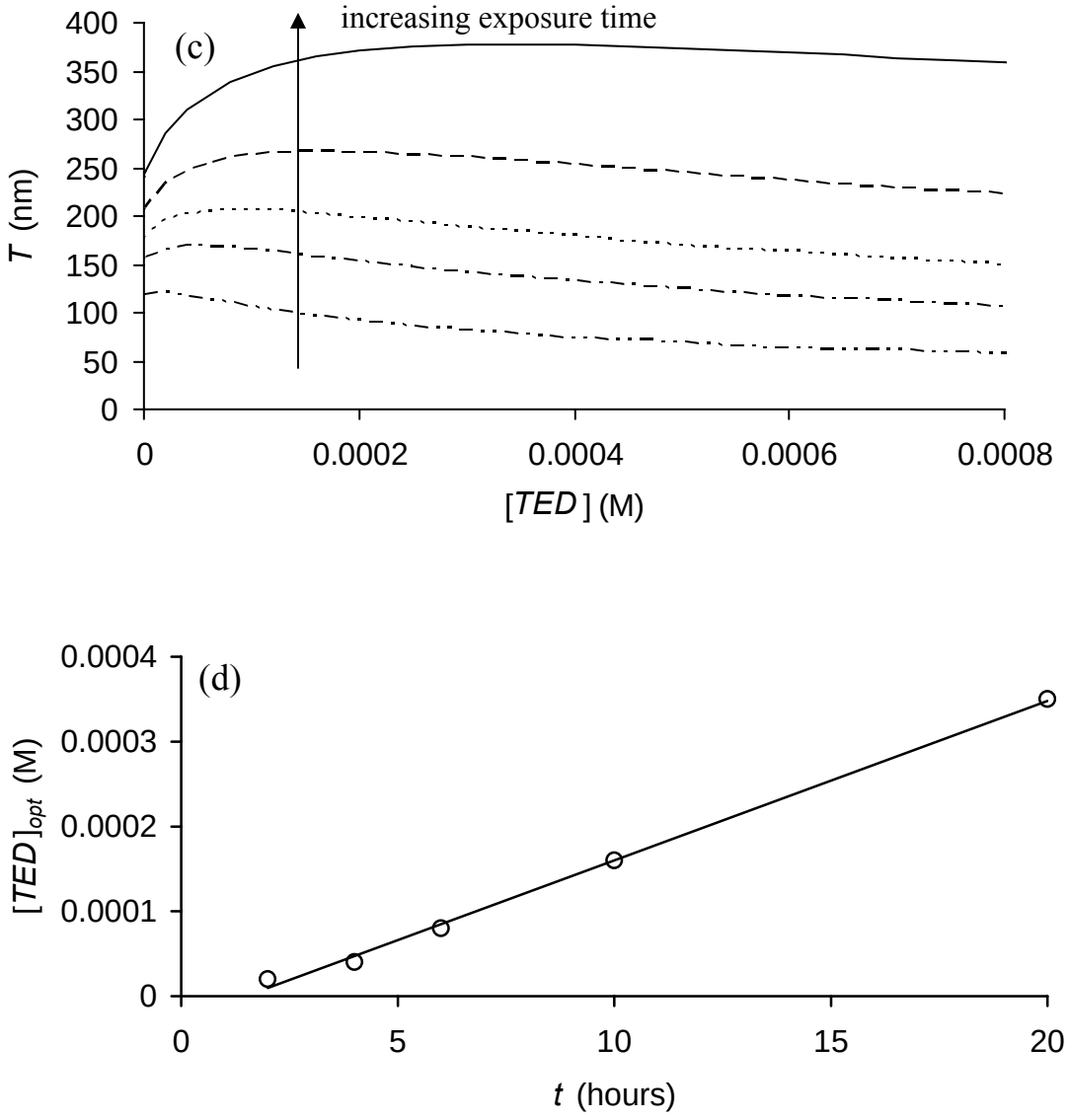

Figure 4.3 a) Simulated maximum PMMA layer thickness as a function of TED concentration. The light intensity used for simulations was 5 mW/cm^2. The maximum thicknesses at all TED concentration are defined as when 99% of the chains are irreversibly terminated. b) Comparison of the PMMA layer thicknesses synthesized at various TED concentrations and measured using variable angle ellipsometry (filled circles) as a function of TED concentration with simulated PMMA layer thicknesses (continuous line). The exposure time was 5.5 hours and light intensity was 5 mW/cm^2. c) Evolution of simulated PMMA layer thickness as a function of TED concentration at various exposure times, using I_0 = 5mW/cm^2. The exposure times of 2 hrs (dashed double-dotted line), 4 hrs (dashed-dotted line), 6 hrs (dotted line), 10 hrs (broken line) and 20 hrs (continuous line) are shown. d) Optimum [*TED*] that maximizes thickness as a function of exposure time. The hollow circles represent the simulated $[TED]_{opt}$ obtained from Figure 4.3c and thin solid line is a best-fit to $[TED]_{opt}$ as a function of exposure time.

In summary, preaddition of TED impacts PMMA layer growth by affecting the equilibrium between active, propagating radicals and dormant PMMA chains. Alternatively, this equilibrium can also be affected by manipulating the activation constant, $k_a^{'}$, *via* changes in light intensity. To investigate how light intensity affects PMMA layer growth, additional experiments and simulations were performed where light intensity was varied while keeping [*TED*] and [*M*] constant.

Effect of Light Intensity on PMMA Layer Growth. Using experimental data and results from simulations, Figure 4.4a shows the effect of light intensity on PMMA layer growth. The PMMA layer growth at I_0 = 5 mW/cm^2 ([*TED*] = 0 M and [*M*] = 4.68 M) matches very well with the simulated PMMA layer growth, which is expected because the model parameters used to simulate layer growth are obtained from best fits of these data at this I_0. However, the model overpredicts layer growth at 2 mW/cm^2. One obvious reason for this overprediction of the experimental data at I_0 = 2 mW/cm^2 is because the proportionality constant $k^{'}$, which relates the molecular weight of PMMA chains with the observed layer thickness, varies with grafting density. Because grafting density and, in turn, layer thickness is impacted by light intensity [42], the value of $k^{'}$ obtained by fitting the experimental thicknesses to the model predictions at one intensity value cannot be used for rigorous tests of behavior at other intensity values. Nevertheless, the trends observed in the experimental thickness data as a function of time are qualitatively predicted using the kinetic model. Both experimental results and simulations indicate that the maximum PMMA layer growth rate observed during the initial stages of SI-PMP increases with light intensity. Furthermore, in the latter stages of polymerization,

the thickness of a PMMA layer grown at lower intensity exceeds the thickness at higher intensity.

In a fashion similar to the analysis of effect of [*TED*] on PMMA layer growth, the effect of light intensity can be understood by studying its effect on the i) maximum growth rate during the initial stages of polymerization, ii) maximum layer thickness, and iii) crossover of thickness versus time profiles. Figure 4.4b shows the effect of light intensity on maximum growth rate. On this log-log plot, the predicted maximum growth rate increases with light intensity with a slope of approximately 0.5, indicating that the maximum growth rate is proportional to $I_0^{1/2}$. This square-root dependence of maximum rate on light intensity is consistent with the model developed in Chapter 2 that incorporates bimolecular termination, and as result, suggests a square root dependence of initial surface-tethered radicals on light intensity [22]. Conversely, the maximum PMMA layer thickness, T_{max} (defined as the thickness at which 99 % of the tethered polymer chains are irreversibly terminated), is inversely proportional to $I_0^{1/2}$ (Figure 4.4c). Analogous yet opposite to the effect of [*TED*] on PMMA layer growth, these effects of light intensity on maximum growth rate and maximum thickness is again a consequence of the trade-off between propagation and irreversible termination reactions. As a result of this trade-off, for a given polymerization time, there exists an optimum light intensity that maximizes PMMA layer thickness (Figure 4.4d). This observation of optimum light intensity is in agreement with the previously obtained results of surface-initiated UV-light induced radical polymerization of styrene [42]. As shown in Figure 4.4e, optimum light intensity is inversely proportional to exposure time.

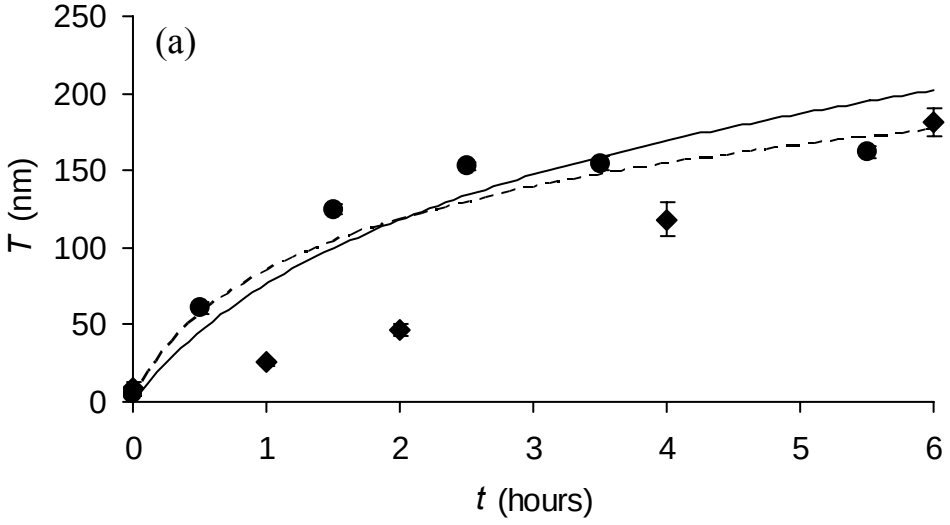
(a)
250
200
150
100
50
0
T (nm)
0
1
2
3
4
5
6
t (hours)

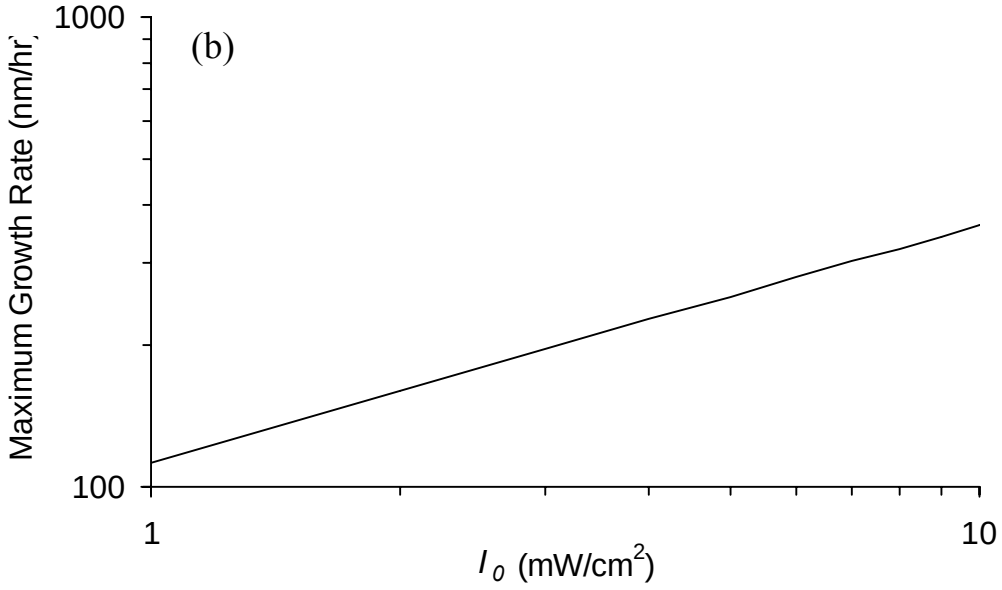
(b)
1000
100
Maximum Growth Rate (nm/hr)
1
10
I0 (mW/cm2)

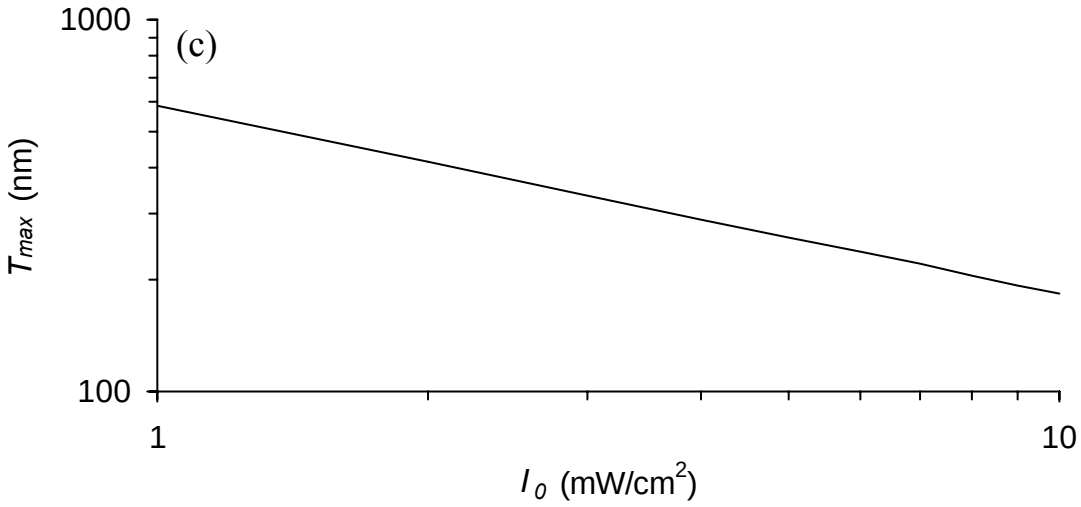
(c)
1000
100
1
10
T_{max} (nm)
I_0 (mW/cm^2)

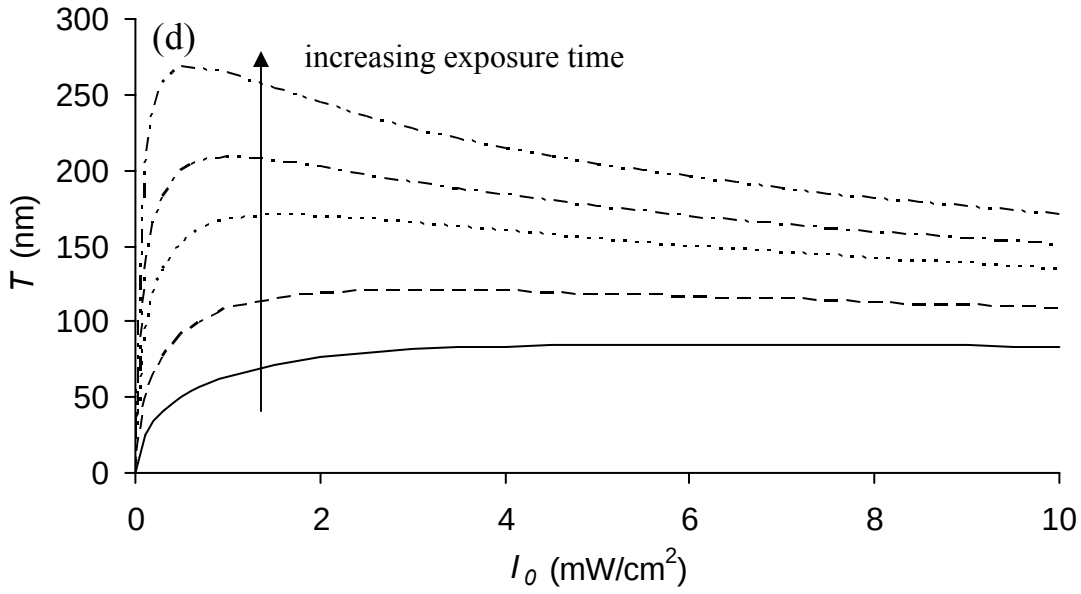
(d)
increasing exposure time
300
250
200
150
100
50
0
0
2
4
6
8
10
T (nm)
I_0 (mW/cm^2)

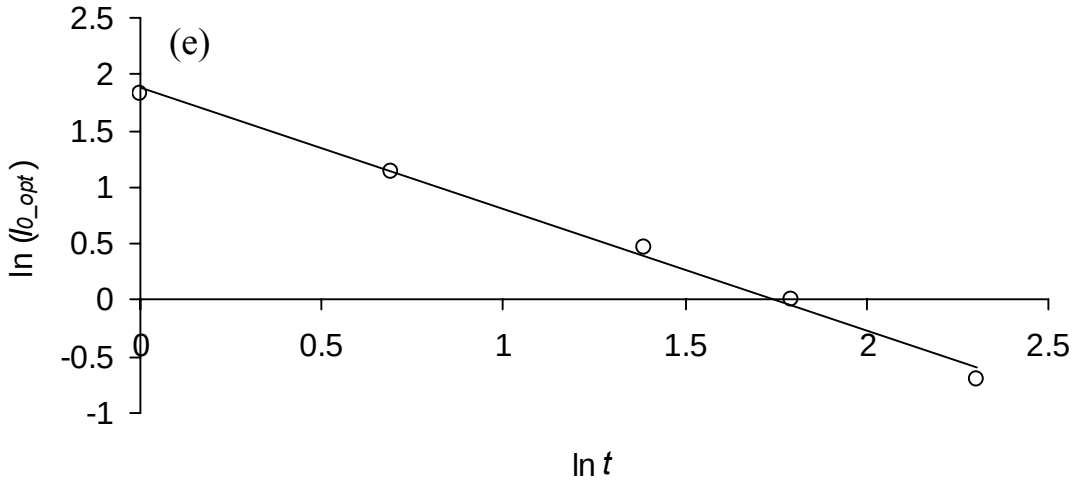

Figure 4.4 a) Comparison of the PMMA layer thicknesses synthesized at various intensities and measured using variable angle ellipsometry as a function of time with simulated PMMA layer thicknesses. The lines in this plot are the simulated PMMA layer thicknesses. Light intensities used were 2 mW/cm^2 (♦; thin line) and 5 mW/cm^2 (●; broken line). b) Simulated maximum rates as a function of light intensity. c) Simulated maximum PMMA layer thickness as a function of light intensity. The maximum thicknesses are defined as the thickness at which 99% of the chains are irreversibly terminated. d) Evolution of simulated PMMA layer thickness as a function of light intensity at various exposure times. The exposure times were 1 hr (continuous line), 2 hrs (broken line), 4 hrs (dotted line), 6 hrs (dashed-dotted line) and 10 hrs (dashed double-dotted line). The [*TED*] used for simulations was 0 M. e) Optimum light intensity that maximizes layer thickness as a function of exposure time. [*TED*] used for simulations was 0 M. The hollow circles represent the simulated I_{0_opt} obtained from Figure 4.4d and thin solid line is a best-fit to I_{0_opt} as a function of exposure time.

Effect of [*TED*] and Light Intensity on Reinitiation Ability of PMMA Layers.

As discussed earlier, increasing [*TED*] and decreasing light intensity affect the PMMA layer growth in similar fashion. To investigate how these two parameters affect the reinitiation ability of PMMA layers, I defined a "fraction of non-terminated species", f_{NT}, which represents the fraction of surface-tethered photoiniferter molecules that have produced actively growing PMMA chains at a particular point during the SI-

PMP process, and tracked f_{NT} as the layer grows. As shown by eq 9, f_{NT} can be represented as the ratio of active propagating radicals plus dormant yet non-terminated PMMA chains, $[STR-DTC]_D$), to the initial photoiniferter concentration:

$$f_{NT} = \frac{[STR\bullet]+[STR-DTC]_D}{[STR-DTC]_0} \tag{9}$$

It should be noted $[STR-DTC]_D$ represents the concentration of dormant (reversibly terminated polymer chains) and obtained using eq 10.

$$[STR-DTC]_D = (1-f_{NI})[STR-DTC]_0 - \frac{[STR\bullet]}{[STR-DTC]_0} \tag{10}$$

where f_{NI} is the fraction of noninitiated chains, defined in eq 11:

$$f_{NI} = \exp(-k_a^{'}t) \tag{11}$$

Thus, f_{NT} represents the concentration of chains in the layer that can initiate and/or propagate during reinitiation in the presence of a second monomer to form block copolymer structures. Consequently, f_{NT} provides a measure of the reinitiation ability of any (PMMA) brush layer.

Figures 4.5a and 4.5b show the effect of [*TED*] and light intensity on reinitiation ability of PMMA layers, respectively, as the layer grows. The shapes of curves in Figures

4.5a and 4.5b immediately suggest that TED and light intensity have marked differences in their impact on continuation of layer growth. As evident from Figure 4.5a, for a given PMMA layer thickness, f_{NT} and, in turn, reinitiation ability increase with increasing [*TED*]. Additionally, Figure 4.5a suggests that f_{NT} increases at low thicknesses (at shorter exposure times), goes through a maximum, and then decreases as higher thicknesses (or longer exposure times) are reached. This pattern of behavior of f_{NT} as a function of PMMA layer thickness (or exposure time) is a consequence of the balance between initiation and irreversible termination reactions involved in SI-PMP. During the initial stages of SI-PMP, initiation reactions dominate, resulting in a build-up of growing surface-tethered polymer chains (active or dormant). Once a significant number of surface-tethered photoiniferter species initiate and begin forming PMMA chains, irreversible termination reactions become dominant (as more and more chains irreversibly terminate as the reaction progresses), leading to a decrease in f_{NT} as thickness (or exposure time) increases.

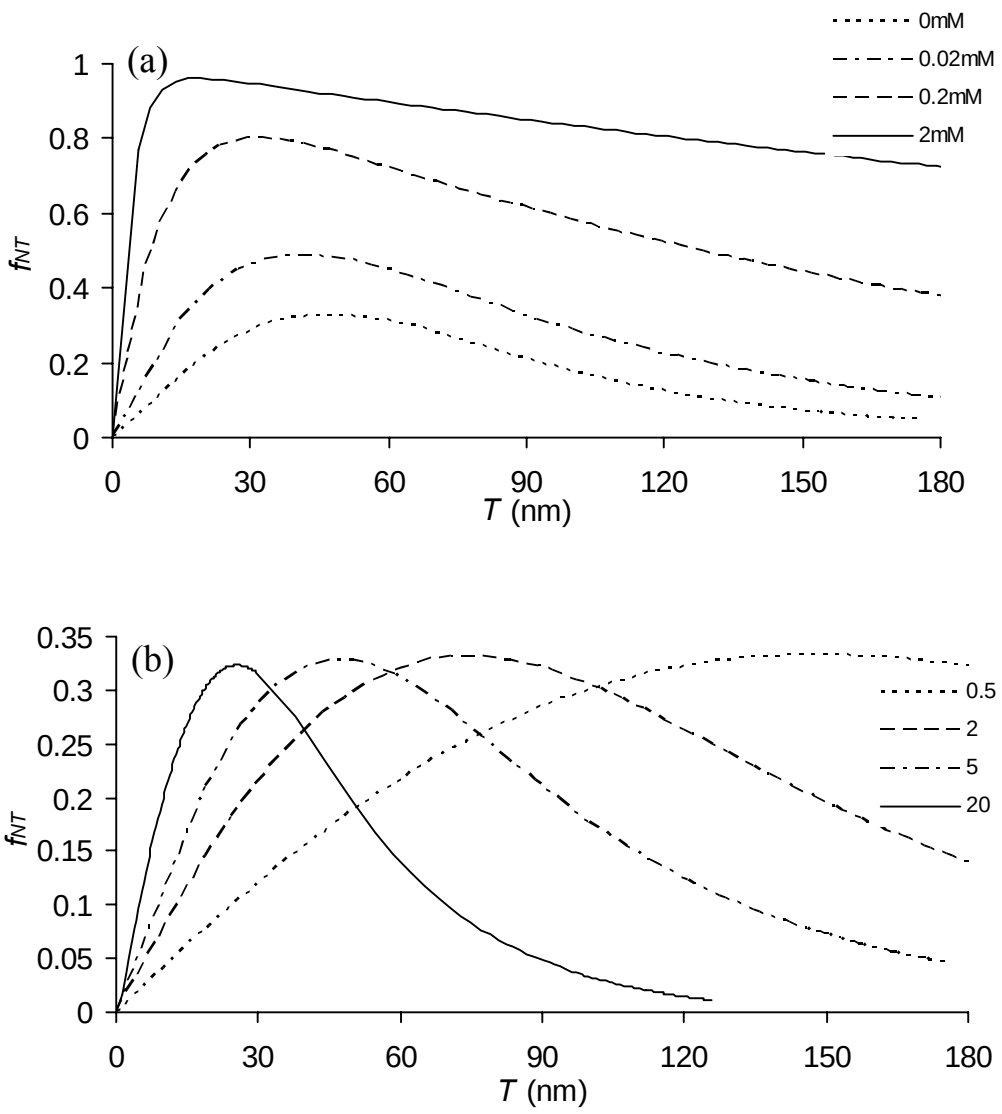

Figure 4.5 a) Simulated fraction of non-terminated species as a function of thickness of PMMA layers at various TED concentrations. TED concentrations were 0 M (dotted line), 2×10^{-5} M (dashed-dotted line), 2×10^{-4} M (broken line) and 2×10^{-3} M (continuous line). The light intensity used for simulations was 5 mW/cm^2. b) Simulated fraction of non-terminated species as a function of thickness of PMMA layers at various light intensities. The light intensities were 0.5 mW/cm^2 (dotted line), 2 mW/cm^2 (broken line), 5 mW/cm^2 (dashed-dotted line) and 20 mW/cm^2 (continuous line). TED concentration used for simulations was 0 M.

Because the addition of actively growing chains to any PMMA layer via initiation of the photoiniferter molecules depends on light intensity, the time or layer thickness at which the f_{NT} profile reaches its maximum value is also affected by light intensity as shown in Figure 4.5b. Because the initiation process is prolonged as light intensity is decreased, the PMMA layer thickness (or exposure time) at which the maximum f_{NT} occurs increases as light intensity is decreased. However, the maximum f_{NT} value is independent of light intensity.

This leads to a significant conclusion: while increasing [*TED*] improves the reinitiation ability of the tethered PMMA layers, decreasing light intensity does not improve reinitiation ability. Rather, decreasing light intensity results in an increase in layer thickness (or exposure time) at which maximum reinitiation ability is achieved. Also, it is worth emphasizing that during reinitiation (a second polymerization) of PMMA layers formed using the SI-PMP process to form a block copolymer brush, surface-tethered photoiniferter molecules that were not initiated when the PMMA brush was made will initiate and propagate growth of the second polymer (hereafter referred to as P2) directly from the substrate surface. In this case, a mixed brush consisting of PMMA-*block*-P2 chains, homopolymer PMMA chains irreversibly terminated during the first exposure, and P2 homopolymer chains will be made. The relative amount of P2 chains attached directly to surface and P2 chains attached to pre-existing PMMA chains can be represented by the ratio f_{NI} / f_{NT}.

For an existing PMMA layer with $f_{NI} / f_{NT} >> 1$, homopolymer P2 chains tethered directly to surface will be prevalent following a second polymerization (reinitiation with second monomer). Conversely, for a PMMA layer with $f_{NI} / f_{NT} << 1$,

the second polymerization step will result largely in the formation of PMMA-*block*-P2 chains. To identify the photopolymerization conditions that favor the formation of block-copolymers rather than mixed polymer brushes (and vice-versa), one should examine the impact of various reaction conditions on f_{NI}/f_{NT}. In order to make a fair comparison, sets of photopolymerization conditions must be chosen where the PMMA layers have grown to identical states. Specifically, I seek pairs of conditions where both PMMA layer thickness and fraction of irreversibly terminated chains vary identically as a function of time. Such photopolymerization conditions can be readily identified by choosing those with similar surface-tethered radical concentration ($[STR\bullet]$) profiles. Knowing that increasing [*TED*] and decreasing light intensity affect PMMA layer growth in similar fashion, I chose to compare f_{NI}/f_{NT} for PMMA layers synthesized in the presence of TED (photopolymerization condition set A: [*TED*] = 2×10^{-4} M; I_0 = 5 mW/cm^2) and in absence of TED but at a lower intensity (photopolymerization condition set B: [TED] = 0 M; I_0 = 0.5 mW/cm^2).

Figure 4.6a shows how PMMA layers synthesized at reaction conditions A and B exhibit identical radical concentrations and fraction of terminated chains as functions of PMMA layer thickness (Note that the fraction of terminated chains is given by $f_T = 1 - f_{NT} - f_{NI}$ and thus is consistent with the fact that the definition of f_{NT} considers only initiated chains). Therefore, PMMA *layers* of identical thickness, when synthesized under either set of reaction conditions, will have identical fractions of species that can initiate and propagate ($f_{NI} + f_{NT}$) to form P2 chains during the second polymerization step. However, in these two systems, the individual PMAA *chains* are initiated at

different rates, and therefore, result in different reinitiation abilities for the PMMA chains formed under each reaction set.

Figure 4.6b shows the comparison of f_{NI}/f_{NT} for PMMA layers synthesized under photopolymerization conditions A (solid line) and B (broken line) as a function of layer thickness. This ratio provides a quantitative indication of the type of layer architecture that will be formed by reinitiation and growth of P2 chains from the already formed PMMA brush. The dotted line at $f_{NI}/f_{NT} = 1$ represents the situation where, after the second polymerization step (reinitiation), the layer will consist of an equal number of P2 chains attached to the underlying PMMA chains (diblock copolymer) and P2 chains attached directly to surface (P2 homopolymer). Thus, at this condition, the layer is a mixture of diblock copolymers and P2 homopolymers. As shown in Figure 4.6b, in the region below the dotted line where $f_{NI}/f_{NT} << 1$, diblock copolymer formation is favored compared to formation of P2 homopolymer. Conversely, formation of a homopolymer mixed brush is favored for systems with low initiation rates and/or low reinitiation abilities ($f_{NI}/f_{NT} >> 1$). For both sets of reaction conditions described in Figure 4.6b, f_{NI}/f_{NT} decreases as PMMA layer thickness increases. However, f_{NI}/f_{NT} drops much more quickly as a function of thickness under condition A (with TED) than observed for condition B (no TED). Therefore, PMMA layers synthesized under photopolymerization condition A favor formation of block copolymer structures over a much broader range of thickness values than PMMA layers synthesized under condition B. Furthermore, without TED present (condition B), block copolymer formation is only favored for PMMA layers greater than 100nm thick. According to Figure 4.6a, by this point in the photopolymerization over 40% of the initial

photoiniferter sites have been terminated. This means that even under ideal block copolymer formation conditions, no more than 60% of the PMMA chains will reinitiate to form PMMA-*block*-P2 chains. Alternatively, by using a relatively small concentration of TED (condition A), diblock copolymer brushes can be readily formed from PMMA layers less than 50 nm in thickness when less than 20% of the total initiator sites have been terminated. Taken together, these predictions indicate that PMMA layers synthesized in presence of a higher [TED] and at higher light intensities are more likely to form block-copolymer brushes after the second polymerization step (reinitiation) as compared to PMMA layers synthesized at lower [TED] and lower light intensities.

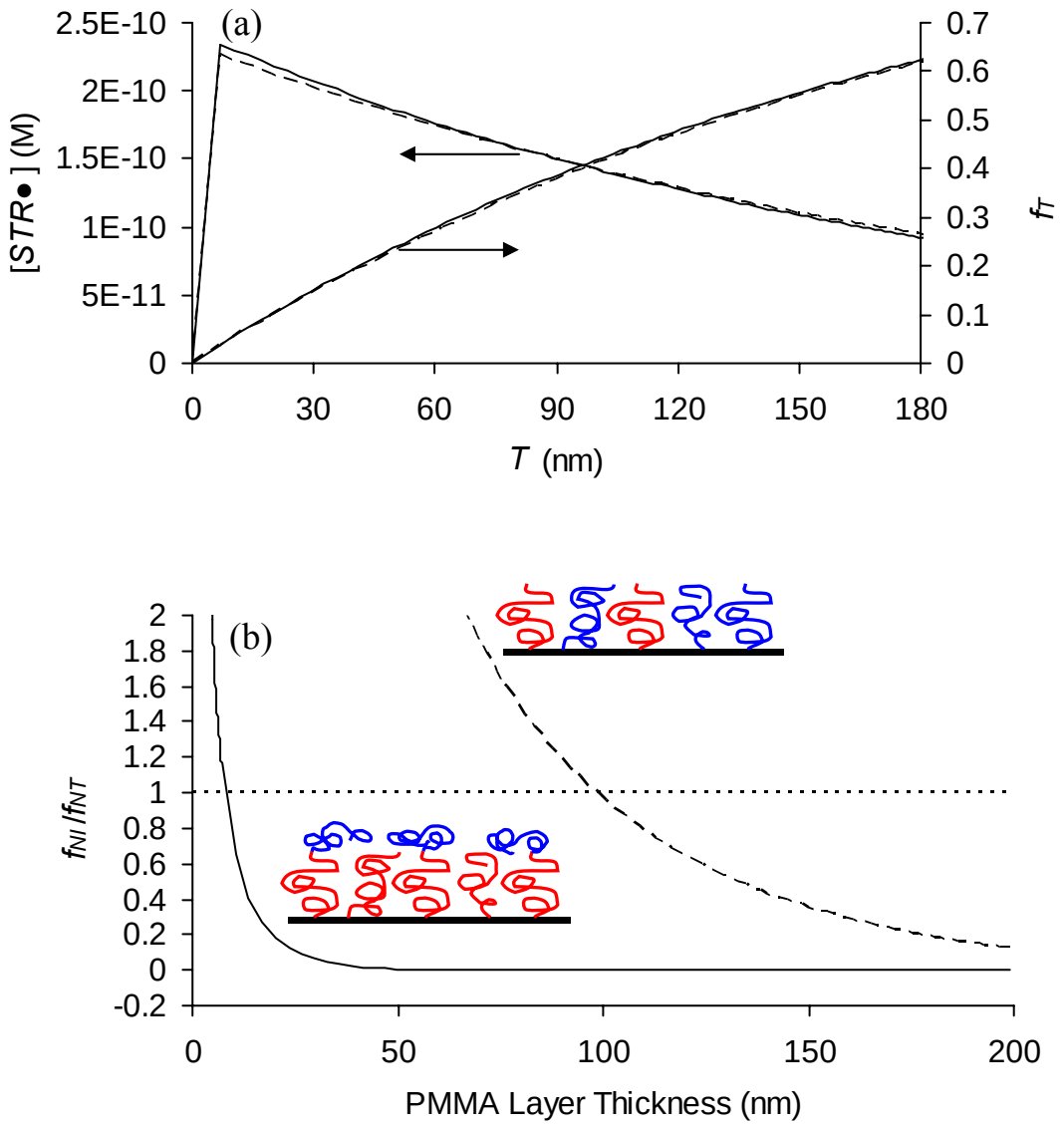

Figure 4.6 a) Comparison of simulated surface-tethered radical concentrations and fraction of terminated species as a function of thickness of PMMA layers synthesized at [*TED*] = 2×10^{-4} M; I_0 = 5 mW/cm^2 (continuous line) and [*TED*] = 0 M; I_0 = 0.5 mW/cm^2 (broken line). b) Comparison of simulated ratio of fraction of uninitiated photoiniferter species to fraction of non-terminated species as a function of thickness of PMMA layers synthesized at [*TED*] = 0.0002 M; I_0 = 5 mW/cm^2 (continuous line) and [*TED*] = 0 M; I_0 = 0.5 mW/cm^2 (broken line).

Effect of Initial Photoiniferter Concentration on Kinetics of Growth and Reinitiation Ability of PMMA Layers. Because thickness of the PMMA layer is impacted by grafting density, the initial photoiniferter concentration, $[STR\text{-}DTC]_0$, plays an important role in the growth kinetics of PMMA layers. In order to generalize the effect of $[STR\text{-}DTC]_0$ at all $[TED]$, in the described simulations, the effect of $[STR\text{-}DTC]_0$ was examined by simulating PMMA layer growth as a function of time at various $[TED]/[STR-DTC]_0$ ratios. It was observed that for a given $[TED]/[STR-DTC]_0$ ratio, PMMA layer thickness varies identically as a function of time at all $[STR-DTC]_0$ when normalized with square root of $[STR-DTC]_0$ (Figure 4.7a). This normalization strategy was verified for the values of $[STR-DTC]_0$ ranging from 2×10^{-6} to 2×10^{10} M. As shown in Figure 4.7a, increases in $[TED]/[STR-DTC]_0$ affect the normalized PMMA layer thickness in a fashion similar to the effect of $[TED]$ on PMMA layer growth described earlier (Figure 4.1). Similarly, as shown in Figure 4.7b, the pattern of behavior captured by the reinitiation ability as a function of normalized PMMA layer thickness with increases in $[TED]/[STR-DTC]_0$ is identical to that observed for the effect of $[TED]$ on reinitiation ability (Figure 4.5a) at $[STR-DTC]_0$ of 2×10^5 M. This indicates that this normalization strategy can be used to predict the thickness and reinitiation ability of PMMA layers with any desired value of $[TED]/[STR-DTC]_0$ and $[STR-DTC]_0$ if the thickness profile is available for a PMMA layer polymerized at any arbitrary $[STR-DTC]_0$ value.

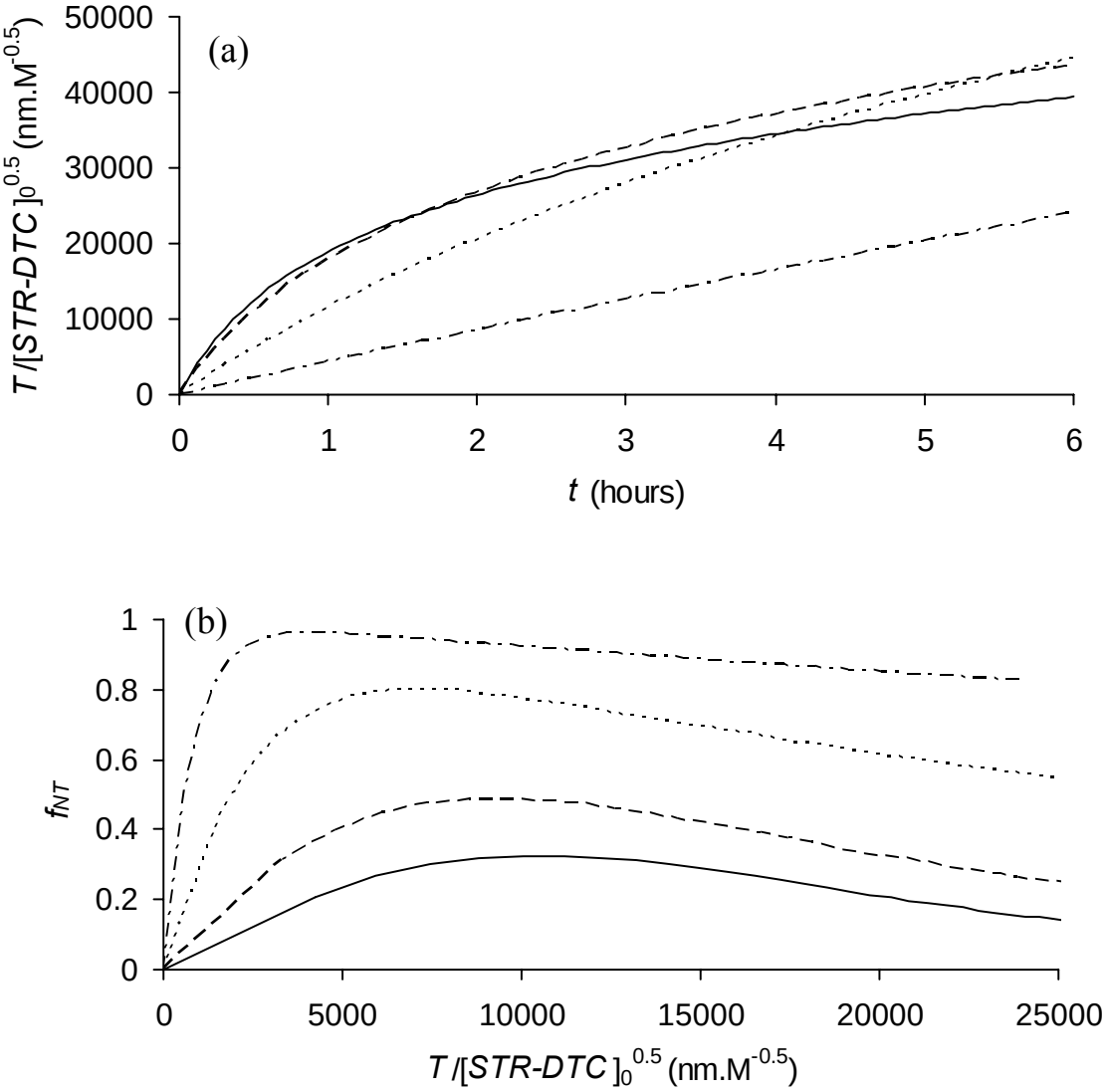

Figure 4.7 Effect of [*TED*]/[*STR-DTC*]$_0$ on a) evolution of PMMA layer thickness normalized with square root of [*STR-DTC*]$_0$ as a function of exposure time and b) fraction of non-terminated chains as a function of PMMA layer thickness normalized with square root of [*STR-DTC*]$_0$. [*TED*]/[*STR-DTC*]$_0$ were 0 (continuous line), 1 (broken line), 10 (dotted line) and 100 (dashed-dotted line). The light intensity used for simulations was 5 mW/cm^2.

4.4 Conclusions

The kinetic model developed in this work provides significant insight into surface-initiated photoiniferter-mediated photopolymerization of MMA. Buttressed by experimental results, the model predictions indicate that increasing [*TED*] and decreasing light intensity impact the PMMA layer growth in similar fashions. While the maximum layer growth rate observed during the initial stages of SI-PMP decreases with increasing [*TED*] and decreasing light intensity, the maximum thickness achievable increases. Using simulations I have shown that the effect of [*TED*] and light intensity on the reinitiation ability of PMMA layers are significantly different: Reinitiation ability increases with increasing [*TED*], whereas decreasing light intensity does not improve reinitiation ability, but increases layer thickness (exposure time) at which maximum reinitiation ability is achieved. A comparison of effects of [*TED*] and light intensity on reinitiation ability show that choice of photopolymerization conditions for the first polymerization step (PMMA layer synthesis) is critical to the final structure of the polymer brush created upon reinitiation (second polymerization step). PMMA layers formed in the presence of TED are more likely to form block copolymers as compared to PMMA layers synthesized without TED and at lower light intensity.

It should be pointed out that without *a priori* determination of all the kinetic parameters, the described model is incapable of predicting absolute values of various polymer brush properties (thickness, reinitiation ability). However, the trends predicted by this model are reasonably accurate and, therefore, within its limitations, the model developed in this work may constitute a useful guide for choosing appropriate

photopolymerization conditions for synthesizing well-defined block and mixed polymer brush layers by SI-PMP. These systems are important constructs for the development of "smart" polymer layers that adapt their conformation and display a suite of interfacial properties as environmental conditions are changed.

4.5 References

1. Matyjaszewski, K. "Comparison and Classification of Controlled/Living Radical Polymerizations". *In Controlled/Living Radical Polymerization: Advances in ATRP, NMP and RAFT*; Matyjaszewski, K., Eds.; ACS Symposium Series 768; American Chemical Society; Washington, DC, **2000**; p 2-26.

2. Zhao, B.; Brittain, W. J. "Polymer Brushes: Surface-Immobilized Macromolecules", *Prog. Poly. Sci.* **2000**, *25*, 677-710.

3. Ejaz, M.; Yamamoto, S.; Ohno, K.; Tsujii, Y.; Fukuda, T. "Controlled Graft Polymerization of Methyl Methacrylate on Silicon Substrate by the Combined Use of the Langmuir-Blodgett and Atom Transfer Radical Polymerization Techniques", *Macromolecules* **1998**, *31*, 5934-5936.

4. Matyjaszewski, K.; Miller, P. J.; Shukla, N.; Immaraporn, B.; Gelman, A.; Luokala, B. B.; Siclovan, T. M.; Kickelbick, G.; Vallant, T.; Hoffmann, H.; Pakula, T. "Polymers at Interfaces: Using Atom Transfer Radical Polymerization in the Controlled Growth of Homopolymers and Block Copolymers from Silicon Surfaces in the Absence of Untethered Sacrificial Initiator", *Macromolecules* **1999**, *32*, 8716-8724.

5. Zhao, B.; Brittain, W. J. "Synthesis, Characterization, and Properties of Tethered Polystyrene-*b*-Polyacrylate Brushes on Flat Silicate Substrates", *Macromolecules* **2000**, *33*, 8813-8820.

6. Shah, R. R.; Merreceyes, D.; Husemann, M.; Rees, I.; Abbott, N. L.; Hawker, C. J.; Hedrick, J. L. "Using Atom Transfer Radical Polymerization to Amplify Monolayers of Initiators Patterned by Microcontact Printing into Polymer Brushes for Pattern Transfer", *Macromolecules* **2000**, *33*, 597-605.

7. Ejaz, M.; Tsujii, Y.; Fukuda, T. "Controlled Grafting of a Well-defined Polymer on a Porous Glass Filter by Surface-Initiated Atom Transfer Radical Polymerization", *Polymer* **2001**, *42*, 6811-6815.

8. Kim, J. B.; Huang, W.; Miller, M. D.; Baker, G. L.; Bruening, M. L. "Kinetics of Surface-Initiated Atom Transfer Radical Polymerization", *J. Poly. Sci.:Part A: Poly. Chem.* **2003**, *41*, 386-394.

9. Boyes, S. G.; Granville, A. M.; Baum, M.; Akgun, B.; Mirous, B. K.; Brittain, W. J. "Polymer Brushes–Surface Immobilized Polymers", *Surf. Sci.* **2004**, *570*, 1-12.

10. Husseman, M.; Malmström, E. E.; McNamara, M.; Mate, M.; Mecerreyes, D.; Benoit, D. G.; Hedrik, J. L.; Mansky, P.; Huang, E.; Russell, T. P.; Hawker, C. J. "Controlled Synthesis of Polymer Brushes by "Living" Free Radical Polymerization Techniques", *Macromolecules* **1999**, *32*, 1424-1431.

11. Husemann, M.; Morrison, M.; Benoit, D.; Frommer, J.; Mate, C. M.; Hingsberg, W. D.; Hedrik, J. L.; Hawker, C. J. "Manipulation of Surface Properties by Patterning of Covalently Bound Polymer Brushes", *J. Am. Chem. Soc.* **2000**, *122*, 1844-1845.

12. Bartholome, C.; Beyou, E.; Bourgeat-Lami, E.; Chaumont, P.; Zydowicz, N. "Nitroxide-Mediated Polymerizations from Silica Nanoparticle Surfaces: "Graft from" Polymerization of Styrene Using a Triethoxysilyl-Terminated Alkoxyamine Initiator", *Macromolecules* **2003**, *36*, 7946-7952.

13. Tsujii, Y.; Ejaz, M.; Sato, K.; Goto, A.; Fukuda, T. "Mechanism and Kinetics of RAFT-Mediated Graft Polymerization of Styrene on a Solid Surface. 1. Experimental Evidence of Surface Radical Migration", *Macromolecules* **2001**, *34,* 8872-8878.

14. Baum, M.; Brittain, W. J. "Synthesis of Polymer Brushes on Silicate Substrates Reversible Addition Fragmentation Chain Transfer Technique", *Macromolecules* **2002**, *35*, 610-615.

15. Nakayama, Y.; Matsuda, T. "Surface Macromolecular Architectural Designs Using Photo-Graft Copolymerization Based on Photochemistry of Benzyl *N*,*N*-Diethyldithiocarbamate", *Macromolecules* **1996**, *29*, 8622-8630.

16. Luo, N.; Metters, A. T.; Hutchison, J. B.; Bowman, C. N.; Anseth, K. S. "A Methacrylated Photoiniferter as a Chemical Basis for Microlithography: Micropatterning Based on Photografting Polymerization", *Macromolecules* **2003**, *36*, 6739-6745.

17. Higashi, J.; Nakayama, Y.; Marchant, R. E.; Matsuda, T. "High-Spatioresolved Microarchitectural Surface Prepared by Photograft Copolymerization Using Dithiocarbamate: Surface Preparation and Cellular Responses", *Langmuir* **1999**, *15*, 2080-2088.

18. Kobayashi, T.; Takahashi, S.; Fujii, N. "Silane Coupling Agent Having Dithiocarbamate Group for Photografting of Sodium Styrene Sulfonate on Glass Surface", *J. App. Polym. Sci.* **1993**, *49*, 417-423.

19. de Boer, B.; Simon, H. K.; Werts, M. P. L.; van der Vegte, E. W.; Hadziioannou, G. ""Living" Free Radical Photopolymerization Initiated from Surface-Grafted Iniferter Monolayers", *Macromolecules* **2000**, *33*, 349-356.

20. Qin, S. H.; Qiu, K. Y. "A New Polymerizable Photoiniferter for Preparing Poly(methyl methacrylate) Macromonomer ", *Eur. Poly. J.* **2001**, *37*, 711-717.

21. Nakayama, Y.; Matsuda, T. "*In-Situ* Observation of Dithiocarbamate-Based Surface Photograft Copolymerization Using Quartz Crystal Microbalance", *Macromolecules* **1999**, *32*, 5405-5410.

22. Rahane, S. B.; Kilbey, S. M., II; Metters, A. T. "Kinetics of Surface-Initiated Photoiniferter-Mediated Photopolymerization", *Macromolecules* **2005**, *38*, 8202-8210.

23. Rahane, S. B.; Metters, A. T.; Kilbey, S. M., II "Impact of Added Tetraethylthiuram Disulfide Deactivator on the Kinetics of Growth and Reinitiation of Poly(methyl methacrylate) Brushes Made by Surface-Initiated Photoiniferter-Mediated Photopolymerization", *Macromolecules* **2006**, *39*, 8987-8991.

24. Fischer, H. "The Persistent Radical Effect in "Living" Radical Polymerization", *Macromolecules* **1997**, *30*, 5666-5672.

25. Fischer, H. "The Persistent Radical Effect in Controlled Radical Polymerizations", *J. Poly. Sci. Part A: Poly. Chem.* **1999**, *37*, 1885-1901.

26. Butté, A.; Storti, G.; Morbidelli, M. "Kinetics of "Living" Free Radical Polymerization", *Chem. Eng. Sci.* **1999**, *54*, 3225-3231.

27. Zhu, S. "Modeling of Molecular Weight Development in Atom Transfer Radical Polymerization", *Macromol. Theory Simul.* **1999**, *8*, 29-37.

28. He, J.; Li, L.; Yang, Y. "Monte Carlo Simulation on Rate Enhancement of Nitroxide-Mediated Living Free-Radical Polymerization", *Macromol. Theory Simul.* **2000**, *9*, 463-468.

29. Zhang, M.; Ray, W. H. "Modeling of "Living" Free-Radical Polymerization Processes. I. Batch, Semibatch, and Continuous Tank Reactors", *J. App. Poly. Sci.* 2002, *86*, 1630-1662.

30. Wang, A. R.; Zhu, S. "Modeling the Reversible Addition-Fragmentation Transfer Polymerization Process", *J. Poly. Sci. Part A: Poly. Chem.* **2003**, *41*, 1553-1566.

31. Wang, A. R.; Zhu, S. "Calculations of Monomer Conversion and Radical Concentration in Reversible Addition-Fragmentation Chain Transfer Radical Polymerization", *Macromol. Theory Simul.* **2003**, *12*, 663-668.

32. Genzer, J. "In Silico Polymerization: Computer Simulation of Controlled Radical Polymerization in Bulk and on Flat Surfaces", *Macromolecules* **2006**, *39*, 7157-7169.

33. Sankhe, A. Y.; Husson, S. M.; Kilbey, S. M., II "Direct Polymerization of Surface-Tethered Polyelectrolyte Layers in Aqueous Solution via Surface-Confined Atom Transfer Radical Polymerization", *J. Poly. Sci. Part A: Poly. Chem.* **2007**, *45*, 566-575.

34. Harris, B. P.; Metters, A. T. "Generation and Characterization of Photopolymerized Gradient Polymer Brushes", *Macromolecules* **2006**, *39*, 2764-2772.

35. Odian, G. *Principles of Polymerization*, 4th ed., Wiley: New Jersey, **2004**.

36. Lovell, L. G.; Elliott, B. J.; Brown, J. R.; Bowman, C. N. "The Effect of Wavelength on the Polymerization of Multi(meth)acrylates with Disulfide/Benzilketal Combinations", *Polymer* **2001**, *42*, 421-429.

37. Plyusnin, V. F.; Kuznetzova, E. P.; Bogdanchikov, G. A.; Grivin, V. P.; Kirichenko, V. N.; Larionov, S. V. "Dithiocarbamate Radicals in Laser Flash Photolysis of Thiuram Disulfide and Dithiocarbamate Anion: Calculation of Optical Spectra", *J. Photochem. Photobiol. A: Chem.* **1992**, *68*, 299-308.

38. Sankhe, A. Y.; Husson, S. M.; Kilbey, S. M., II "Effect of Catalyst Deactivation on Polymerization of Electrolytes by Surface-Confined Atom Transfer Radical Polymerization in Aqueous Solutions", *Macromolecules* **2006**, *39*, 1376-1383.

39. Gopireddy, D.; Husson, S. M. "Room Temperature Growth of Surface-Confined Poly(acrylamide) from Self-Assembled Monolayers Using Atom Transfer Radical Polymerization", *Macromolecules* **2002**, *35*, 4218-4221.

40. Hairer, E.; Wanner, G. *Solving Ordinary Differential Equations II: Stiff and Differential-Algebraic Problems*, 2nd ed., Springer-Verlag: Germany, **2002**, Chapter IV.7, pp 102-117.

41. Doi, T.; Matsumoto, A.; Otsu, T. "Radical Polymerization of Methyl Acrylate by Use of Benzyl *N*,*N*-Diethyldithiocarbamate in Combination with Tetraethylthiuram Disulfide as a 2-Component Iniferter", *J. Poly. Sci. Part A: Poly. Chem.* **1994**, *32*, 2911-2918.

42. Prucker, O.; Schimmel, M.; Tovar, G.; Knoll, W.; Rühe, J. "Microstructuring of Molecularly Thin Layers by Photolithography", *Adv. Mater.* **1998**, *10*, 1073-1077.

CHAPTER 5

SWELLING BEHAVIOR OF RESPONSIVE POLY(METHACRYLIC ACID)-*BLOCK*-POLY(*N*-ISOPROPYLACRYLAMIDE) BRUSHES SYNTHESIZED USING SURFACE-INITIATED PHOTOINIFERTER-MEDIATED PHOTOPOLYMERIZATION

Surface-initiated photoiniferter-mediated photopolymerization (SI-PMP) in presence of tetraethylthiuram disulfide (TED) is used here to directly synthesize surface-grafted poly(methacrylic acid)-*block*-poly(*N*-isopropylacrylamide) (PMAA-*b*-PNIPAM) layers. The response of these PMAA-*b*-PNIPAM bi-level brush layers to changes in pH, temperature and ionic strength is investigated using *in-situ* multi-angle ellipsometry to measure changes in solvated layer thickness. As expected, PMAA blocks swell as pH is increased, with the maximum change in the thickness occurring near pH = 5, and PNIPAM blocks exhibit lower critical solution temperature (LCST) behavior, marked by a broad transition between extended and collapsed states and a decrease in the LCST due to added ions in the buffer solution. The response of the bi-level brushes to changes in added salt at constant pH is complex, as the swelling behavior of both the weak polyelectrolyte, PMAA, and thermoresponsive PNIPAM is affected by changes in ionic strength. The work described in this chapter demonstrates not only the robustness of SI-PMP for making novel, bi-level stimuli-responsive brushes, but also the complex links between synthesis, structure, and response of these interesting materials.

5.1 Introduction

The term "stimuli-responsive polymer" has been applied widely to describe polymers that exhibit a significant change in conformation and properties in response to external triggers. Over the past decade there has been tremendous interest in the synthesis and properties of synthetic stimuli-responsive polymers, particularly surface-tethered layers of these materials [1-6]. Surface coatings of stimuli-responsive polymers can be used to tailor and reversibly switch a wide array of interfacial properties, such as wettability, elastic modulus, surface energy, adhesion and friction. Consequently, these coatings (or "smart surfaces") are proposed as suitable platforms for chemical gates on membranes [7,8] or in microfluidic devices [9], vehicles for pulsatile/stealth drug delivery [10,11], biosensors [12,13] and molecular motors [14] to name a few. Multicomponent materials, whereby each constituent responds to one or more stimuli, are especially attractive because they provide a way to design surface layers that elicit a suite of responses.

One of the most widely used approaches to create soft interfacial layers is to tether polymer chains to a surface. When end-anchored at the solid-fluid interface at a sufficiently high tethering density, the chains of the layer stretch away from the surface to alleviate lateral crowding. The cilia-like layer of polymer chains extending away from the surface is often referred to as a "polymer brush". The stretched configuration of the chains and the crowded nature of the interfacial layer is the origin of many of the useful properties of polymer brushes: these layers resist compression and aggregation, effectively dissipate shear stresses, and respond reversibly to changes in their solution

environment. Polymer brushes have been used widely as well-defined model systems to study structure-property relationships because tethering the chain to the surface provides the opportunity to study chain stretching as a function of tethering density, molecular weight, solvent quality, pH, salt concentration (ionic strength) and temperature [1,4,15-26].

In this chapter, I report the use of surface-initiated, photoiniferter-mediated photopolymerization (SI-PMP) to create homopolymer and block copolymer brushes of poly(methacrylic acid) (PMAA) and poly(*N*-isopropylacrylamide) (PNIPAM). SI-PMP has certain advantages over other surface-initiated controlled radical polymerization techniques such as atom transfer radical polymerization (ATRP), nitroxide-mediated free-radical polymerization (NMP) and reversible addition fragmentation transfer (RAFT) because SI-PMP can be carried out at room temperature and is amenable to lithographic methods for readily creating micropatterned interfacial layers [27,28]. Additionally, because light is the activating agent, SI-PMP is well suited for the direct synthesis of polyelectrolytes (PMAA, in this study) [29], alleviating problems with, for example, catalyst complexation, dissociation, or disproportionation that occurs during ATRP of electrolytic monomers in protic media [30-32].

The response characteristics of the constituent materials used in this study are well known. Because of the weakly ionizable carboxylate groups along the backbone, the degree of dissociation of PMAA can be changed by adjusting the pH of the solution. As the net charge of the PMAA changes, there is a corresponding change in its hydrodynamic volume. The effect of pH, ionic strength and valency on the swelling of weak polyacids (PMAA or poly(acrylic acid), for example) has been studied by various

groups [15-17,30,33-35]. The thickness of these polyacid layers increases with pH, but the thickness may increase or decrease as a function of salt concentration, depending upon whether the counterion concentration outside of the layer is greater or less than that within the brush [35]. However, the swelling response of PMAA brushes to changes in pH and ionic strength at elevated temperatures (higher than room temperature) has not been investigated.

On the other hand, PNIPAM is perhaps the most widely studied thermo-responsive polymer. In deionized water it exhibits lower critical solution temperature (LCST) behavior: at ~32 ºC PNIPAM undergoes a coil-to-globule phase transition induced by expulsion of water from the chain [36]. Though the thermoresponsive behavior of PNIPAM coils and hydrogels in aqueous solution has been investigated extensively [36], the behavior of surface-grafted homo-PNIPAM brushes to the changes in temperature has been studied only in recent years. Surface plasmon resonance measurements by Lopez et al. [24] indicate that the phase transition of homo-PNIPAM brushes occurs over a broad temperature range centered around 32 ºC. Neutron reflectivity studies of Kent and coworkers demonstrated similar broad transitions of homo-PNIPAM brushes. Additionally, Kent et al. [23] and Leckband et al. [26] investigated the effect of grafting density and molecular weight of homo-PNIPAM chains on phase behavior. Their studies indicate that the LCST of homo-PNIPAM brushes depends upon the molecular weight and grafting density of chains: the swollen-collapsed transition is more pronounced for PNIPAM brushes of higher molecular weight and grafting density. Genzer et al. [25] showed that the LCST of PNIPAM brushes decreases as the concentration of salt in solution increases.

Despite the fact that PMAA and PNIPAM homopolymer brushes have been synthesized and studied by many groups, the synthesis and swelling behavior of bi-level, diblock copolymer brushes made from these responsive materials has not been reported previously. To this end, I have used SI-PMP in the presence of tetraethylthiuram disulfide (TED) to create PMAA-*b*-PNIPAM brushes. As shown in previous chapters and publications, SI-PMP in the presence of TED preserves the active end-groups of the surface-tethered chains, thereby allowing the molecular weight of the brush chains, as manifest by layer thickness, to be controlled and multi-block copolymers to be made [28]. Through experimental results reported in this chapter, I demonstrate the robustness of SI-PMP for making novel block copolymer brushes and how these brushes respond to various external stimuli.

5.2 Experimental

Materials. Purities and preparations of reagents and solvents required for the synthesis of photoiniferter, *N*,*N*-(diethylamino)dithiocarbamoyl-benzyl(trimethoxy)silane (SBDC), and for the formation of self-assembled monolayers (SAMs) of this iniferter on silicon surfaces are described in detail in Chapter 2 (and Appendix B for the synthesis of SBDC) and a previous publication [27]. Neutral alumina (Acros, Brockmann I type), hexane (Aldrich, 95%), benzene (Aldrich, 99%), methanol (Aldrich, 99.9%) and tetraethylthiuram disulfide (TED, Sigma, 97%) were used as received. Methacrylic acid (MAA, Aldrich, 99%) was dehibited by passing it through a neutral alumina column. *N*-

isopropylacrylamide (NIPAM, Aldrich, 97%) was recrystallized from benzene/hexane solution (50% v/v) and dried under vacuum prior to use.

Salts, acids and bases used to make buffer solutions include sodium phosphate dibasic (NaH_2PO_4, Riedel de Haën, 99%), glacial acetic acid (Acros), phosphoric acid (Mallinckrodt, 85%), hydrochloric acid (VWR, 50% v/v in water), sodium hydroxide (Alfa Aesar, 97%), 2-(*N*-morpholino)ethane sulfonic (MES) free acid (Amersco, >99%), and sodium chloride (Fisher Scientific, >99%), and these salts, acid and bases were used as received. The ionic strength of the buffer solutions was adjusted by adding sodium chloride in the amounts indicated in Table G1 of Appendix G, which lists the amounts of acid/base and sodium chloride required to make 1 L buffer solutions of various pH and ionic strengths. As needed, hydrochloric acid or sodium hydroxide was added to a buffer solution to precisely adjust the pH (within ± 0.1 pH unit of the target). All the buffer solutions were made using Millipore (Milli-Q) filtered water.

General Methods. The synthesis and characterization of SBDC are described in Appendix B and Chapter 2. The protocol used to make SAMs of this photoiniferter on silicon surfaces were also described in Chapter 2. Briefly, piranha acid-cleaned silicon wafers were placed individually in oven-dried test tubes. These wafer-containing test tubes were then flame-dried and 4 mL of an anhydrous toluene solution containing the photoiniferter (at 2 mM) was transferred to each test tube. The depositions were allowed to proceed for ~12 h at room temperature under nitrogen. Finally, after the deposition, the photoiniferter-modified silicon wafers were sonicated, rinsed with toluene and dried with a stream of dry nitrogen gas.

Synthesis of Homo-PMAA and Homo-PNIPAM Brushes. For the synthesis of homo-PMAA layer, a 50% v/v solution (5 mL) of MAA in Milli-Q filtered water was prepared in air-free Schlenk tube and degassed by four consecutive freeze-pump-thaw cycles. The degassed MAA solution was transferred via syringe to a preassembled reaction cell containing the photoiniferter-modified silicon wafers. The protocol for assembly of the reaction cell is described in Chapter 2 and a previous publication [27]. The assembly of the reaction cell and transfer of degassed monomer solution is carried out in a glove box where the oxygen level is kept below 1 ppm. The fully-assembled reaction cell was removed from glove box and exposed to a collimated UV-light for 1 hour at light intensity of 25 mW/cm^2. The details of UV exposure system are described previously [27]. After the photopolymerization, the PMAA-derivatized silicon wafers were sonicated, rinsed with water and then dried with a nitrogen stream. For the synthesis of homo-PNIPAM layer, a 25% w/w solution of NIPAM in methanol was prepared in an air-free Schlenk tube and degassed by three consecutive freeze-pump-thaw cycles. The protocols for the assembly of the reaction cell and photopolymerization are identical to those for MAA photopolymerization. The PNIPAM-modified silicon wafers were sonicated and rinsed with methanol and dried with a stream of nitrogen.

Synthesis of PMAA-*b*-PNIPAM Layers. For the synthesis of PMAA-*b*-PNIPAM layers, firstly, PMAA layers were synthesized. These PMAA layers were synthesized at light intensity of 15 mW/cm^2, MAA concentration of 50 % v/v in water and TED concentration of 0.2 mM (based on the volume of solution of MAA in water). The protocols for monomer preparation, assembly of reaction cell, photopolymerization and postpolymerization treatments are identical to those described for synthesis of homo-

PMAA brushes. PMAA layers were then reinitiated with NIPAM as a monomer, and for the reinitiation experiments, preparations, photopolymerization, and postpolymerization treatments were analogous to those followed for NIPAM polymerization. (Conditions for reinitiation with NIPAM: light intensity = 5 mW/cm^2, [NIPAM] = 25 % w/w in methanol, [TED] = 0 mM and exposure time = 3.5 h.)

Characterization. A Beaglehole Instruments phase-modulated Picometer™ ellipsometer that employs a photoelastic birefringence modulator to modulate the polarization of the incident light beam (λ = 632.8 nm) was used to measure the dry and solvated thicknesses of SBDC SAMs, PMAA, PNIPAM and PMAA-*b*-PNIPAM layers. For dry layer thickness measurements, refractive indices of 1.45, 1.48 and 1.50 were used for SBDC, PMAA and PNIPAM, respectively. The ellipsometric angles ψ and Δ of dry layers were measured by changing the angle of incidence from 80° to 35° in steps of 1 degree (with an accuracy of better than 0.01°). These ellipsometric angles as a function of incident angle were fitted using a Cauchy model (Igor Pro. software package) to determine the thickness. Dry layer thickness measurements were taken at five different points on every sample.

To investigate the response of PMAA, PNIPAM and PMAA-*b*-PNIPAM layer thicknesses to external stimuli, *in-situ* ellipsometric measurements were performed. All of the measurements were carried out in a cylindrical liquid flow cell made of a special annealed glass that does not bend or refract light. The polymer-modified silicon wafers were clamped on a Teflon stage, which was placed in the flow cell [37]. The contacting buffer solutions of given pH were circulated continuously through the flow cell using a peristaltic pump (Cole Parmer model 7520-00 Masterflex with model 7518-10 Easy-

Load™ pump module). It should be noted that for measurements in liquids, each sample remained in the *in-situ* ellipsometry setup while buffer solutions were exchanged and circulated through the flow cell. This allowed measurements to be made on the same spot, alleviating any uncertainty that lateral heterogeneity of samples may cause. The temperature of the buffer solutions was adjusted (within ± 0.2 °C) by heating the buffer solutions using a Corning PC-220 hot plate. A refractive index of 1.33 was used for all the buffer solutions at all of the temperatures. In a manner analogous to dry-layer thickness measurements, for solvated thickness measurements the ellipsometric angles ψ and Δ were measured by changing the angle of incidence from 80° to 50°, and these ellipsometric angles as a function of incident angle were fitted using a single-layer Cauchy model to determine the thickness and refractive index of the stretched polymer layers. The standard deviation in the measurement of polymer layer thicknesses in swollen state was ± 6 nm. This standard deviation was calculated from three repeat *in-situ* ellipsometric thickness measurements on a PMAA-*b*-PNIPAM layer, for which one set of data (data collected without changing the measurement spot) are shown in Figure 5.5 in the Results and Discussion section. The dry layer thickness at the measurement spot was 54.7 nm (PMAA block thickness in dry state = 18.4 nm and PNIPAM block thickness in dry state = 36.3 nm).

5.3 Results and Discussion

While SI-PMP is a robust method for growing polymer brushes and photoiniferter mediated photopolymerization is, in general, known to be compatible for polymerization

of wide array of monomers, including styrenic, acrylate, acrylamides and acidic monomers [29,38,39], care must be exercised to establish conditions that preserve the ability to reinitiate growth. In Chapter 3, I showed that preaddition of TED, which undergoes homolytic cleavage to provide a source of deactivating, dithiocarbamyl radicals to the reaction mixture enables formation of block copolymers by SI-PMP [28]. Thus, prior to synthesis of responsive brushes, we examine the ability to reinitiate PMAA layers in the presence of NIPAM.

Growth and Reinitiation of PMAA Layers. Figure 5.1 shows the evolution of dry PMAA layer thickness as a function of exposure time and the thicknesses of PNIPAM layers grown by reinitiating those PMAA layers. The PMAA brushes were synthesized using a light intensity of 15 mW/cm^2, a MAA concentration of 50 % v/v (in deionized water) and a TED concentration of 0.2 mM. These PMAA layers were reinitiated in the presence of NIPAM monomer (25 % w/w in methanol) at light intensity of 5 mW/cm^2 for 3.5 hours. Based on the kinetic modeling studies of SI-PMP reported in Chapter 4, because nearly all of the photoiniferter molecules are activated at this light intensity (15 mW/cm^2), the PMAA layers synthesized at these photopolymerization conditions are more likely to form block copolymer layers of PMAA-*block*-PNIPAM, rather than forming a mixed brush consisting of both PMAA and PNIPAM chains tethered directly to the substrate. As shown in Figure 5.1, PMAA layer thickness increases with exposure time; however, the layer growth was observed to be nonlinear, particularly beyond 2 h, suggesting that even with preaddition of 0.2 mM TED, irreversible termination reactions occur during growth of the weak polyacid layer. Figure 5.1 also shows that the PNIPAM block thickness decreased with exposure time for

PMAA layer synthesis. This decrease in PNIPAM block thickness (with increasing PMAA exposure time) can be partly attributed to an increase in the number of irreversible termination reactions that occur during PMAA layer growth.

It should also be noted that the thickness of PNIPAM block (36.3 ± 3.2 nm) reinitiated from the PMAA layer synthesized for 0.5 hours is significantly less than the thickness of PNIPAM layer (132.2 ± 3.8 nm) synthesized directly from a photoiniferter-modified silicon wafer at reinitiation conditions (described below). This difference in the thicknesses could possibly be due to low cross-over efficiency from PMAA to NIPAM. Another possibility is that because the active end groups are distributed throughout the PMAA layer (not simply confined to the edge of the layer), transport of NIPAM to the active end groups during reinitiation is hindered. Both of these effects would result in extension of only a fraction of PMAA chains with NIPAM, thereby leading to the behavior observed. Nevertheless, the results shown in Figure 5.1 suggest that with the appropriate selection of photopolymerization conditions, we are able to manipulate the thicknesses of PMAA and PNIPAM blocks. It should be noted that reinitiation of PMAA layers in the presence of NIPAM was done at identical photopolymerization conditions. Assuming that the molecular weights of PNIPAM chains synthesized at identical conditions are approximately identical, the variation in the thicknesses of PNIPAM blocks is due to variation in the concentration of PNIPAM chains per unit area. However, in the present study, the grafting density and molecular weight of chains are not assessed, and the effects of these parameters on the responsive nature of bi-level block copolymer layers could be a focus of future research.

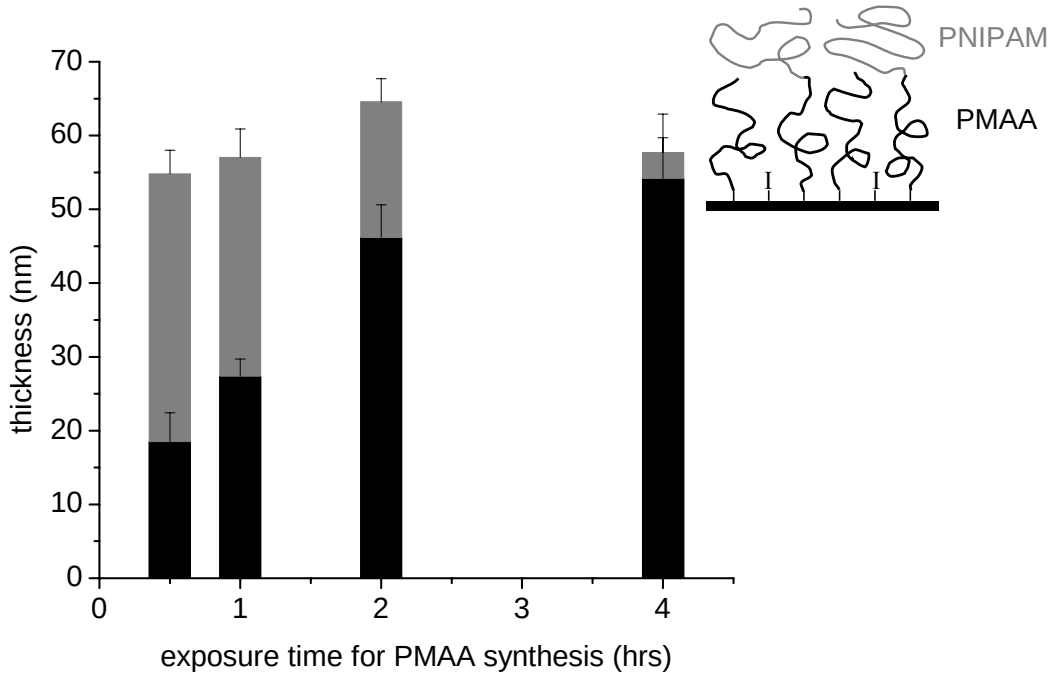

Figure 5.1 Evolution of PMAA layer thickness (black bars) as a function of exposure time and thicknesses of PNIPAM blocks (grey bars) synthesized by reinitiating each PMAA layer with NIPAM at constant conditions. PMAA layers were synthesized at 15 mW/cm^2, MAA concentration of 50 % v/v in water and [TED] = 0.2 mM. Reinitiation of the PMAA layers with NIPAM was conducted at 5 mW/cm^2, NIPAM concentration of 25 % w/w in methanol and exposure time of 3.5 hours. Error bars represent the standard deviation from the multiple measurements using two identical samples (five measurements per sample). The cartoon in the right corner of the plot is schematic representation of a bi-level PMAA-*b*-PNIPAM brush.

The responsive nature of the PMAA-*b*-PNIPAM layers was investigated by measuring the ellipsometric thicknesses *in-situ* as a function of pH and temperature of contacting buffer solutions. However, in order to dissect the effect of pH and temperature on each block of the PMAA-*b*-PNIPAM bi-level brushes, the effects of pH and temperature on swelling of homo-PMAA layers and homo-PNIPAM layers are first studied.

Response of Homo-PMAA and Homo-PNIPAM Layers to Changes in pH and Temperature. Figure 5.2 shows the results from PMAA stretching experiments as a function of pH and temperature. The dry layer thickness of this PMAA layer (synthesized at a light intensity of 25 mw/cm^2, MAA concentration of 50 % v/v in water and exposure time of 1 hr) was measured to be 58.2 nm. No TED was present during the synthesis of this PMAA layer. As Figure 5.2 indicates, this weak polyelectrolyte (PE) brush responds to changes in pH: as the pH is increased, dissociation (deprotonation) of carboxylate groups and, in turn, repulsive electrostatic interactions cause swelling of the PMAA layer. This pattern of behavior exhibited by the PMAA brush in response to changes in pH mirrors that observed for weak PEs by other researchers [16,30]. The maximum increase in thickness of the PMAA layer occurs in the range of $4 < pH < 6$, centered at ~5, which is consistent with the reported pK_a of PMAA [40]. The swelling results also show that exposure of a dry PMAA brush to the buffer solution at pH = 3, where the PMAA brush is not ionized, swells the layer ~1.5 times its dry-layer thickness. This swelling is simply due to hydration of uncharged PMAA layer [40]. Increasing the pH from 6 to 8 results in insignificant changes in PMAA layer thickness, indicating that the PMAA chains are fully deprotonated above pH = 6. Figure 5.2 also suggests that except when the layer is in its fully protonated form, there is no impact of temperature on the swollen structure of the PMAA homopolymer brush. In the fully protonated form (pH = 3), due to the fact that the hydrogen-bonding interactions reduce as temperature is increased, PMAA layer decreases as temperature increases.

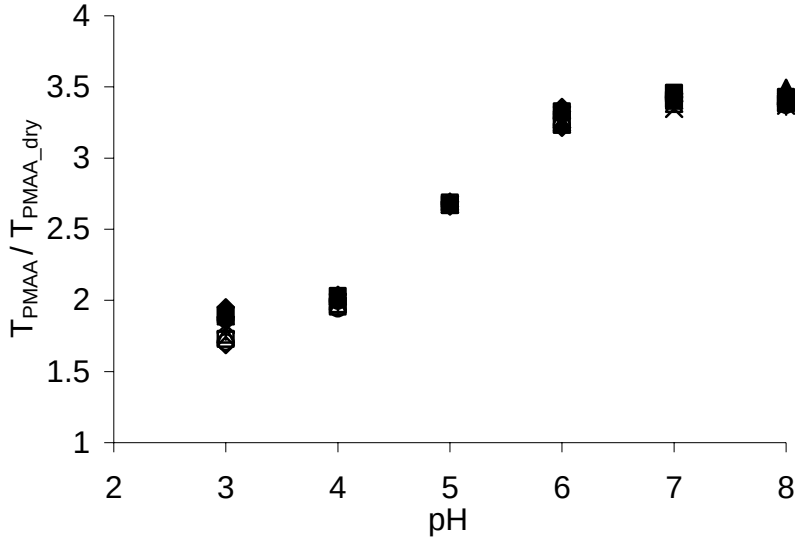

Figure 5.2 Swelling response of a PMAA layer to changes in pH of contacting buffer solutions at various temperatures. PMAA layer was synthesized at light intensity 25 mW/cm^2, MAA concentration of 50 % v/v in water and exposure time of 1 hour. No TED was added while synthesizing this PMAA layer. Dry layer thickness was 58.2 nm. The temperatures of buffer solutions were 22 °C (♦), 24 °C (■), 26 °C (▲), 28 °C (●), 30 °C (×), 32 °C (+), 34 °C (Δ), 36 °C (□), 38 °C (○), 40 °C (◊).

Figure 5.3 displays the swelling response of a 132.2 nm thick PNIPAM brush as a function of temperature and pH. This PNIPAM layer was synthesized at a light intensity of 5 mW/cm^2 and a NIPAM concentration of 25 % w/w in methanol for 3.5 hours. The thermoresponsive nature of this PNIPAM brush is reflected in its transition from a highly swollen state at low temperature to a collapsed state at higher temperatures. It is worth pointing out that at 40 ºC the layer has collapsed nearly to its dry layer thickness. Figure 5.3 also shows that pH appears to have an almost negligible impact on the swelling behavior of the layer.

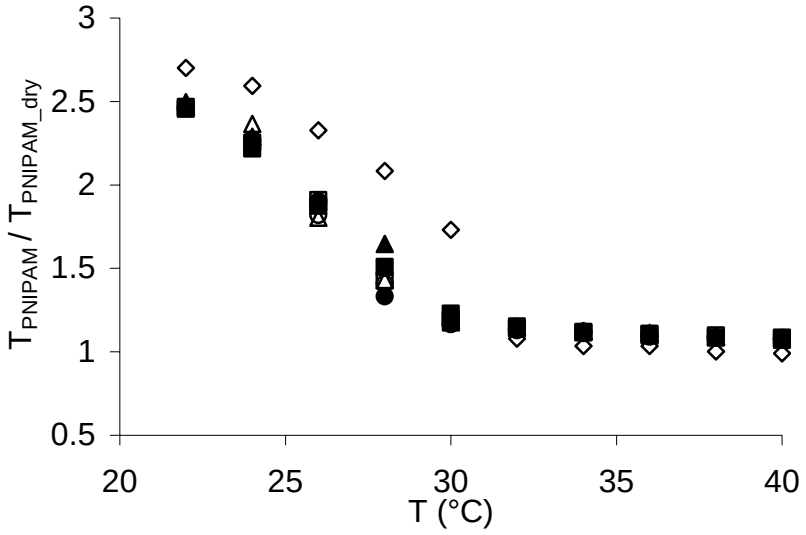

Figure 5.3 Swelling response of a homo-PNIPAM layer to changes in temperature of contacting buffer solutions of various pH and deionized water (pH = 7). The PNIPAM layer was photopolymerized at a light intensity of 5 mW/cm^2, NIPAM concentration of 25 % w/w in methanol and an exposure time of 3.5 hours. No TED was added while synthesizing this PNIPAM layer. Dry layer thickness of this PNIPAM layer was 132.2 nm. The buffer solutions had a pH of 3 (●), 4 (■), 5 (▲), 6 (Δ), 7 (□), 8 (○). The hollow black diamonds (◊) show the response of the PNIPAM layer in deionized water to changes in temperature.

Although the LCST behavior of free PNIPAM chains in water is distinguished by a relatively sharp transition at ~32 ºC, in agreement with reports by Genzer et al. [25] we observe a broadening of the transition, and a lower transition temperature due to added ions (As noted in Experimental section, the ionic strength of the buffer solutions is 154 mM). I also examined the swelling response of this PNIPAM brush in pure, deionized water: the layer displays the same broad transition behavior; however, as anticipated the transition is shifted to higher temperature, with the midpoint of the transition between the swollen and collapsed states occurring at 30 ºC.

Response of PMAA-*b*-PNIPAM Layers to pH and Temperature. Knowing that homo-PMAA and homo-PNIPAM brushes respond to changes in pH and

temperature, respectively, we hypothesized that combining these materials into a bi-level structure (i.e., a PMAA-*b*-PNIPAM brush) should provide additional opportunities to actuate the layer with both pH and temperature. Figures 5.4a and 5.4b show the response of a PMAA-*b*-PNIPAM brush to changes in pH and temperature, respectively. This 57.0 nm-thick (dry) PMAA-*b*-PNIPAM layer was symmetric in terms of the thicknesses of individual blocks in dry state. The thicknesses of the PMAA block and of the PNIPAM block were 27.4 nm and 29.6 nm, respectively.

As shown in Figure 5.4a, over a range of temperatures, the PMAA-*b*-PNIPAM brush responds to pH in a manner analogous to what is seen in the swelling behavior of the homo-PMAA brush. At the highest temperature investigated (40 °C) the brush swelling ratio, defined as the solvated layer thickness normalized by the dried layer thickness, increases from ~1.3 at pH = 3 to ~2.2 at pH = 8, while at the lowest temperature of 22 °C, the swelling ratio increases from ~3.2 at pH = 3 to ~4.2 at pH = 8. Across this temperature range, the pH-induced swelling change occurs mostly between pH = 5 and 6, which is, ostensibly, a result of PMAA block stretching due to increased Coulombic interactions (deprotonation of the carboxyl groups). It is interesting to note that the range of pH over which this swelling transition occurs is narrower in the case of PMAA-*b*-PNIPAM layer as compared to that for homo-PMAA layer, which showed a transition between pH 4-6. The narrower transition could be attributed to the difference in local pH inside the brush and solution pH due to the over-layer of PNIPAM and, in turn buffering effect.

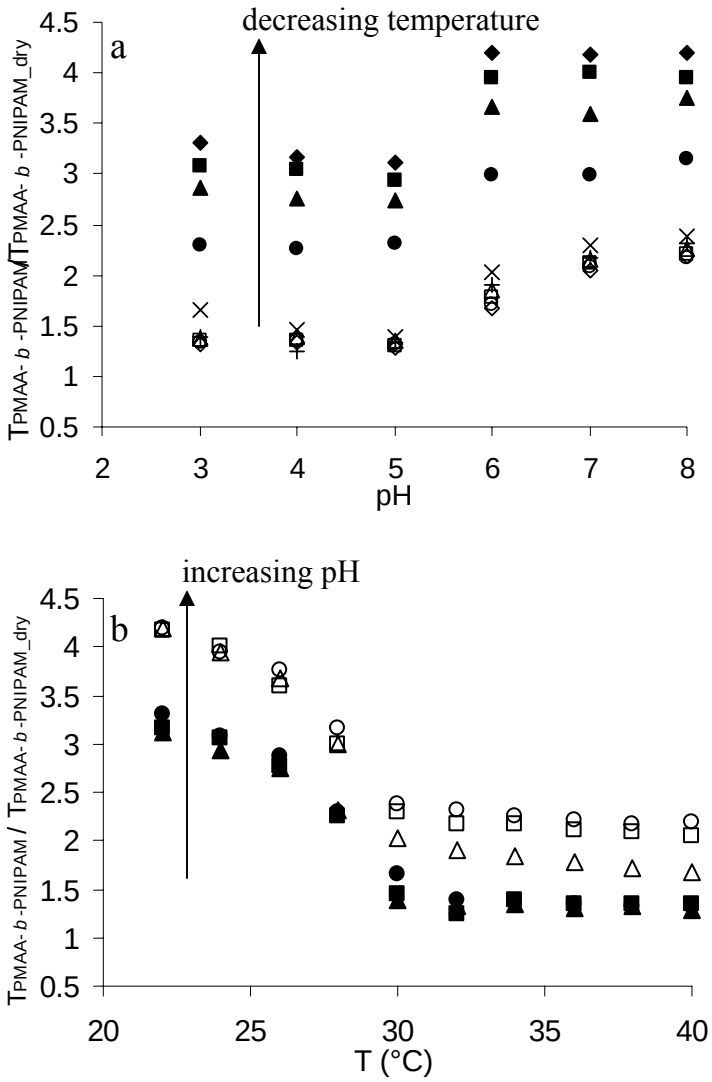

Figure 5.4 a) Response of a symmetric PMAA-*b*-PNIPAM brush to changes in pH. The temperatures were 22 °C (♦), 24 °C (■), 26 °C (▲), 28 °C (●), 30 °C (×), 32 °C (+), 34 °C (Δ), 36 °C (□), 38 °C (○), 40 °C (◊). **b)** Response of a symmetric PMAA-*b*-PNIPAM brush to changes in temperature. The pHs were 3 (●), 4 (■), 5 (▲), 6 (Δ), 7 (□), 8 (○). Dry layer thicknesses of the PMAA and PNIPAM blocks at the spot of *in-situ* ellipsometric measurements were measured to be 27.4 nm and 29.6 nm, respectively.

The data also show that at any pH, the layer can be made to swell (collapse) by decreasing (increasing) the temperature through the LCST. This coil-globule transition of the PNIPAM component of the bi-level PMAA-*b*-PNIPAM brush can be clearly seen in

Figure 5.4b. Similar to a homo-PNIPAM brush, the thermal transition of the PMAA-*b*-PNIPAM brush is broad. Using temperature only and for all pHs examined, the PMAA-*b*-PNIPAM brush can be actuated by a factor of 2 over the range from 22 °C to 40 °C. Using both temperature and pH, this PMAA-*b*-PNIPAM layer can be made to swell ~4.2 times its dry thickness, and a variety of combinations of pH and temperature can be used to set the degree-of-swelling between these limits. Based on the previous conclusion that homo-PNIPAM layer shrinks approximately to its dry thickness at around 40 °C, Figure 5.4 suggests that PMAA block swells ~3.4 times its dry layer thickness at pH = 7 and PNIPAM block swells ~4.7 times its dry thickness at 22 °C.

While the pH and temperature response of the bi-level PMAA-*b*-PNIPAM layer in general reflects the behavior of the constituent blocks acting in an independent fashion, there are some aspects and subtle features worth noting. Swelling of the PNIPAM blocks (in terms of swelling ratios) of the PMAA-*b*-PNIPAM brush is different than that exhibited by homo-PNIPAM brush. This difference in the swelling could be due to the structural differences that spring from the way the homo-PNIPAM layer and PNIPAM blocks were made: grafting density of PNIPAM blocks is probably lower than the grafting density if homo-PNIPAM layers. However, as mentioned earlier, the temperature range over which the swelling (shrinking) of PNIPAM blocks in bi-level brush occurs is identical to the temperature range, over which the homo-PNIPAM layer swells (shrinks). Also, the swelling of the PMAA block of the bi-level system appears to be affected at pH = 6 by the collapse of the PNIPAM layer. One possible explanation for this behavior could be hydrogen bond formation between the amide (-CONH) groups of PNIPAM and carboxylic (–COOH) groups of PMAA [41,42] at temperatures above LCST where the

PNIPAM blocks are collapsed onto the PMAA blocks due to the poor solubility of the PNIPAM chains in the aqueous buffer solutions). Such hydrogen bonding within the layer would result in an overall shrinkage of the bi-level copolymer layer. However, if hydrogen bonding is influencing the pH-dependent actuation, it is not affecting the LCST of PNIPAM block, though the LCST is broad.

Taken together, the results shown in Figures 5.4a and 5.4b clearly indicate that swelling of a bi-level PMAA-*b*-PNIPAM brush, and in turn its solvated thickness, can be controlled easily by choice of pH, temperature or multiple combinations of pH and temperature. It should, however, be noted that the thickness of each block of this PMAA-*b*-PNIPAM layer were nearly equivalent. As suggested by Figure 5.1, with SI-PMP the thicknesses of the two blocks can be manipulated easily by changing photopolymerization conditions. To investigate how an asymmetric PMAA-*b*-PNIPAM layer responds to environmental stimuli, an "asymmetric" a bi-level PMAA-*b*-PNIPAM layer (blocks of different thicknesses) was created, and in-situ stretching swelling measurements were made. Comparing the pH- and temperature-dependent swelling behaviors of an asymmetric PMAA-*b*-PNIPAM system with that of a symmetric PMAA-*b*-PNIPAM system may shed light on how one component of a multi-component, multi-responsive layer affects the swelling of the other component.

Shown in the Figure 5.5 are the results from stretching measurements of an asymmetric PMAA-*b*-PNIPAM layer. The thicknesses of the PMAA and PNIPAM blocks were 18.4 and 36.3 nm, respectively; so this sample had a total dry layer thickness of ~54.7 nm, which is similar to the symmetric layer studied above. As can bee seen in

Figure 5.5, the characteristic swelling behavior of this layer is consistent with the response of the symmetric layer (Figure 5.4).

With similar total thicknesses, the overall swelling of the symmetric and asymmetric PMAA-*b*-PNIPAM is approximately the same (~4.1 times the dry layer thickness) at the lowest temperature (22 °C) and the highest pH (7) investigated in this study. The values of pH and temperature at which the swelling transitions occur are identical to those observed for the symmetric PMAA-*b*-PNIPAM layer. Additionally, based on our results showing that homo-PNIPAM layers shrink to their dry thickness at ~40 °C, the swelling of individual blocks is also identical to that observed for the symmetric PMAA-*b*-PNIPAM brush: the PMAA block swells approximately 3.1 times its dry thickness at highest pH investigated (pH = 7) and the chains of the PNIPAM layer swell ~4.6 times their dry layer thickness at the lowest investigated temperature (22 °C). The fact that the swelling behavior of the constituent blocks of the bi-level brushes remains approximately the same (regardless of individual block thicknesses) suggests that the thickness (and therefore, the molecular weight) of PNIPAM block does not affect the actuation of the PMAA block, and vice-versa. In essence, even though the blocks are joined at a common point, each appears to respond independently to changes in T and pH. The only significant difference between the swelling of the symmetric and asymmetric PMAA-*b*-PNIPAM brushes was the contribution of each individual block to the overall thickness change of the brush: as expected, the thicker block of the block copolymer contributes more to the overall thickness change as compared to the thinner block.

In essence, even though the blocks are joined at a common point, each appears to respond independently to changes in T and pH. The only significant difference between the swelling of the symmetric and asymmetric PMAA-*b*-PNIPAM brushes was the contribution of swelling of individual blocks to the overall thickness change (swelling) of the brush: as expected, the thicker block of the block copolymer contributed more to the overall thickness change as compared to the thinner block.

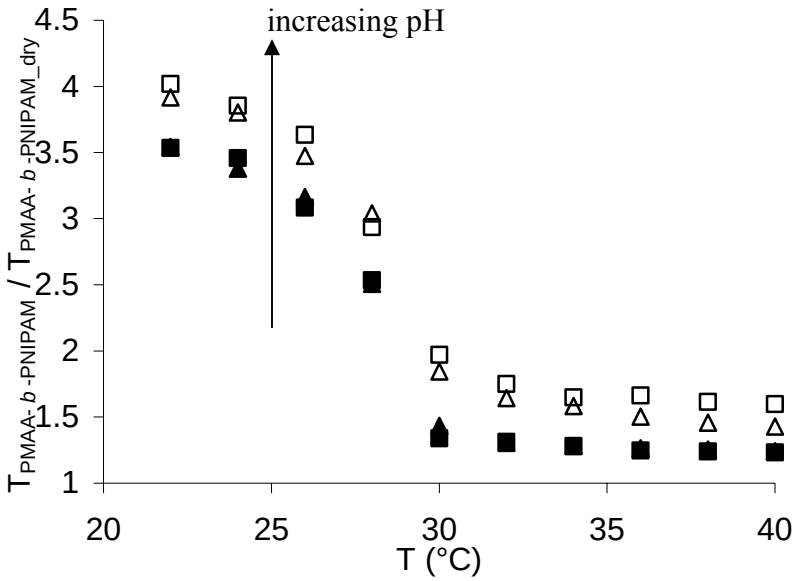

Figure 5.5 Response of an asymmetric PMAA-*b*-PNIPAM brush to changes in pH and temperature. The pHs of buffer solutions were 4 (■), 5 (▲), 6 (Δ), 7 (□). An 18.4 nm-thick PMAA layer was synthesized using a light intensity of 15 mW/cm^2, MAA concentration of 50 % v/v in water, TED concentration of 0.2 mM (based on the volume of solution of MAA in water) and an exposure time of 0.5 hour. PNIPAM layer was synthesized by reinitiating PMAA layer at light intensity of 5 mW/cm^2, NIPAM concentration of 25 % w/w in methanol and exposure time = 3.5 hours. The dry layer thickness of this PNIPAM block was measured to be 36.3 nm.

Effect of Ionic Strength on Swelling of PMAA-*b*-PNIPAM Layers. As noted earlier, an increase in the ionic strength of the contacting solution is known to result in a decrease in the LCST of PNIPAM [25]. Also, added salts play a complex and crucial role in the swelling behavior of weak polyelectrolytes: at low ionic strength (the so-called "osmotic brush" regime), and as salt is added, a weak PE brush will increase its height until the internal salt concentration equals the external salt concentration. When the "salted brush" regime is reached, the weak PE brush will shrink as the ionic strength is increased [16]. Thus, changes in ionic strength affect both blocks of PMAA-*b*-PNIPAM brushes.

Figure 5.6a and 5.6b show the effect of ionic strength on the swelling response of the asymmetric PMAA-*b*-PNIPAM bi-level layer at pH = 7 and 5, respectively. As shown in Figure 5.6a, as the ionic strength is increased from 120 mM to 240 mM, there is a slight (~7 %) decrease in the swelling ratio of the PMAA-*b*-PNIPAM layer at 40 °C. On the other hand, a substantial decrease in the swelling ratio is observed at 28 °C. Similarly, as shown in Figure 5.6b, the swelling ratio decreases slightly at 40 °C and substantially at 28 °C and 30 °C as the ionic strength of the buffer solutions of pH = 5 is increased from 40 mM to 200 mM. The decreases in swelling ratios at 28 °C and 30 °C (around the LCST of PNIPAM) are primarily indicative of a depression of the LCST of PNIPAM with increasing ionic strength, whereas the decreases in swelling ratios at 40 °C could be a combined effect of ionic strength impacting both the PMAA and PNIPAM blocks. However, at this stage it is not possible to speculate on the relative contribution of each individual block to overall swelling. Nevertheless, and more importantly, the observed effects of ionic strength on the swelling behavior of PMAA-*b*-PNIPAM bi-level

brushes indicate that, in addition to pH and temperature, the overall solvated thickness and structure of each block of these layers can be manipulated by changing the ionic strength of aqueous solution.

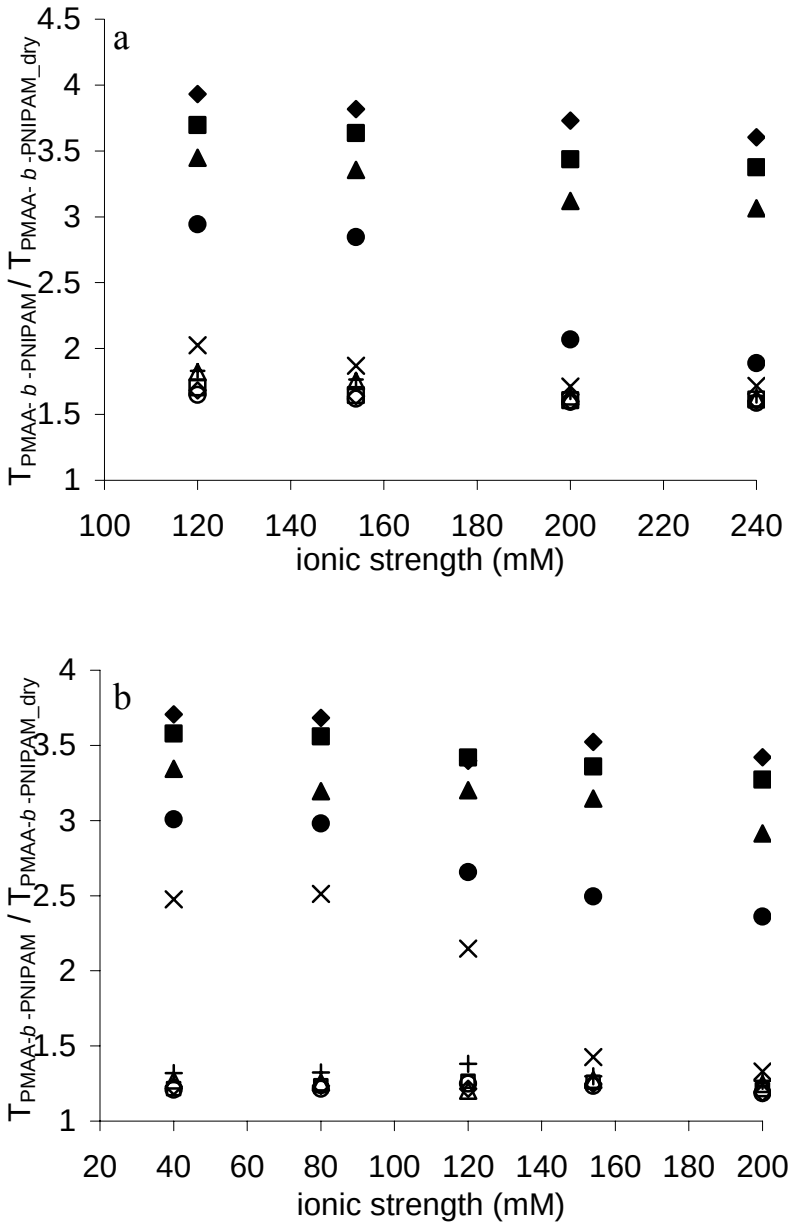

Figure 5.6 Response of an asymmetric PMAA-*b*-PNIPAM brush to changes in ionic strength of buffer solutions of a) pH = 7 and b) pH = 5 at various temperatures. The temperatures were 22 °C (♦), 24 °C (■), 26 °C (▲), 28 °C (●), 30 °C (×), 32 °C (+), 34 °C (Δ), 36 °C (□), 38 °C (○), 40 °C (◊). Dry layer thicknesses of the PMAA and PNIPAM blocks were measured to be 18.4 and 36.3 nm, respectively.

5.4 Conclusions

Responsive PMAA-*b*-PNIPAM layers were synthesized successfully using surface-initiated photoiniferter-mediated photopolymerization. As expected, the actuation of PMAA-*b*-PNIPAM layers depends on pH, temperature and ionic strength. However, each component in PMAA-*b*-PNIPAM layer retains its customary responsive characteristics: the PMAA blocks swell as pH is increased and the PNIPAM blocks exhibit lower critical solution temperature (LCST) behavior. Due to added ions (buffer solutions were used) and surface confinement, the LCST transition of PNIPAM layers occurs at a lower temperature and over a wider range of temperature as compared to the sharp transition at 32 ºC observed in case of free PNIPAM chains in deionized water. While the responsive nature of the PNIPAM blocks in PMAA-*b*-PNIPAM layers is similar to the responsive nature of homo-PNIPAM layers, the pH-induced swelling of PMAA blocks is slightly different than the pH-induced swelling of the homo-PMAA layers. Most importantly, the actuation of PMAA-*b*-PNIPAM layers can be broadly manipulated by changing the pH, temperature, ionic strength, individually or in concert. I expect these changes also impact layer properties, and there is considerable room for future studies aimed at understanding how these changes in structure alter layer properties.

5.5 References

1. Luzinov, I.; Minko, S.; Tsukruk, V. V. "Adaptive and Responsive Surfaces through Controlled Reorganization of Interfacial Polymer Layers ", *Prog. Polym. Sci.* **2004**, *29*, 635-698.

2. Gil, E. S.; Hudson, S. M. "Stimuli-responsive Polymers and their Bioconjugates", *Prog. Polym. Sci.* **2004**, *29*, 1173-1222.

3. Russell, T. P. "Surface-responsive Materials", *Science* **2002**, *297*, 964-967.

4. Brittain, W. J.; Boyes, S. G.; Granville, A. M.; Baum, M.; Mirous, B. K.; Akgun, B.; Zhao, B.; Blickle, C.; Foster, M. D. "Surface Rearrangement of Diblock Copolymer Brushes-Stimuli Responsive Films", *Adv. Polym. Sci*. **2006**, *198*, 125-147.

5. Alarcon, C. D. H.; Pennadam, S.; Alexander, C. "Stimuli Responsive Polymers for Biomedical Applications", *Chem. Soc. Rev*. **2005**, *34*, 276-285.

6. Zhou, F.; Huck, W. T. S. "Surface Grafted Polymer Brushes as Ideal Building Blocks for "Smart" Surfaces", *Phys. Chem. Chem. Phys.* **2006**, *8*, 3815.

7. Ito, Y.; Ochiai, Y.; Park, Y. S.; Imanishi, Y. "pH-Sensitive Gating by Conformational Change of a Polypeptide Brush Grafted onto a Porous Polymer Membrane", *J. Am. Chem. Soc.* **1997**, *119*, 1619-1623.

8. Zhang, H.; Ito, Y. "pH Control of Transport through a Porous Membrane Self-Assembled with a Poly(acrylic acid) Loop Brush", *Langmuir* **2001**, *17*, 8336-8340.

9. Barker, S. L. R.; Ross, D.; Tarlov, M. J.; Gaitan, M.; Locascio, L. E. "Control of Flow Direction in Microfluidic Devices with Polyelectrolyte Multilayers", *Anal. Chem.* **2000**, *72*, 5925-5929.

10. Kikuchi, A.; Okano, T. "Pulsatile Drug Release Control Using Hydrogels", *Adv. Drug Delivery Rev.* **2002**, *54*, 53-77.

11. Kost, J.; Langer, R. "Responsive Polymeric Delivery Systems", *Adv. Drug Delivery Rev.* **2001**, *46*, 125-148.

12. Roy, I.; Gupta, M. N. "Smart Polymeric Materials: Emerging Biochemical Applications", *Chem. Biol.* **2003**, *10*, 1161.

13. Yang, C. C.; Tian, Y.; Jen, A. K. Y.; Chen, W. C. "New Environmentally Responsive Fluorescent *N*-isopropylacrylamide Copolymer and its Application to DNA Sensing", *J. Polym. Sci., Part A.: Polym. Chem.* **2006**, *44*, 5495-5504.

14. Santer, S.; Rühe, J. "Motion of Nano-objects on Polymer Brushes", *Polymer* **2004**, *45*, 8279-8297.

15. Rühe, J.; Ballauff, M.; Biesalski, M.; Dziezok, P.; Grohn, F.; Johannsmann, D.; Houbenov, N.; Hugenberg, N.; Konradi, R.; Minko, S.; Motornov, M.; Netz, R. R.; Schmidt, M.; Seidel, C.; Stamm, M.; Stephan, T.; Usov, D.; Zhang, H. "Polyelectrolyte Brushes", *Adv. Polym. Sci*. **2004**, *165*, 79-150.

16. Biesalski, M.; Johannsmann, D.; Rühe, J. "Synthesis and Swelling Behavior of a Weak Polyacid Brush", *J. Chem. Phys.* **2002**, *117*, 4988-4994.

17. Konradi, R.; Rühe, J. "Binding of Oppositely Charged Surfactants to Poly(methacrylic acid) Brushes", *Macromolecules* **2005**, *38*, 6140-6151.

18. Balastre, M.; Li, F.; Schorr, P.; Yang, J.; Mays, J.; Tirrell, M. "A Study of Polyelectrolyte Brushes Formed from Adsorption of Amphiphilic Diblock Copolymers Using the Surface Forces Apparatus", *Macromolecules* **2002**, *35*, 9480-9486.

19. Raviv, U.; Giasson, S.; Kampf, N.; Gohy, J.–F.; Jérôme, R.; Klein, J. "Lubrication by Charged Polymers", *Nature* **2003**, *425*, 163-165.

20. Tian, P.; Uhrig, D.; Mays, J. W.; Watanabe, H.; Kilbey, S. M., II, "Role of Branching on the Structure of Polymer Brushes Formed from Comb Copolymers", *Macromolecules* **2005**, *38*, 2524-2529.

21. Kilbey, II, S. M.; Watanabe, H.; Tirrell, M. "Structure and Scaling of Polymer Brushes near the Theta Condition", *Macromolecules* **2001**, *34*, 5249-5259.

22. Yim, H.; Kent, M. S.; Satija, S.; Mendez, S.; Balamurugan, S. S.; Lopez, G. P. "Evidence for Vertical Phase Separation in Densely Grafted, High-Molecular-Weight Poly(*N*-isopropylacrylamide) Brushes in Water", *Phys. Rev. E* **2005**, *72*, 051801.

23. Yim, H.; Kent, M. S.; Mendez, S.; Balamurugan, S. S.; Balamurugan, S.; Lopez, G. P.; Satija, S. "Temperature-Dependent Conformational Change of PNIPAM Grafted Chains at High Surface Density in Water", *Macromolecules* **2004**, *37*, 1994-1997.

24. Balamurugan, S.; Mendez, S.; Balamurugan, S. S.; O'Brien, II, M. J.; Lopez, G. P. "Thermal Response of Poly(*N*-isopropylacrylamide) Brushes Probed by Surface Plasmon Resonance", *Langmuir* **2003**, *19*, 2545-2549.

25. Jhon, Y. K.; Bhat, R. R.; Jeong, C.; Rojas, O. J.; Szleifer, I.; Genzer, J. "Salt-Induced Depression of Lower Critical Solution Temperature in a Surface-Grafted Neutral Thermoresponsive Polymer", *Macromol. Rapid Commun*. **2006**, *27*, 697.

26. Plunkett, K. N.; Zhu, X.; Moore, J. S.; Leckband, D. E. " PNIPAM Chain Collapse Depends on the Molecular Weight and Grafting Density", *Langmuir* **2006**, *22*, 4259-4266.

27. Rahane, S. B.; Kilbey, II, S. M.; Metters, A. T. "Kinetics of Surface-Initiated Photoiniferter-Mediated Photopolymerization", *Macromolecules* **2005**, *38*, 8202-8210.

28. Rahane, S. B.; Metters, A. T.; Kilbey, II, S. M. "Impact of Added Tetraethylthiuram Disulfide Deactivator on the Kinetics of Growth and Reinitiation of Poly(methyl methacrylate) Brushes Made by Surface-Initiated Photoiniferter-Mediated Photopolymerization", *Macromolecules* **2006**, *39*, 8987-8991.

29. Harris, B. P.; Kutty, J. K.; Fritz, E. W.; Webb, C. K.; Burg, K. J. L.; Metters, A. T. "Photopatterned Polymer Brushes Promoting Cell Adhesion Gradients", *Langmuir* **2006**, *22*, 4467.

30. Ayres, N.; Boyes, S. G.; Brittain, W. J. "Stimuli-Responsive Polyelectrolyte Polymer Brushes Prepared *via* Atom-Transfer Radical Polymerization", *Langmuir* **2007**, 23, 182-189.

31. Osborne, V. L.; Jones, D. M.; Huck, W. T. S. "Controlled Growth of Triblock Polyelectrolyte Brushes", *Chem. Commun.* **2002**, *17*, 1838-1839.

32. Tsarevsky, N. V.; Pintauer, T.; Matyjaszewski, K. "Deactivation Efficiency and Degree of Control over Polymerization in ATRP in Protic Solvents", *Macromolecules* **2004**, *37*, 9768-9778.

33. Biesalski, M.; Johannsmann, D.; Rühe, J. "Electrolyte-Induced Collapse of a Polyelectrolyte Brush", *J. Chem. Phys.* **2004**, *120*, 8807.

34. Zhang, H. N.; Rühe, J. "Swelling of Poly(methacrylic acid) Brushes: Influence of Monovalent Salts in the Environment", *Macromolecules* **2005**, *38*, 4855-4860.

35. Currie, E. P. K.; Sieval, A. B.; Fleer, G. J.; Cohen Stuart, M. A. "Polyacrylic Acid Brushes: Surface Pressure and Salt-Induced Swelling", *Langmuir* **2000**, *16*, 8324-8333.

36. Dhara, D.; Chatterji, P. R. "Phase Transition in Linear and Cross-Linked Poly(*N*-Isopropylacrylamide) in Water: Effect of Various Types of Additives", *J. Macromol. Sci.: Rev. Macromol. Chem. Phys*. **2000**, *40*, 51-68.

37. Alonzo, J.; Huang, Z.; Liu, M.; Mays, J. W.; Dadmun, M.; Kilbey, S. M., II "Looped Polymer Brushes Formed by Self-Assembly of Poly(2-vinylpyridine)-Polystyrene-Poly(2-vinylpyridine) Triblock Copolymers at the Solid-Fluid Interface. Kinetics of Preferential Adsorption", *Macromolecules* **2006**, *39*, 8434-8439.

38. Luo, N.; Metters, A. T.; Hutchison, J. B.; Bowman, C. N.; Anseth, K. S. "A Methacrylated Photoiniferter as a Chemical Basis for Microlithography: Micropatterning Based on Photografting Polymerization", *Macromolecules* **2003**, *36*, 6739-6745.

39. Nakayama, Y.; Matsuda, T. "*In-Situ* Observation of Dithiocarbamate-Based Surface Photograft Copolymerization Using Quartz Crystal Microbalance", *Macromolecules* **1999**, *32*, 5405-5410.

40. Kharlampieva, E.; Sukhishvilli, S. A. "Polyelectrolyte Multilayers of Weak Polyacid and Cationic Copolymer: Competition of Hydrogen-Bonding and Electrostatic Interactions", *Macromolecules* **2003**, *36*, 9950-9956.

41. Bulmus, V.; Ding, Z.; Long, C. J.; Stayton, P. S.; Hoffman, A. S. "Site-Specific Polymer-Streptavidin Bioconjugate for pH-Controlled Binding and Triggered Release of Biotin", *Bioconjugate Chem.* **2000**, *11*, 78-83.

42. Xia, F.; Feng, L.; Wang, S.; Sun, T.; Song, W.; Jiang, W.; Jiang, L. "Dual-responsive Surfaces that Switch between Superhydrophilicity and Superhydrophobicity", *Adv. Mater.* **2006**, *18*, 432-436.

CHAPTER 6

CONCLUSIONS AND RECOMMENDATIONS

6.1 Conclusions

Through this dissertation, I report findings of kinetic and mechanistic investigation of surface-initiated photoiniferter-mediated photopolymerization (SI-PMP) of methyl methacrylate and the application of SI-PMP for the synthesis of multiresponsive polymer brushes. While the initial rate of poly(methyl methacrylate) (PMMA) layer growth was observed to have first-order dependence on monomer concentration, the overall growth was found to be nonlinear as a function of time. Modeling studies in combination with experimental observations of PMMA layer growth as functions of exposure time, monomer concentration and light intensity suggest that SI-PMP suffers from irreversible bimolecular termination reactions, which lead to loss of surface-tethered radicals and in turn, cessation of layer growth.

The problem of irreversible termination reactions was attributed to be the consequence of insufficient concentration of deactivating dithiocarbamyl radicals in the SI-PMP system. Therefore, tetraethylthiuram disulfide (TED), a source of dithiocarbamyl radicals, was added to the system. The studies of the impact of TED on the growth of PMMA by SI-PMP revealed interesting trade-offs: As expected, TED reduces the rate of growth of the layers and decreases the extent of irreversible termination reactions that

lead to cessation of polymerization; however, at long times the dithiocarbamyl radicals generated from TED can initiate polymerization in solution, resulting in monomer consumption, which can further retard the rate of propagation. Reinitiation studies using styrene support the contention that preaddition of TED helps to preserve the active ends, leading to an increase in reinitiation efficiency and block copolymer formation, as manifest by increasing PS-block thicknesses with increasing TED concentration, [TED].

The effects of various photopolymerization conditions such as initial photoiniferter concentration, light intensity and TED concentration were further investigated by simulating SI-PMP process. In combination with experimental observations, simulation of SI-PMP using the rate-based model indicate that increasing [TED] and decreasing light intensity impact the PMMA layer growth in similar fashions. While the maximum layer growth rate observed during the initial stages of SI-PMP decreases with increasing [TED] and decreasing light intensity, the maximum thickness attainable increases. However, simulations also indicate that the effects of [TED] and light intensity on the reinitiation ability of PMMA layers are significantly different: reinitiation ability increases with increasing [TED]; whereas decreasing light intensity does not improve reinitiation ability, but increases layer thickness (exposure time) at which maximum reinitiation ability is achieved. Comparison of effects of [TED] and light intensity on reinitiation ability indicate that choice of photopolymerization conditions for the first polymerization step (PMMA layer synthesis) is critical to the final structure of the polymer brush created upon reinitiation (second polymerization step). PMMA layers formed in the presence of TED are more likely to form block copolymers as compared to PMMA layers synthesized without TED and at lower light intensity.

The findings of the simulation studies about the choice optimum photopolymerization conditions were applied to successfully synthesize multiresponsive poly(methacrylic acid)-*block*-poly(*N*-isopropylacrylamide) (PMAA-*b*-PNIPAM) layers. The actuation of PMAA-*b*-PNIPAM layers depends on pH, temperature and ionic strength, as expected. However, each component in PMAA-*b*-PNIPAM layer retains its customary responsive characteristics: PMAA block swells as pH is increased and PNIPAM block exhibits a lower critical solution temperature (LCST) behavior. Due to added ions (buffer solution) and surface confinement, PNIPAM brush transition occurs at a lower temperature and over a wider range of temperature as compared to the sharp transition at 32 ºC observed in case of free PNIPAM chains in deionized water. While the responsive nature of PNIPAM blocks in PMAA-*b*-PNIPAM layers is similar to the responsive nature of homo-PNIPAM layers, the pH-induced swelling of PMAA blocks is slightly different than the pH-induced swelling of homo-PMAA layers.

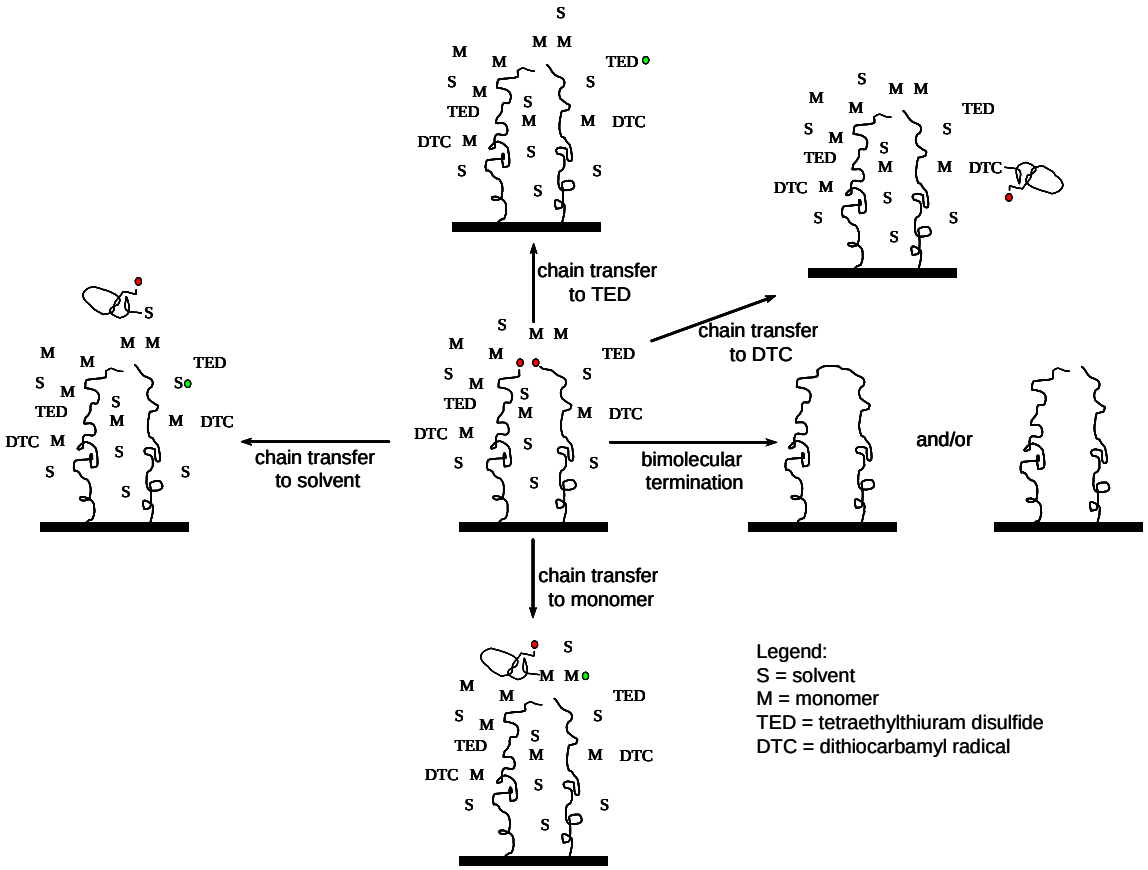

Figure 6.1 Schematic representation of SI-PMP and possible side-reactions involved in SI-PMP.

6.2 Recommendations

The findings reported in this dissertation prove the robustness of SI-PMP to synthesize homo- and block copolymer layers. The following recommendations, especially in the field of responsive polymer layers, are suggested to advance the work reported in this dissertation:

1) Preliminary studies in this work (please refer to Appendix H) and reports of responsive nature of random PMAA-*co*-PNIPAM layers in the literature [1] suggest that both pH- and thermoresponsive characteristics of PMAA and PNIPAM, respectively can be tuned by changing the comonomer compositions. A bi-level brush that consists of PMAA-*b*-(PMAA-*co*-PNIPAM) or (PMAA-*co*-PNIPAM)-*b*-PNIPAM layer can form a multiresponsive layer with predefined responsive characteristics.

2) Grafting density is known to affect the swelling of both polyelectrolyte (PE) and PNIPAM brushes [2-4]. In the current work, no efforts were made to evaluate the grafting density and reinitiation efficiency (and in turn, chain density of PNIPAM blocks) of PMAA layers. The investigation of effects of grafting density and reinitiation efficiency of PMAA layers on the responsive behavior of PMAA-*b*-PNIPAM system could be instrumental in design of these multiresponsive layers.

3) With subtle modifications in the photoiniferter chemistry, previous researchers have shown that SI-PMP can be used to grow polymer brushes from polymeric substrates. Growing multiresponsive polymer brushes using SI-PMP from the polymeric substrates would be more practical in terms of applications in the field of drug delivery.

6.3 References

1. Xia, F.; Feng, L.; Wang, S.; Sun, T.; Song, W.; Jiang, W.; Jiang, L. “Dual-responsive Surfaces that Switch between Superhydrophilicity and Superhydrophobicity”, *Adv. Mater.* **2006**, *18*, 432-436.

2. Rühe, J.; Ballauff, M.; Biesalski, M.; Dziezok, P.; Grohn, F.; Johannsmann, D.; Houbenov, N.; Hugenberg, N.; Konradi, R.; Minko, S.; Motornov, M.; Netz, R. R.; Schmidt, M.; Seidel, C.; Stamm, M.; Stephan, T.; Usov, D.; Zhang, H. “Polyelectrolyte Brushes”, *Adv. Polym. Sci*. **2004**, *165*, 79-150.

3. Plunkett, K. N.; Zhu, X.; Moore, J. S.; Leckband, D. E. “ PNIPAM Chain Collapse Depends on the Molecular Weight and Grafting Density”, *Langmuir* **2006**, *22*, 4259-4266.

4. Currie, E. P. K.; Sieval, A. B.; Fleer, G. J.; Cohen Stuart, M. A. “Polyacrylic Acid Brushes: Surface Pressure and Salt-Induced Swelling”, *Langmuir* **2000**, *16*, 8324-8333.

APPENDICES

Appendix A

Copyright Permissions

ACS PUBLICATIONS DIVISION
APR - 2 2007
COPYRIGHT OFFICE

Karen Buehler

From: Santosh [srahane@clemson.edu]
Sent: Sunday, April 01, 2007 7:56 PM
To: Copyright
Subject: Permission for reproducing figures from a ACS journal

Dear Sir/Madam,

I am completing a doctoral dissertation at Clemson University entitled "Kinetics of Surface-Initiated Photoiniferter-Mediated Photopolymerization and Synthesis of Stimuli-Responsive Polymer Brushes". I would like to include in the Introduction of my dissertation following figures:

1) Figure 7 from the article published in *Macromolecules* **1996**, *29*, 8622-8630,
2) Figure 5 from the article published in *Macromolecules* **2000**, *33*, 349-356,
3) Figure 1b from the article published in *Macromolecules* **1999**, *32*, 5405-5410, and
4) Figure 2b from the article published in *Macromolecules* **1999**, *32*, 5405-5410.

I would appreciate your permission to use these figures for my doctoral dissertation. You can contact me at:

Santosh B. Rahane
127 Earle Hall,
Dept. of Chemical and Biomolecular Engineering,
Clemson University,
Clemson, SC-29634
Phone: 864-656-7381
Fax: 864-656-0784

If you need further information, please email me at srahane@clemson.edu.

Thank you,
Santosh B. Rahane.

PERMISSION TO REPRINT IS GRANTED BY THE AMERICAN CHEMICAL SOCIETY

ACS CREDIT LINE REQUIRED. Please follow this sample: Reprinted with permission from (reference citation). Copyright (year) American Chemical Society.

* OR "REPRINTED IN PART..."

APPROVED BY: C. Arleen Courtney 4/3/07
ACS Copyright Office

☐ **If box is checked, author permission is also required. See original article for address.**

republication
<republication@wiley.com>
04/04/2007 11:20 AM
Please respond to republication <republication@wiley.com>

To <republication@wiley.com>
cc
bcc
Subject Republication/Electronic Request Form

A01_First_Name: Santosh
A02_Last_Name: Rahane
A03_Company_Name: Clemson University
A04_Address: 127 Earle Hall, Dept of Chemical and Biomolecular Engineering
A05_City: Clemson
A06_State: SC
A07_Zip: 29631
A08_Country: USA
A09_Contact_Phone_Number: 864-656-7381
A10_Fax: 864-656-0784
A11_Emails: srahane@clemson.edu
A12_Reference:
A13_Book_Title: Journal of polymer science. Part A, Polymer chemistry
A40_Book_or_Journal: Journal
A14_Book_Author:
A15_Book_ISBN:
A16_Journal_Month: February
A17_Journal_Year: 2003
A18_Journal_Volume: 41
A19_Journal_Issue_Number: 3
A20_Copy_Pages: Figure 1 on page no. 389
A21_Maximum_Copies: dissertation
A22_Your_Publisher: Clemson University
A23_Your_Title: Kinetics of Surface-Initiated Photoiniferter-Mediated Photopolymerization and Synthesis of Stimuli-Responsive Polymer Brushes
A24_Publication_Date: May 2007
A25_Format: print
A31_Print_Run_Size:
A41_Ebook_Reader_Type:
A26_If_WWW_URL:
A27_If_WWW_From_Adopted_Book:
A28_If_WWW_Password_Access: No
A45_WWW_Users:
A29_If_WWW_Material_Posted_From:
A30_If_WWW_Material_Posted_To:
A42_If_Intranet_URL:
A32_If_Intranet_From_Adopted_Book:
A33_If_Intranet_Password_Access: No
A48_Intranet_Users:
A34_If_Intranet_Material_Posted_From:
A35_If_Intranet_Material_Posted_To:
A36_If_Software_Print_Run:
A37_Comments_For_Request:

Wiley STM

PERMISSION GRANTED
BY: 4/5/07
Global Rights Dept., John Wiley & Sons, Inc.

NOTE: No rights are granted to use content that appears in the work with credit to another source

Appendix B

Synthesis of the Photoiniferter, *N*,*N*-(Diethylamino)dithiocarbamoylbenzyl-(trimethoxy)silane (SBDC)

The procedure for synthesis of SBDC is reported by de Boer et al. [*Macromolecules* **2000**, *33*, 349-356] and, in brief, involves an overnight reaction between *p*-(chloromethyl)phenyltrimethoxysilane (1) and *N*,*N*-diethyldithiocarbamate (2) in dry tetrahydrofuran (THF) at room temperature (Figure B.1).

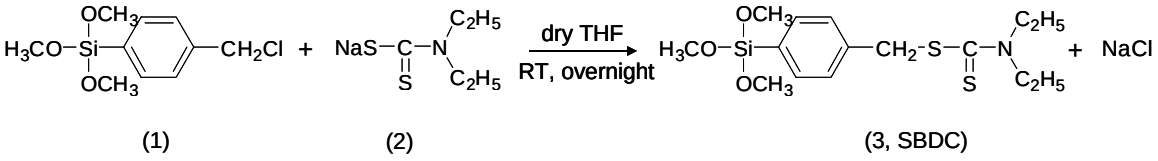

(1) (2) (3, SBDC)

Figure B1 Synthesis of *N*,*N*-(Diethylamino)dithiocarbamoylbenzyl(trimethoxy)silane (SBDC).

The detailed synthesis and separation procedure is described below:

1) 250 ml (containing a stirbar) and 100 ml round bottom flasks were flame-dried.
2) The flame-dried flasks were transferred to glove-box, where both oxygen and water levels are kept below 1 ppm.
3) A solution of reactant (**2**) (2.04 g, 12 mmol) in anhydrous THF (approximately 25 ml) was prepared in 100 ml flask.

4) A solution of reactant (**1**) (2.64 ml, 18 mmol) in anhydrous THF (10 ml) was prepared in 250 ml flask containing stir-bar.
5) The solution of reactant (**2**) was added slowly (over a period of 20 minutes) to the 250 ml flask containing solution of reactant (**1**).
6) The reaction mixture was stirred overnight at room temperature.
7) A white precipitate (NaCl) was formed, and during the reaction period, the solution became yellow.
8) The NaCl precipitate was filtered off, and the solution was concentrated by evaporating THF.
9) The remaining yellow liquid was vacuum-distilled in a Kugelrohr apparatus by increasing the temperature slowly to 160 °C at pressure of approximately 3 to 4 mbar.
10) Vacuum-distillation in a Kugelrohr apparatus yielded nearly pure product (**3**, SBDC).
11) The final product, SBDC, was transferred to a 5 ml flame-dried round bottom flask, which was stored in a dry-box.

Appendix C

Test to Investigate Whether Initial Lag Observed is a Consequence of Radical Inhibition

Hypothesis:

The test of the initial lag was based on the hypothesis that if the initial lag is a result of inhibitor- or oxygen-mediated radical inhibition, then using monomer solution that is exposed to UV-light at certain photopolymerization conditions in presence of photoiniferter-modified silicon wafers for exposure time longer than the initial lag period observed for those photopolymerization conditions, a subsequent surface-initiated photoiniferter-mediated photopolymerization (SI-PMP) should not result in a initial lag period.

Results and Discussion:

SI-PMP of methyl methacrylate (MMA) was carried out at MMA concentration of 4.68 M and light intensity of 5 mW/cm^2 for exposure time longer than the initial lag period (2 hours in the current studies). At the MMA concentration of 4.68 M and light intensity of 5 mW/cm^2, as shown in Figure 1.5, initial lag period was observed to be approximately 0.5 hours. After 2 hours of exposure, the photopolymerization cell was then transferred to the glove-box without disturbing the assembly. In the glovebox, already exposed monomer solution was drawn out of the reaction cell using a syringe. This monomer solution was used for synthesizing PMMA layers using SI-PMP from fresh PI-modified silicon wafers. Figure C1 shows the evolution of PMMA layer growth as a function of time at 5 mW/cm^2. As shown in figure, initial lag is still present

suggesting that inhibitor- or oxygen-mediated radical-inhibition is not the cause of initial lag observed in PMMA layer growth by SI-PMP.

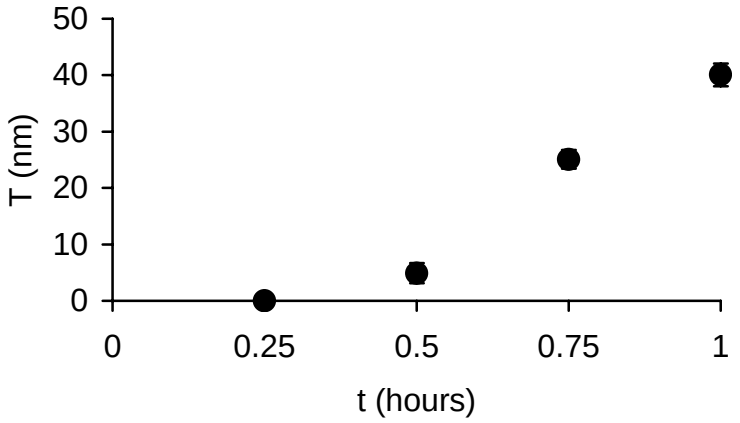

Figure C1 Evolution of PMMA layer thickness as a function of time. The MMA solution used to synthesize the PMMA layers was preexposed to UV-light at monomer concentration of 4.68 M and light intensity of 5 mW/cm^2 for 2 hours in the presence of photoiniferter-modified silicon wafers.

Appendix D

Test to Investigate Whether Initial Lag Observed is a Consequence of Quick Termination of Surface-Tethered Radicals Generated During Initial Stages

Hypothesis:

To test whether the initial lag is a consequence of termination of surface-tethered radicals due to proximity (high concentration) of radicals during the initial stages of surface-initiated photoiniferter-mediated photopolymerization (SI-PMP), evolution of poly(methyl methacrylate) (PMMA) layer growth at initial photoiniferter concentration lower than that corresponding to the photoiniferter monolayer was studied. This test was based on the hypothesis that by reducing the initial photoiniferter concentration, the concentration of surface-tethered radicals generated, and in turn, the extent of termination reactions during the initial stages should decrease resulting in shorter initial lag period.

Results and Discussion:

Figure D1 shows the effect of photoiniferter concentration on PMMA layer growth. In these experiments, photoiniferter concentration was systematically varied by pre-exposing the photoiniferter-modified silicon wafers to UV-light in presence of only toluene at light intensity of 1 mW/cm^2 and for different exposure times. The photoiniferter concentrations were quantified by following procedure.

Photoiniferter-modified silicon wafers were exposed to toluene at 5 mW/cm^2 for an array of exposure times. These pre-exposed layers were then reinitiated using styrene as a monomer for 4 hours and at 5 mW/cm^2. Concentration of styrene in toluene was 4.34

M. The normalized thicknesses of PS layers (T_{PS}/T_{PS0} where, T_{PS} is the thickness of PS layer grown from a pre-exposed PS PI-modified wafer and T_{PS0} is the thickness of PS layer grown from an un-exposed PI-modified wafer) as a function of PS were fitted to exponential decay model for initiation kinetics (eq D1) and the decay constant ($k_a^{'}$) was obtained (thin line in Figure D2) from the data fitting. Using information about the decay constant at 5 mW/cm^2, initiation kinetics at 1 mW/cm^2 were predicted (dotted line in Figure D2). The prediction of initiation kinetics at 1 mW/cm^2 were validated by comparing the predicted normalized PS layer thicknesses with the normalized thicknesses of PS layers synthesized from PI-modified wafers pre-exposed to toluene at 1 mW/cm^2 and for various exposure times. The values of T_{PS}/T_{PS0} were used as a measure of initial photoiniferter concentration.

$$\frac{[STR-DTC]}{[STR-DTC]_0} = 1 - \exp\left(k_a^{'} t\right) \tag{D1}$$

This procedure not only facilitates quantifying initial photoiniferter concentration, but also provides insight into the initial stages of SI-PMP. It is worth noting that the normalized thicknesses plotted in Figure D2 exhibit an exponential decrease as observed in case of initiation kinetics typically. In a situation when significant initial termination events occur during the initial stages, the thicknesses of PS layers synthesized from photoiniferter-modified layers pre-exposed to toluene for long times (for example, 2 or 4 hours at light intensity of 5 mW/cm^2) would be higher than those shown in Figure D2. The fact that these thicknesses were very low (or negligible) suggests that termination reactions are not dominant during the initial lag period.

Additionally, as shown by the arrows in Figure D1, decreasing initial photoiniferter concentration did not result in decrease in the initial lag period. These observations support the conclusion that the initial lag period cannot be fully described by significant chain termination in the initial stages of layer growth.

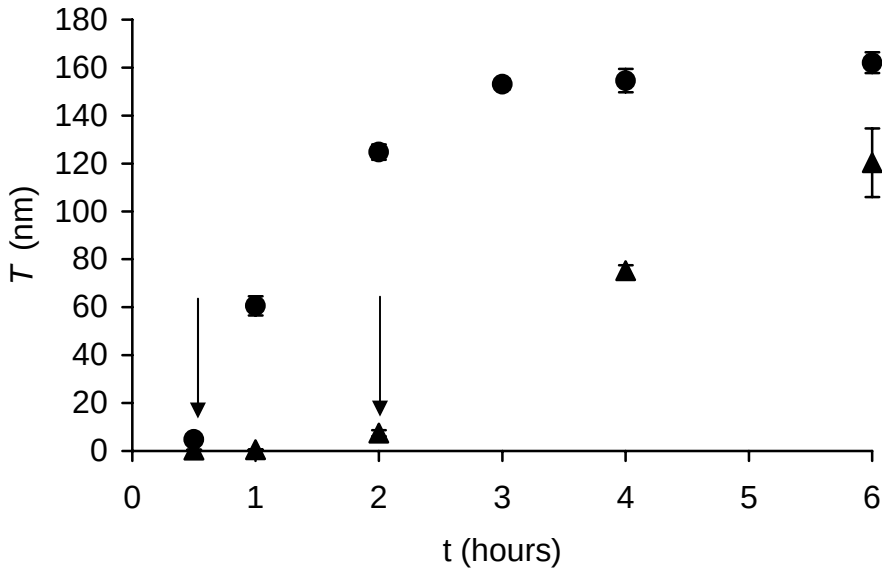

Figure D1 Comparison of the PMMA layer thicknesses synthesized at various initial photoiniferter concentrations and measured using variable angle ellipsometry as a function of time with simulated PMMA layer thicknesses. Photoiniferter concentrations used were $[I_M]_0$ M (●) and $0.3[I_M]_0$ (▲) where, $[I_M]_0$ represents the photoiniferter concentration that corresponds to a photoiniferter monolayer.

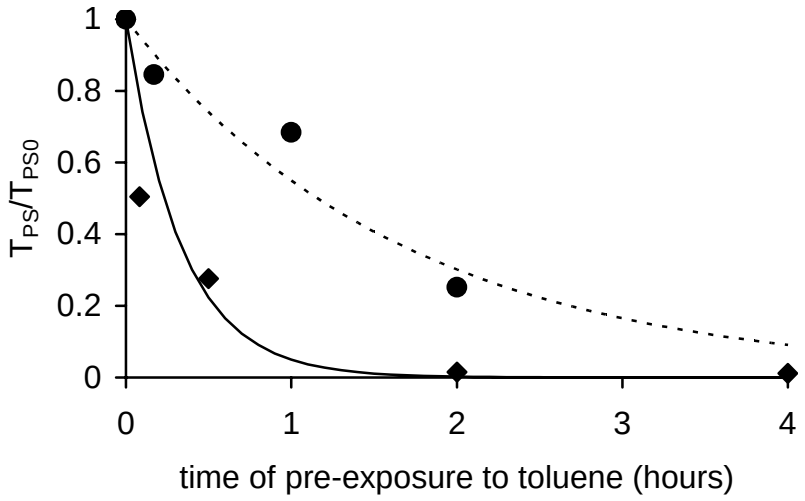

Figure D2 Initiation kinetics of surface-tethered photoiniferter investigated through reinitiation of photoiniferter-modified silicon wafers pre-exposed to toluene. Photoiniferter-modified wafers were pre-exposed to toluene at 5 mW/cm^2 (♦) and 1 mW/cm^2 (●).

Appendix E

Derivation and Predictions of "Chain Transfer to Solvent Alone" and "Chain Transfer to Solvent and Monomer Together" Models to Determine the Prevalent Termination Mechanism

Eq E1 represents the PMMA layer growth rate. *For assumptions and simplifications, please refer to Chapter 2*.

$$\frac{dT}{dt} = k[STR\bullet][M] \tag{E1}$$

The layer growth is affected by various termination reactions including bimolecular termination and chain transfer reactions. In this appendix, kinetic models are developed when chain transfer to solvent alone and chain transfer to solvent and monomer together are dominant termination mechanisms.

Chain Transfer to Solvent Alone:

Eq E2 represents time rate of change of surface-tethered radical concentration due to chain transfer to solvent.

$$-\frac{d[STR\bullet]}{dt} = k_{ct-S}[STR\bullet][S] \tag{E2}$$

Integrating Eq E2 yields the following time-dependent expression for surface-tethered radical concentration:

$$[STR\bullet] = [STR\bullet]_0 \exp(-k_{ct-S}[S]t) \tag{E3}$$

Substituting Eq E3 in Eq E1 and then solving for $T(t)$ yields the following expression for PMMA layer thickness as a function of exposure time, t.

$$T = \frac{k}{k_{ct-S}}\frac{[M]}{[S]}[STR\bullet]_0\{\exp(-k_{ct-S}[S]t_{brush}) - \exp(-k_{ct-S}[S]t)\} + T_{brush} \tag{E4}$$

Figure E1 shows the comparison of predictions of chain transfer to solvent model with the experimental obtained thicknesses as a function of time. Similar to the analysis of bimolecular termination and chain transfer to monomer model done in Chapter 2, the lumped kinetic parameters in Eq E4 were obtained by fitting the experimental data at 4.68 M monomer concentration with the model predictions, and these lumped parameters were then used to predict the thicknesses at monomer concentrations of 1.17 M and 2.34 M. As shown in Figure E1, the thicknesses at monomer concentrations of 1.17 and 2.34 M are significantly underpredicted, suggesting that chain transfer to solvent is not the dominant termination mechanism in SI-PMP for the reaction conditions investigated.

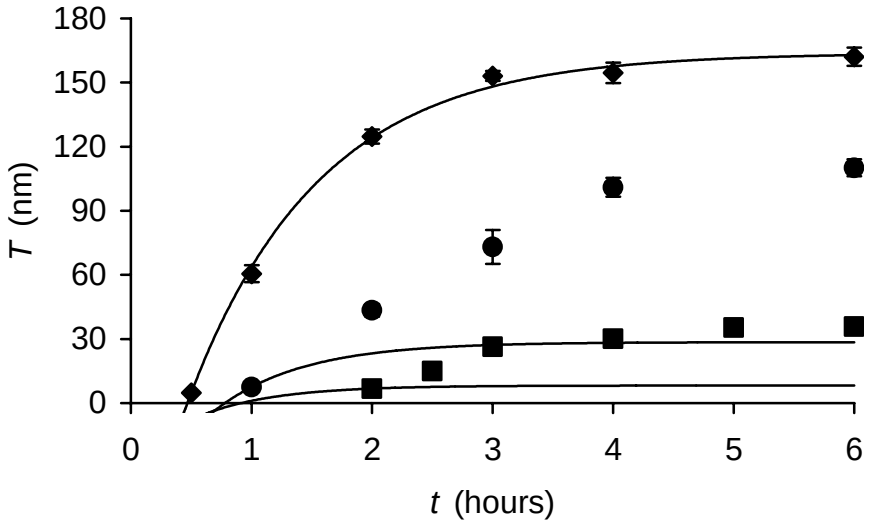

Figure E1 Comparison of the PMMA layer thicknesses measured using variable angle ellipsometry as a function of exposure time with model predictions (thin lines) for chain transfer to solvent. Irradiation intensity is 5 mW/cm^2 and methyl methacrylate concentrations in toluene are (■) 1.17, (●) 2.34, and (♦) 4.68 M.

Chain Transfer to Solvent and Monomer:

Eq E5 represents time rate of change of surface-tethered radical concentration due to chain transfer to solvent and monomer.

$$-\frac{d[STR\bullet]}{dt} = k_{ct}[STR\bullet][M] + k_{ct-S}[STR\bullet][S] \tag{E5}$$

Integrating Eq E5 yields the following time-dependent expression for surface-tethered radical concentration:

$$[STR\bullet] = [STR\bullet]_0 \exp[-(k_{ct}[M] + k_{ct-S}[S])t] \tag{E6}$$

Substituting Eq E6 in Eq E1 and then solving for $T(t)$ yields following expression for PMMA layer thickness as a function of t when chain transfer to both monomer and solvent are considered dominant termination mechanisms.

$$T = \frac{k[M]}{k_{ct}[M] + k_{ct-S}[S]}[STR\bullet]_0 \{\exp[-(k_{ct}[M] + k_{ct-S}[S])t_{brush}] - \exp[-(k_{ct}[M] + k_{ct-S}[S])t]\} + T_{brush} \quad \text{(E7)}$$

Figure E2 shows the comparison of predictions of "chain transfer to monomer and solvent together" model with the experimental obtained thicknesses as a function of time. The lumped kinetic parameters in Eq E7 were obtained by fitting the experimental data at 4.68 M monomer concentration with the model predictions and these lumped parameters were then used to predict the thicknesses at monomer concentrations of 1.17 M and 2.34 M. As shown in Figure E2, the thicknesses at monomer concentration 2.34 M are reasonably predicted using the model. However, the thicknesses at monomer concentrations at 1.17 M are overpredicted.

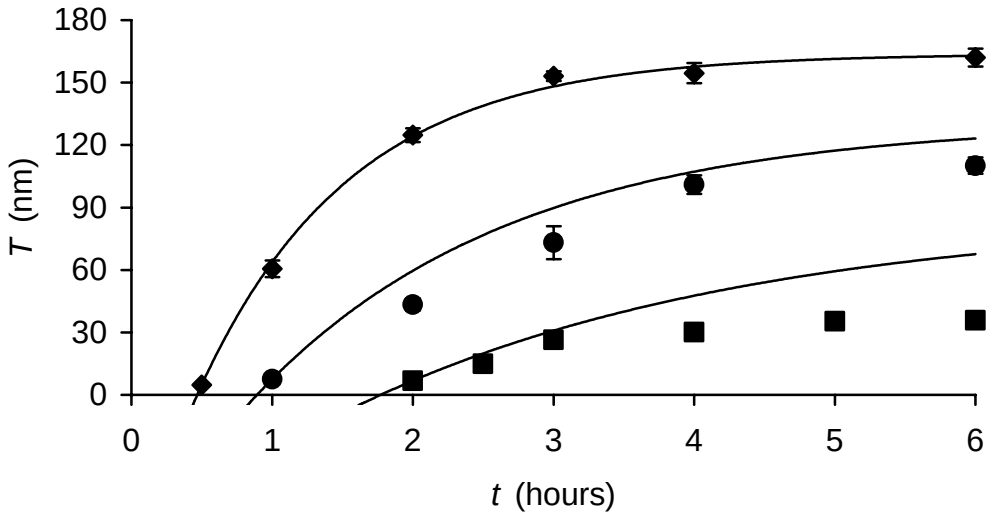

Figure E2 Comparison of the PMMA layer thicknesses measured using variable angle ellipsometry as a function of exposure time with model predictions (thin lines) for chain transfer to monomer and solvent. Irradiation intensity is 5 mW/cm^2 and methyl methacrylate concentrations in toluene are (■) 1.17, (●) 2.34, and (♦) 4.68 M.

Appendix F

Derivation of Pseudo-steady State Model

Pseudo-steady model is developed by simplifying the comprehensive model (eq F1 through F5) through application of certain assumptions; it is useful for the validation of comprehensive model.

$$\frac{d[STR\bullet]}{dt} = k_a^{'}[STR - DTC] - k_{t,rev}[STR\bullet][DTC\bullet] - k_t[STR\bullet]^2 \quad \text{(F1)}$$

$$\frac{d[STR - DTC]}{dt} = -k_a^{'}[STR - DTC] + k_{t,rev}[STR\bullet][DTC\bullet] \quad \text{(F2)}$$

$$\frac{d[DTC\bullet]}{dt} = k_{a,TED}^{'}[TED] - k_{t,TED}[DTC\bullet]^2 + k_a^{'}[STR - DTC] - k_{t,rev}[STR\bullet][DTC\bullet] \quad \text{(F3)}$$

$$\frac{d[TED]}{dt} = -k_{a,TED}^{'}[TED] + k_{t,TED}[DTC\bullet]^2 \quad \text{(F4)}$$

$$\frac{dT}{dt} = k^{'}k_p[STR\bullet][M] \quad \text{(F5)}$$

Application of assumption of no irreversible termination simplifies eq F1 to yield eq F6.

$$\frac{d[STR\bullet]}{dt} = k_a^{'}[STR-DTC] - k_{t,rev}[STR\bullet][DTC\bullet] \quad \text{(F6)}$$

Assumption of pseudo-steady state for the surface-tethered carbon radicals yields eq F7:

$$[STR-DTC]_s = \frac{k_{t,rev}[STR\bullet]_s[DTC\bullet]_s}{k_a^{'}} \quad \text{(F7)}$$

where $[STR-DTC]_s$ is the concentration of surface-tethered radicals reversibly-terminated by dithiocarbamyl radicals at pseudo-steady state, $[STR\bullet]_s$ is the concentration of surface-tethered radicals at pseudo-steady state and $[DTC\bullet]_s$ is the concentration of dithiocarbamyl radicals at pseudo-steady state.

A mole balance for reversibly deactivated surface-tethered species yields eq F8 for $[STR-DTC]_s$.

$$[STR-DTC]_s = [STR-DTC]_0 - [STR\bullet]_s \quad \text{(F8)}$$

Substituting eq F8 into eq F7 and simplifying yields

$$[STR\bullet]_s = \frac{f_1 k_a [STR-DTC]_0}{f_1 k_a + [DTC\bullet]_s} \quad \text{(F9)}$$

Pseudo-steady state concentration of dithiocarbamyl radicals can be obtained by applying pseudo-steady state analysis to eq F3. In case of excess TED, the contribution of DTC●

radicals generated from low-area substrates is negligible as compared to DTC● radicals generated from free TED in the solution, simplifying eq F3 to yield eq F10.

$$\frac{d[DTC\bullet]}{dt} = k_{a,TED}^{'}[TED] - k_{t,TED}[DTC\bullet]^2 \tag{F10}$$

As discussed earlier, applying pseudo-steady state analysis to eq F10 yields eq F11 for pseudo-steady state concentration of dithiocarbamyl radicals.

$$[DTC\bullet]_s = \sqrt{\frac{k_{a,TED}^{'}[TED]_s}{k_{t,TED}}} \tag{F11}$$

Substituting this expression for $[DTC\bullet]_s$ into eq F9 and replacing $[TED]_s$ by $[TED]_0$ (initial concentration of TED) for the initial stages of SI-PMP, yields eq F12 for pseudo-steady state concentration of surface-tethered radicals during the initial stages of SI-PMP in presence of excess TED.

$$[STR\bullet]_s = \frac{k_a^{'}[STR - DTC]_0}{k_a^{'} + \sqrt{\frac{k_{a,TED}^{'}[TED]_0}{k_{t,TED}}}} \tag{F12}$$

This expression for $[STR\bullet]_s$ can be substituted in eq F5 to obtain the (maximum) growth rate of the PMMA layers.

Appendix G

Buffer Recipes

pH	ionic strength (mM)	Acid/base	mass of acid/base (g)	mass of NaCl (g)
3	154	phosphoric acid	4.9	6.4
4	154	acetic acid	3.0	8.5
5	154	acetic acid	3.0	6.9
6	154	MES free acid	9.8	7.7
7	154	NaH_2PO_4	7.1	2.5
8	154	NaH_2PO_4	7.1	0.6
5	40	acetic acid	3.0	0.4
5	80	acetic acid	3.0	2.7
5	120	acetic acid	3.0	4.9
5	200	acetic acid	3.0	9.6
7	120	NaH_2PO_4	7.1	0.6
7	200	NaH_2PO_4	7.1	5.1
7	240	NaH_2PO_4	7.1	7.4

Table G1 Amounts of acids/bases and sodium chloride required to make 1 L buffer solutions of given pH and ionic strengths.

Appendix H

Preliminary Investigation of Responsive Nature of a Random Poly(methacrylic acid)-*co*-poly(*N*-isopropylacrylamide) layer as a function of pH and Temperature

To study the responsive nature of a random copolymer of methacrylic acid (MAA) and *N*-isopropylacrylamide (NIPAM), a 142.4 nm-thick poly(methacrylic acid)-*co*-poly(*N*-isopropylacrylamide) (PMAA-*co*-PNIPAM) layer was synthesized at light intensity of 10 mW/cm^2, monomer (MAA:NIPAM = 1:1 by mass) concentration of 25 % w/w in methanol/water mixture (1:1 v/v), TED concentration of 0.0 mM and an exposure time of 6 hours. Based on the reactivity ratios of methacrylic acid and acrylamide (as a first approximation to the reactivity ratio of *N*-isopropylacrylamide) and Equation H1 [1], the random copolymer should consist of approximately 62 % of methacrylic acid comonomer.

$$F_{MAA} = \frac{r_{MAA} f_{MAA}^2 + f_{MAA} f_{NIPAM}}{r_{MAA} f_{NIPAM}^2 + 2 f_{MAA} f_{NIPAM} + r_{NIPAM} f_{NIPAM}^2} \quad \text{(H1)}$$

In this equation, F_{MAA} is the fraction of MAA in PMAA-*co*-PNIPAM layer, r_{MAA} is the reactivity ratio of MAA (1.63) [2], f_{MAA} is the fraction of MAA in monomer mixture (0.5, in this study), r_{NIPAM} is the reactivity ratio of acrylamide (0.57) [2], and f_{NIPAM} is the fraction of MAA in monomer mixture (0.5, in this study).

Figure H1 shows the results from PMAA-*co*-PNIPAM layer stretching experiments as a function of pH and temperature. As shown in the Figure, while the

PMAA-*co*-PNIPAM layer responds to pH, the lower critical solution transition behavior (LCST) of random copolymer disappeared. It is believed that at high fractions of methacrylic acid, the random copolymer is sufficiently hydrophilic to offset the hydrophobic temperature sensitive component, NIPAM. This observation of disappearance of LCST behavior is consistent with previously reported temperature-dependent swelling of poly(*N*-isopropylacrylamide-*co*-poly(acrylic acid) (PNIPAM-*co*-PAA) hydrogels [3], which suggests that PNIPAM-*co*-PAA hydrogels with more than 20 mol % of PAA, did not exhibit LCST behavior. The results of PNIPAM-*co*-PAA hydrogels also suggest that the copolymer composition could be varied to tune pH- and temperature-dependent actuation of these hydrogels.

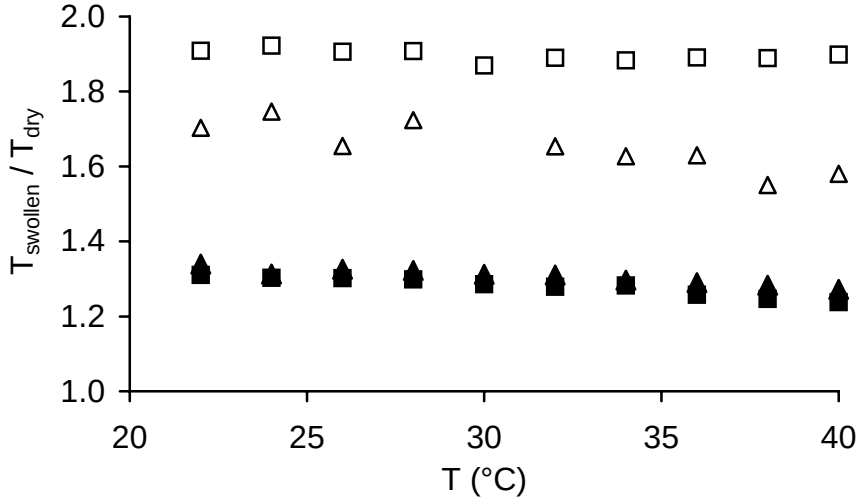

Figure H1 Response of a random PMAA-*co*-PNIPAM brush to changes in pH and temperature. The pHs of buffer solutions were 4 (■), 5 (▲), 6 (Δ), 7 (□). An 142.4 nm-thick PMAA-*co*-PNIPAM layer was synthesized using a light intensity of 10 mW/cm^2, monomer (MAA:NIPAM = 1:1 by mass) concentration of 25 % w/w in methanol/water mixture (1:1 v/v), TED concentration of 0.0 mM and an exposure time of 6 hours.

References

1. Odian, G. In "Principles of Polymerization", 4th ed.; Wiley-Interscience: New Jersey, **2004**; p 464-543.

2. Ueda, A.; Nagai, S. In "Polymer Handbook", 4th ed.; Brandup, J., Immergut, E. H., Grulke, E. A., Eds.; Wiley-Interscience: New Jersey, 1999; Vol. 1, p II/97.

3. Yoo, M. K.; Sung, Y. K.; Lee, Y. M.; Cho, C. S. "Effect of Polyelectrolyte on the Lower Critical Solution Temperature of Poly(N-isopropylacrylamide) in the Poly(NIPAAm-*co*-acrylic acid) Hydrogel," *Polymer* **2000**, *41*, 5713-5719.